Title
Deconstructing Retinal Ganglion Cell Axonal Regeneration in Xenopus laevis

Author
Fague, Lindsay

Publication Date
2022

Peer reviewed|Thesis/dissertation

Deconstructing Retinal Ganglion Cell Axonal Regeneration in *Xenopus laevis*

by

LINDSAY MARIE CATHERINE FAGUE

DISSERTATION

Submitted in partial satisfaction of the requirements for the degree of

DOCTOR OF PHILOSOPHY

in

Biochemistry, Molecular, Cellular, and Developmental Biology

in the

OFFICE OF GRADUATE STUDIES

of the

UNIVERSITY OF CALIFORNIA

DAVIS

Approved:

_____

Nicholas Marsh-Armstrong, Chair

_____

Marie Burns

_____

Anna La Torre

Committee in Charge

2022

Table of Contents

Acknowledgements

The work contained in the following pages would almost by definition have been impossible to achieve without the guidance of a great principal investigator. For that alone I owe a great scientific debt, but I will also add that in a much larger sense, my entire identity as both a scientist and a person have been indelibly shaped for the better by the tireless guidance, encouragement, and assistance of my mentor, Dr. Nicholas Marsh-Armstrong. Nick, I have the highest respect for you equally as a scientist and a human being – your commitment to meaningful, rigorous, and honest science without compromising the "whole person" in the process has been an inspiration for me to achieve the highest standard of both research and personal integrity. Thanks for taking a chance on me as the first graduate student you took on at Davis, and thanks for always practicing what you preach. Whether it was showing up for a long Sunday of experiments, encouraging all of us to debate with you about our results, or allowing me leave to visit my family when I needed it, you continually prove that you care both about your science and your people. You challenge us as you challenge yourself, and it is an inspiration for all of us to follow.

I am also forever indebted to my thesis committee members Dr. Marie Burns and Dr. Anna La Torre. Anna, your enthusiasm for science is infectious and your questions are always on point – in fact, as you well know, one of your early questions at our joint lab meetings inspired an entire 3 figures' worth of data for my first paper. Thank you for always "showing up", mentally as well as physically, to help those around you on their way. From undergraduates to fellow professors, know that your positivity and energy are so motivating to us all. Thank you for keeping our fires burning on those days it starts to flicker. Marie, my profound respect for the depth of your knowledge and the rigor of your work is equaled only by my admiration for your

compassion, vision, and insight as a person. I love how critically and creatively you approach the world; your questions always make me think more deeply than I had before. You truly make me believe that anything is possible and that joy can be found both inside and out of the lab, and your unique, encouraging, and enlightening perspective has given me more peace and hope than I can ever say. Thank you for being someone I can turn to with my most personal (or most practical) of questions and who will always give me the direction I need to carry on.

And finally, a massive thank you also to the Joint Vision Friday Lab Group: to the lab heads, Dr. Nadean Brown, Dr. Tom Glaser, Dr. Ala Moshiri, and Dr. Sergei Simo, to my now-graduated colleagues Dr. Joel Miesfield, Dr. Adam Miltner, and Dr. Jisoo Han, and to all the current members for their ongoing participation and collaboration. The lively discussions, teaching, learning, and advice shared in these meetings have been absolutely instrumental to my growth as a scientist. I love the collaboration of this group, the openness of sharing both resources and knowledge, and the way these discussions have made me grow so comfortable asking any question I might have at any scientific presentation, even outside of Davis. Thank you for quelling my fears and teaching me that science at its best is generous, helpful, and interactive. You have truly set a high standard to follow.

If I have achieved anything worth reporting in the pages that follow, it is only because of all of you. Thank you for everything.

Abstract

The retinal ganglion cells (RGCs) of the optic nerve are essential for transmission of visual information to the brain. Diverse insults to the optic nerve result in partial to total vision loss as the axons of RGCs are destroyed. In glaucoma, axons are injured at the optic nerve head; in other optic neuropathies, axons can be damaged along the entire visual pathway. In all cases, as mammals cannot regenerate injured central nervous system cells, once the axons are lost, vision loss is irreversible.

However, RGC axons of the African clawed frog *Xenopus laevis* are capable of regeneration and functional reinnervation of central brain targets following injury. In this dissertation, I describe a novel tadpole optic nerve crush (ONC) procedure and assessments of axon growth and brain innervation based on live imaging of RGC-specific transgenes which can be used to assay putative regeneration-associated genes *in vivo.* Using these assays with a CRISPR/Cas9-based F0 knockout screen, I report that the MAPKKK dual leucine zipper kinase (*dlk*) is necessary for regeneration of RGC axons following injury. Loss of Dlk does not affect vision as assessed by a behavioral assay but does block functional vision restoration after ONC. Dlk absence does not affect axonal outgrowth of RGCs either during development or from RGCs generated in the retina after the injury, but only affects the axonal regeneration of those RGCs whose axons were injured. While Dlk loss does not alter the acute change in mitochondria movement that occurs within RGC axons soon after injury, it does completely block the activation of the transcription factor c-Jun within RGCs days after the injury. Taken together, these results show that Dlk is essential for the axonal injury signal to reach the nucleus, suggesting that the difference between species that can and cannot regenerate their RGC axons after injury is likely the transcriptional response downstream of a MAPK cascade.

While mechanisms intrinsic to retinal ganglion cells, such as Dlk-dependent signal activation, are critical to successful RGC regeneration, RGC interactions with myeloid and glial cell populations in the retina and optic nerve are also highly likely to affect RGC survival and regeneration. Thus, using the same tadpole optic nerve crush assay, I further report that ablation of myeloid cells using a novel cell-type specific inducible transgene also delays optic nerve regeneration and reinnervation of the optic tectum following ONC. The absence of myeloid cells also results in a significant delay in clearance of cellular debris derived from the injury site. Additionally, removal of cellular debris immediately follows myeloid cell influx into both brain and optic nerve, indicating that debris removal by myeloid cells may be required for axonal regeneration.

My work elucidates two key aspects of an evolutionarily conserved successful regeneration response, one cell intrinsic and one cell extrinsic. Understanding the molecular mechanisms utilized by a regeneration-capable species may be essential to the rational design of future clinical interventions to regrow the optic nerve. My work also suggests that a combination of different molecular and cellular interventions will likely be the only way to achieve axonal regeneration sufficient for functional recovery of vision.

Chapter 1: The Basic Science of Optic Nerve Regeneration

Neurons and the Nervous System

The ability to sense the difference between a hot drink and a cold one, form memories, play hockey or climb mountains, watch a sunset, and complete a Ph.D are all due to neurons – specialized cells which capture, encode and transmit information via electrochemical signaling to understand the environment and direct all body functions. Neurons consist of a cell body, containing the nucleus, many organelles; dendrites, projecting tendrils which connect with other neurons or cells to collect input; and axons, which relay information onward to other neurons. Information relay occurs via a process known as synaptic transmission. Synaptic transmission begins when the axons of a sending neuron release neurotransmitters, often at a synapse with another neuron's dendrites. Neurotransmitters are small proteins which bind to receptors on the receiving axons' dendrites and create a physiological change which results in an electrical impulse being created within the receiving neuron (2). Beginning from the neuronal soma and progressing down to the axonal tips, voltage-gated ion channels open to allow an influx of charged ions which depolarize the membrane potential of the axon. The insulating myelin sheath, layers of cell membranous material produced from a myelinating cell that wraps around the length of the axon, is critical for fast signal propagation down the axon (3, 4). Once the electrochemical wave has reached the axon terminus, it induces the formation and release of vesicles containing neurotransmitters, which are released from the axon tips of one neuron (presynaptic terminals) and fuse with the dendritic tips of the next receiving axons (postsynaptic terminals) to begin the process anew. Thus, an electrochemical signal can be relayed through a network of axons before it terminates at its eventual target, whether that is a signal integration

center in the brain responsible for translating those signals or a motor neuron which then converts the neuronal signal into a contraction of the actin-myosin muscle tissue.

The nervous system is divided functionally into two connected but distinct systems, the central nervous system and the peripheral nervous system. The central nervous system (CNS) includes all regions of the brain and the spinal cord and the retina in the eye (5); the peripheral nervous system (PNS) accounts for all other sensory and motor neurons in other regions of the body (6). Though signal transmission occurs in the same manner in both systems, subtle distinctions in structure in function, which will be discussed later, create significant difference between CNS and PNS neurons. For this dissertation and for the entirety of my thesis work, I have focused on one major and compelling difference: while damage to PNS neurons is to an extent repairable in most vertebrates (7), the CNS in those same species is largely incapable of regeneration, meaning that any damage sustained is irreversible.

Introduction to the Retina and Optic Nerve

The visual system is part of the CNS and is made up of the eye, the optic nerve, and their visual targets in the brain. At the back of the eye lies the retina, a multi-layered thin neural tissue which collects light information and transmits it to the brain (Figure 1.1). The innermost layer of the retina is comprised of photoreceptors, specialized cells which absorb photons of light to create vision. Photoreceptors include both rods (responsible for low-light vision) and cones (responsible for high-acuity, bright light vision). In mice, rods outnumber cones by almost 20 times and contain a single light-sensing pigment known as rhodopsin; by contrast, cones contain one of several opsins, each specialized for absorption of a specific wavelength of light, thus allowing for color vision (8). In most mammals, the centermost region of the retina allows for the

highest-acuity vision due to a higher ratio of cones to rods; in primates this centermost region, known as the fovea, is completely devoid of rods and has a higher concentration of both cones and retinal ganglion cells (and therefore, the lowest ration of cones-per-ganglion cell) than anywhere else in the retina (9). Both rods and cones are partially regulated by inhibitory feedback from horizontal cells (8). The photoreceptor cells synapse onto bipolar cells in the next layer of the retina, which then transmit the visual stimuli largely to amacrine cells, although some bipolars connect directly to retinal ganglion cells (RGCS) (10). Amacrine cells are a diverse population whose key functions include lateral inhibition of the signals sent by the photoreceptor cells and are essential for functions such as the perception of movement (11). Retinal ganglion cells occupy the most peripheral layer of the retina and are unique in that though their dendrites and soma are located within the retina, their axons extend out of the retina through the optic nerve and to the brain, making them the sole projecting cell which connects the retina to the brain. In addition to these major cell types, the retina also contains several types of glial cells, notably Muller glia, astrocytes and microglia. The major glial cell type in the retina, Muller glia, function in neurotransmitter uptake, water and metabolite transport and regulation, energy production, and protection against oxidative stress, functions typically carried out elsewhere in the CNS by astrocytes (3, 12). Microglia are the major resident immune cells of the retina; upon detection of a disease or injury to the retina, they convert from a resting to an activated state and proliferate rapidly to respond to the insult (13).

Aside from the long projecting axons of RGCs, the optic nerve is also comprised of several support cell types, including astrocytes, oligodendrocytes, oligodendrocyte precursor cells, and their own population of resident microglia. Astrocytes in the optic nerve serve a similar function to that of Muller glia in the retina – they are important for water transport,

metabolism, ion regulation, signaling, and most recently have been shown to play a role in phagocytosis of debris produced from RGCs (3, 14). Oligodendrocytes myelinate RGC axons with layers of membranes to enable fast signal propagation, and also produce growth factors to assist with signaling (4). Finally, resident microglia in the ON, similar to those in the retina, sense damage to axons and activate a phagocytic and proliferative response upon injury or neurotoxic stress; they have also been found to cross-activate astrocytes into a similarly reactive state (13, 15). Together each of these neuronal cell types contribute to the homeostasis of the optic nerve and its ability to successfully transmit the visual signals collected by the retina to the brain for processing and analysis. In both retina and optic nerve there also is vasculature, with their constituent cell types, endothelial cells and pericytes, but also immune cells that may derive from the circulation but migrate into the tissues under conditions of stress or disease (16).

Retinal Ganglion Cells

Retinal ganglion cells (RGC) are among the first neuronal cell types to be born within the retina (17, 18). Soon after the birth and differentiation of RGCs, there is the extension of the major axon towards the developing optic nerve head, followed by the growth of branched processes that eventually become the dendritic arbor and terminate within the inner plexiform layer (IPL). The dendrites of RGCs form synapses with amacrine cells and bipolar cells within the IPL, and the axons of RGCs make contacts with various visual processing loci within the brain (19).

RGCs are remarkable in their diversity of both structure and function. Over 40 subtypes of RGCs have been identified in the rodent retina, and each subtype shows vast differences in their responses to light, their overall morphology and dendritic organization, and their axonal

projections (20, 21). The earliest classification of RGCs was done purely based on morphological observation by Ramón y Cajal in the late nineteenth century, and indeed, morphology remains an important factor in the identification and classification of RGC subtypes (22, 23). Later work discovered that RGCs are highly selective in their stimulus response. RGCs which depolarize with increases in light intensity are classified as ON RGCs, while RGCs that hyperpolarize in response to light and respond instead when light intensity decreases are called OFF RGCs (17, 24). Interestingly, the dendrites of ON RGCs stratify in the outer portion of the IPL, while OFF-RGCs stratify in the inner IPL, and On-Off RGCs, which will respond to both increases and decreases in light, have arborization in both areas of the IPL; this important early finding linked RGC structure to function (25). Further physiological identifiers of RGC subtypes also includes the direction-selective RGCs (dsRGCs), which depolarize in response to only a particular direction of movement stimulus; ON-OFF dsRGCs respond regardless of whether the stimulus is light or dark, and ON ds-RGCs respond only when the stimulus is an increase in light intensity and RGCs (24, 26). Other RGCs can be partially classified by biochemical markers; for example, alpha RGCs are more neurofilament-rich than many other RGCs (24). Additionally, there are at least 5 subtypes of melanopsin-expressing RGCs (intrinsically photosensitive RGCs or ipRGCs), which are themselves capable of absorbing photons of light (27-29). Most recently, single-cell sequencing and optogenetic techniques are enabling even more precise and detailed descriptions of RGC molecular and physiological signatures, which will likely result in better categorization of known subtypes and further subdivision of new RGC types (20, 30).

In addition to their structural and functional diversity, RGCs project to a wide variety of different brain targets. These projections are not entirely subtype specific, but a class of RGCs tends to project to only a subset of brain regions, and each brain region typically receives input

from only a dozen or less types of RGCs. For example, ipRGCs project to at least 12 brain regions, chief among these being the suprachiasmatic nucleus (SCN), where they assist in regulating the circadian clock, the hypothalamus and the olivary pretectal nucleus, a region at the midbrain which functions in pupillary light reflexes (27, 29, 31). The superior colliculus (SC), a brain region which integrates basic ocular stimuli with motor responses and orients the head in response to motion, receives input from at least 8 subtypes of RGCs including both alpha and ipRGCs (31). Others subtype of RGCs also innervate these same regions, along with many others, including to the lateral geniculate nucleus (LGN), the major image-forming center of the brain for complex stimuli, the pre-tectal nucleus, and the thalamus (19, 24). Overall, in mammals, there are over 24 brain regions which receive input from RGCs and contribute to the brain's processing of visual information collected by the retina (32).

In general, each RGC cell provides a specific type of information regarding visual stimulus to a specific area of the brain, which integrates these signals into a single image incorporating the motion, light intensity, color, edge differentiation information, and so on transmitted by individual RGCs. Loss of or injury to any single RGC cell type or group of RGCs would thus result in an incomplete image and severely impact the ability of the organism to respond to visual stimulus. Importantly, the lack of regenerative capacity in the CNS means that any injury or disease to the optic nerve, and specifically the axons of RGCs which comprise the main cell type of the optic nerve, results in irreparable vision loss. Clinically, a large number of

acute or progressive pathologies have been identified which regularly cause such RGC axonal damage, and a number of the most prevalent are discussed next.

Common optic neuropathies with injury to retinal ganglion cell axons

Glaucoma is the most common optic neuropathy resulting from RGC axonal damage and the leading cause of irreversible blindness worldwide, projected to affect over 100 million people

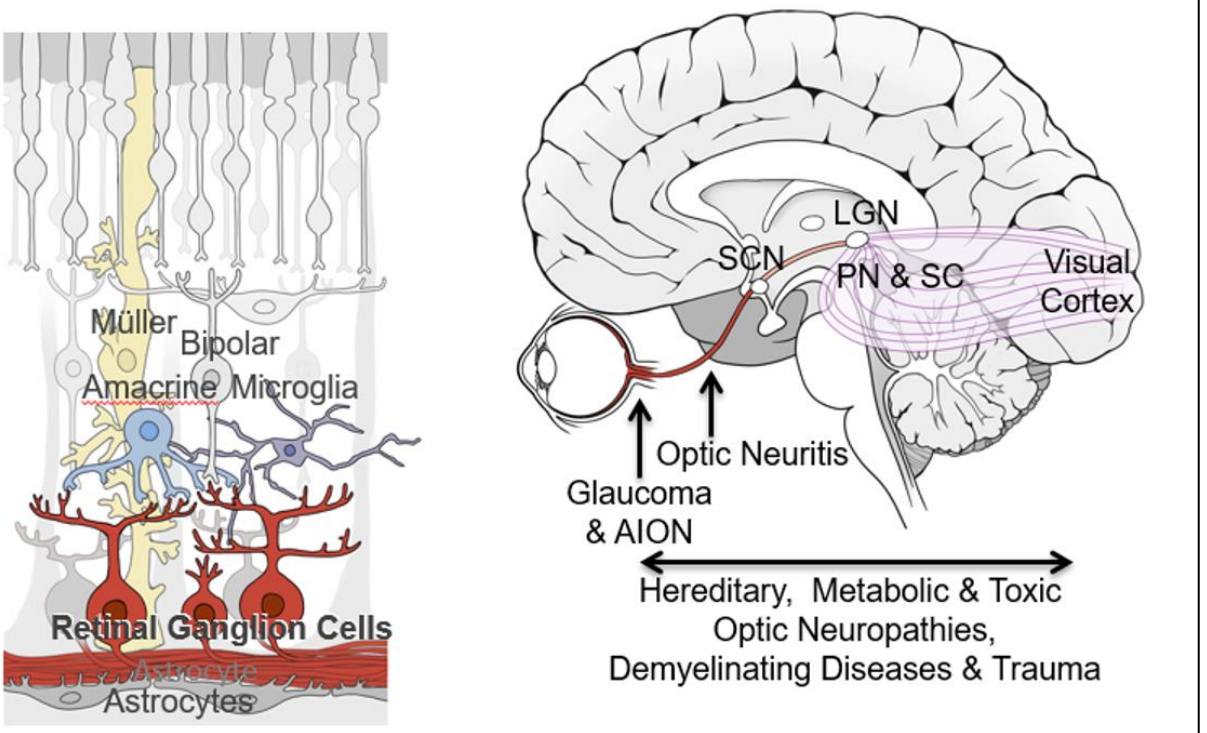

Figure 1.1: **Simple schematics of the retina and human brain emphasizing cells and areas relevant to optic nerve regeneration**. Various optic neuropathies affect different parts of the optic nerve; for example, glaucoma and AION/NAION affect the optic nerve head, while other insults can affect the optic nerve, optic tract and optic radiation. Visual information carried by RGC axons is processed by multiple regions of the brain, in addition to the lateral geniculate nucleus (LGN) that carries most image forming visual information to the visual cortex. Among these other brain nuclei are the superchiasmatic nucleus (SCN), pretectal nuclei (PN) and superior colliculi, which mediate diverse non-image-forming aspects of vision. In the retina, RGCs receive synapses from amacrines and bipolar cells, and are in close contact with glia (Müller cells and astrocytes) as well as microglia.

(From Fague, Liu and Marsh-Armstrong, 2021).

by 2040 (33). Glaucoma is frequently, though not always, associated with elevated intraocular

pressure, and the optic nerve head is generally believed to be the site of the axonal injury (Figure 1.1) (34). In classical glaucomatous neuropathies, elevated intraocular pressure impinging on the unmyelinated portions of RGC axons in the optic nerve head (ONH) is believed to cause damage to and eventual degradation of these axons (34-36). At the same time, elevated IOP is not a universal characteristic of the disease. Studies on different populations find that between 30-38% of Caucasian patients, about 57% of patients of African extent, and 52-92% of Asian patients have normal IOP levels (37-41). Clearly, glaucoma is not a purely hypertensive disease; many unknown factors likely contribute to its development, as is the case with other ON diseases. Glaucoma even in its earliest stages has also been found to cause overall damage to the macula, the central-most region of a primate eye with the highest density of both photoreceptors and RGCs, causing an thinning of the retinal nerve fiber layer and inner plexiform layer, as might be expected giving the overall progressive loss of RGCs in this disease (42). Current glaucoma treatment mainly focuses on the pressure-associated probable causes of glaucoma by seeking to lower intraocular pressure using eye drops or surgical procedures. However, even with such treatment in patients with high-IOP associated glaucoma, progression of vision loss still occurs in many patients (43).

Other optic neuropathies can occur at the optic nerve head but have much shorter time-courses. Ischemic optic neuropathies, either nonarteritic or arteritic, involve sudden visual loss, sometimes worsening over days or weeks as the ischemia continues, accompanied by painless edema of the optic disc (44). AION is typically caused by giant cell arteritis and results in severe visual damage, while NAION may stem from small-vessel disease in the nerve and some visual improvement within months is common (44-46).

Other insults affect other parts of the visual pathway. Optic neuritis, acute inflammation of the ON, is characterized by abrupt central vision loss and pain with eye movement. Most commonly associated with multiple sclerosis, patients often recover full vision but can progress to irreversible vision loss (44, 46). Interestingly, color vision loss is disproportionately affected in optic neuritis compared to ischemic optic neuropathies, suggesting different RGC populations may be affected in each (44). Traumatic optic neuropathy, while relatively rare, typically occurs following head injuries. It is severe and most often irreversible, similar to the optic nerve crush procedure utilized for laboratory studies (47). Besides head trauma, the ON can sustain acute physical damage as a result of tumors, compression, and infections (44, 46). Increased intracranial pressure can also cause optic neuropathy, for example in pseudotumor cerebri syndrome and space-flight associated neuro-ocular syndrome (48, 49). The pathophysiology in the traumatic situations, and quite likely all optic atrophies, is likely to be multifactorial, involving a primary injury followed by a response to this injury which further damages other axons (50, 51).

Several hereditary disorders also result in ON damage, including the mitochondria related Leber's hereditary optic neuropathy and various genetic dominant optic atrophies (52, 53). In addition, other common neurodegenerative diseases such as Alzheimer's disease, Parkinson's disease, and Huntington's Disease all appear to affect RGCs, quite possibly through axonal damage (54, 55). While treatment of these ideally addresses the underlying etiology, in principle they too might benefit from the ability to regrow axons.

In summary, RGC damage can result from many diseases, occur at various speeds and severities, and may even affect different RGCs subgroups. Unfortunately, once any significant damage to RGC axons has occurred, the RGCs will die, and no treatment currently exist to either

halt RGC death or initiate axonal regrowth. Importantly, as we describe below, the clinical window for neuroprotection and regeneration-based interventions is very limited, as they need to act after axonal damage but prior to RGC cell death.

Axonal Response to Injury in the Central Nervous System: A timeline

Understanding when to implement an axonal regeneration strategy clinically requires understanding the progression of degeneration after RGC axon injuries. Here we focus mainly on insight gained from the most widely used experimental models, those based on optic nerve crush (ONC) in rodents, though some insight derives from other models, including spinal cord injuries (noted below). ONC involves controlled crushing of the ON with forceps several millimeters behind the globe, where nearly all axons are myelinated, leaving the ON sheath and the vasculature supplying the ON intact (56). Though some degeneration mechanisms are context and injury dependent, as noted elsewhere (57, 58), most ON injury scenarios likely unfold through similar mechanisms to what is outlined here.

Milliseconds to hours after injury

Immediately following injury in both in-vivo spinal cord and neuronal cell culture models, calcium (Ca^{2+}) enters the injury site through voltage-gated calcium channels (59-61). An ex-vivo murine spinal cord model also found that Ca^{2+} is released from the axoplasmic reticulum, possibly contributing to a secondary degenerative signal (62). Removal of this extracellular Ca^{2+} by a chelator delays axonal degeneration (60, 61). Both astrocytes and retinal ganglion cells express several types of mechanosensitive TRP channels which mediate Ca2+ influx in response to pressure or stretch injuries (63, 64). Ca^{2+} influx may be dependent on

concurrent Na^+ entry in some types of injuries, and in a neuroinflammatory model the majority of Ca^{2+} enters instead through nanoruptures in the plasma membrane (59, 61). Importantly, live spinal cord imaging found that a "recoverable period" exists for hours after the initial insult; either Ca^{2+} clearance or nanorupture resolution protects axons from later swelling and degeneration (65). This increased Ca^{2+} activates calpains, ubiquitous cysteine proteases, mechanistically linking injury-induced calcium signaling to subsequent axonal degeneration by cytoskeletal degradation (66). Live-imaging of rat ON shows that within hours of injury, the axons swell and fragment on both sides of the injury (67). In murine spinal cord, the same fragmentation process can be completely blocked by calpain inhibitors (68).

First days after injury

At this point the proximal (closest to the eye) and distal axonal segments begin distinct degenerative processes. In both CNS and peripheral PNS axons, the distal axon segments fragment through a process called Wallerian degeneration (explained further below), in which the cytoskeleton is degenerated, the axon first forms swellings and then fragments into self-enclosed units, and the myelin disintegrates into elliptical structures (69, 70). The proximal axonal segment forms a retraction bulb, elliptical in shape and several times the axonal diameter. This bulb grows progressively larger over weeks as the axonal cytoskeleton depolymerizes and the axon dies back towards the soma (71, 72). The retraction bulb is the antithesis of the well-organized growth cones typical of developing or regenerating neurons. In a growth cone, actin structures (lamellipodia and filopodia) at the growing tip are separated from elongating microtubule "beams" by a clearly defined transitional zone (71). In contrast, studies on sciatic nerves found that retraction bulbs feature disorganized, mis-oriented microtubules and no clear

separation between microtubule and actin structures (72). Polymerization of both actin and microtubules are critical. Pharmacologic stabilization of microtubules promotes regeneration of CNS spinal cord neurons (72, 73). Additionally, combined knockdown in RGCs of two non-muscle myosin II isoforms (motor proteins involved in the movement and restructuring of actin, and normally present in the growth cone transitional zone) promoted marked regeneration persisting for weeks after injury (74). In murine spinal cord, while some axons attempt regeneration by neurite sprouting, these sprouts lack directionality, grow only a small distance past the injury site, and ultimately retract (68). Axonal transport of mitochondria also increases in the proximal stump of injured murine intercostal neurons, and this increase in mitochondria axonal localization may be important, at least it is so in *C. elegans* motor neuron regeneration (75, 76).

Around the first day after injury the cell's injury response machinery has already been triggered, and studies in sciatic neurons, motor neurons, and RGCs all found that similar molecular injury signals travel from the axonal injury site back to the soma (77-80). Infiltrating neutrophils arrive on the first day post-ONC and are reported to express at least one pro-regenerative factor, oncomodulin (81, 82).

The critical first week

In the first week following ONC the inflammatory response reaches its peak. Infiltrating monocyte-derived macrophages arrive at the optic nerve after the first day (83, 84). Of note, immunohistochemical classification of microglia vs. macrophages (and thus, their relative contributions) remains difficult, as macrophages take on a microglial-like molecular profile upon infiltration and activation in the CNS (85, 86); however, new retinal single-cell profiling

experiments have made huge strides in determining the full complement of different myeloid cells involved in injury responses (16). Astrocytes at the injury site in the ON degenerate by 3 days and begin to repopulate by day 7 (87). Optic nerve head astrocytes become reactive, losing many fine processes and shrinking in total area covered, but thickening both their soma and primary processes (88). Retinal microglia increase in number, presumably through proliferation (89). The retinal ganglion cell soma receives the signal that it has been damaged within the first week, and many stress responses are subsequently activated (78, 90, 91). Whether the RGC will die or regenerate is determined in that first week after injury, and this fate depends on various intrinsic and extrinsic factors, described next.

Response of RGCs to Axonal Damage: Intrinsic and Extrinsic Mechanisms

Upon receiving the axon injury signal, the cell eventually will either complete a self-destruction program or successfully regenerate its axons. As discussed below, these are related but separable processes. Both intrinsic (internal to the RGC) and extrinsic (mediated by other cell types) factors affect these two decisions, and as such, they will be discussed separately.

Intrinsic pathways

The fact that RGCs exhibit very different regrowth capacities at different developmental stages demonstrates the importance of intrinsic factors to RGC regeneration. When embryonic or post-natal hamster retinal explants were cultured with either embryonic or post-natal tectal explants, the embryonic retinas showed far greater neurite innervation into the tectal tissues, regardless of the tectal tissue age (92). Similarly, rat RGCs purified prior to birth show markedly greater neurite extension than those harvested after birth. Furthermore, amacrine-conditioned

media, but not bipolar conditioned media, converted embryonic retinal explants into a reduced-growth, postnatal-like state, suggesting that biochemical signals from amacrines may cause a postnatal "switch" in RGC regenerative ability (93). A molecular understanding of this innate programming is therefore critical. Interestingly, the innate programming of survival and regeneration appear to be controlled by at least partially distinct pathways, as discussed next.

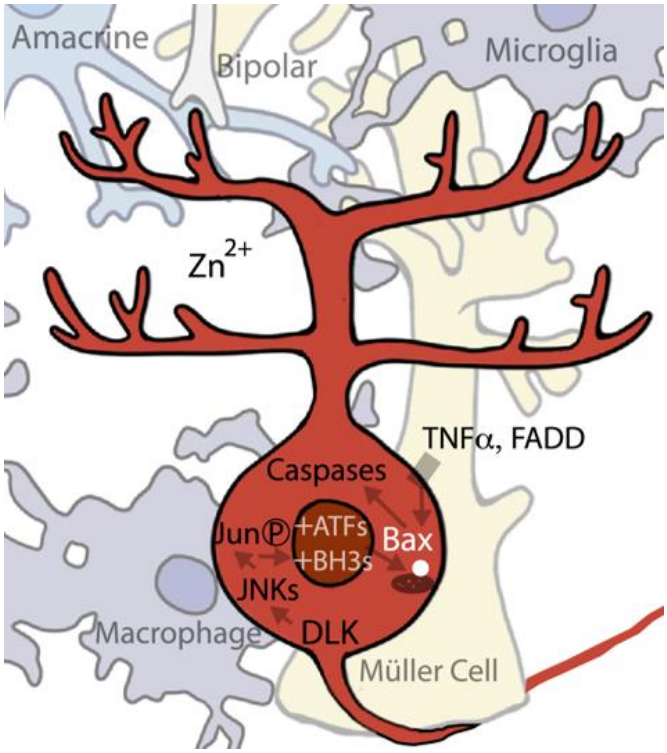

Figure 1.2. RGC cell death pathways. Both pathways internal to RGCs and factors released from surrounding cell types contribute to the apoptotic cell death of injured RGCs. The signaling protein DLK is produced in injured axons and transported back to the RGC cell soma. There, it activates the intrinsic Jun/JNK signaling pathway, which regulates key genes mediating the cellular injury response. Among these, Jun activates BH3 proteins, which then interact with the cell-death protein BAX, triggering BAX translocation to the mitochondrial outer membrane. This results in release of cell-death promoting molecules including cytochrome C, which ultimately activate the caspases. Jun also activates the ER stress signaling molecules, ATFs, which contribute to intrinsic apoptotic cell-death pathways. Meanwhile, external to the cell, high levels of zinc (Zn^{2+}) are released from amacrine cells, which synapse onto RGCs, contributing to RGC cell death. Additionally, the extrinsic apoptotic pathway is activated by the release of TNF-alpha, FADD, and other cell-death promoting molecules released from nearby Müller glia and microglia. Finally, RGC cellular decay exposes specific membrane components to the external environment, and these components act as an 'eat-me' signal to recruit activated microglia and macrophages, which invade and phagocytose dying cell membranes and organelles.

(From Fague, Liu and Marsh-Armstrong, 2021).

Intrinsic Pathways: Survival

BAX and the intrinsic apoptotic pathway

Some of the most powerfully neuroprotective measures characterized to date involve the

intrinsic apoptotic pathway, which triggers programmed cell death in response to injury or stress signals (reviewed in Syc-Mazurek 2020 (94), Maes 2017 (95)). The pathway was discovered when developmental *C. elegans* screens found several *ced* (cell death abnormal) genes. Absence of these genes resulted in complete loss of programmed cell death during development (96-98) Mammalian homologs to most *ced* genes have now been found, including *Ced-3*/caspase-9, *ced-4*/Apaf1 and *ced-9*/Bcl-2 (96, 99). Bcl-2 belongs to a large gene family which includes pro-apoptotic genes (e.g. Bax), anti-apoptotic genes (Bcl-2, Bcl-XL) and the BH3-only genes (95). Following ER stress or extracellular death signals, BH3-only proteins interact with Bax and mediate translocation and insertion of Bax into the mitochondrial outer membrane (95, 100, 101) (Figure 1.2). Bax-mediated membrane permeabilization triggers the mitochondrion to release pro-apoptotic factors including cytochrome c, which interacts with Apaf-1 to activate downstream caspases (cysteine protease effectors of cell death) (100, 102). In the retina, the balance between Bax and Bcl-2 mediates cell survival after injury. Overexpression of Bcl-2 is neuroprotective both during development and after ON injury (103). Conversely, Bax is pro-apoptotic, so its absence is protective. Nearly 90% of RGC somas survive in the mouse Bax knock-out up to 18 months following ONC, although in these mice, RGC-specific gene markers are downregulated, the cells atrophy, and the surviving cells no longer function electrophysiologically as RGCs (104-106). However, within 4-8 weeks of ONC, Bax knockout mice can still activate an apoptotic response if transfected with Bax, though this ability later disappears as the cells become entirely quiescent (106). These results show that RGC death can be slowed, thus offering the possibility of prolonging the therapeutic window for intervention.

DLK/LZK: A critical injury signal

While several pathways likely alert the soma of cell injury, among the most critical is a mitogen-activated protein kinase (MAPK) signaling cascade (107). MAPK cascades are diverse pathways that convey information to the cell in response to a wide range of extracellular signals (108). One of these cascades, the JNK (c-Jun N-terminal kinases) cascade, is triggered by dual leucine zipper kinase/leucine zipper kinase (DLK/LZK) signaling in response to axonal injury in both PNS and CNS neurons in mice (77, 78). In both *C. elegans* sensory neurons and murine RGCs, DLK/LZK are retrogradely transported from the axonal site of injury back to the soma, and the cascade (DLK > MAP2Ks > JNKs) ultimately phosphorylates the transcription factor Jun, which regulates key genes mediating the cellular injury response (78, 109). DLK also mediates the retrograde transport of other potential injury-signaling molecules, including Stat3 (signal transducers and activators of transcription 3)(77). Importantly, compared to WT animals, DLK knockout mice show far fewer gene expression changes post-injury, pointing to the importance of this signaling factor (78, 110). Along with Jun, profiling studies have placed DLK/LZK upstream of many transcription factors key to the fate of RGCs, including Klf6, Atf3, and Sox11 (78, 80). Also downstream of DLK and the JNK cascade are the endoplasmic reticulum (ER) stress response genes CHOP (official name: DDIT3) and Atf3 (activating transcription factor 3), and the intrinsic apoptotic pathway already described (BH3s > Bax > caspases) (78, 111-113). Atf3 is associated with stress response in both CNS and PNS tissues, and in the PNS, it has been linked to regenerative capacity (113). Atf3 and Atf4 are both upregulated following ON injury of various types (114, 115). Functional studies on these genes, however, have yielded nuanced results. While a dual JNK2/3 knockout protects from RGC cell death in the context of murine ONC, it does not offer similar protection in a mouse glaucoma

model (116, 117), though complete loss of all JNKs would likely have more pronounced effects (80, 94). There are many reasons why the JNK pathway may be more important in some types of injury. One is that there are other cell death pathways differentially activated by different types of injury. Autophagy, a program by which cells catabolize themselves, for example, can be activated by various insults, and can push towards or away from cell death, depending on the context. Autophagy-related genes (including ATGs and Lc3-II) are upregulated after ONC in mice (90, 118). Genetic deletion of ATG5 or ATG4 increases RGC death, and enhancement of autophagy via rapamycin decreased RGC death in a rat optic nerve transection model (118, 119). Importantly, though the DLK-initiated JNK cascade initiates cell death in mammalian RGCs, the same pathway also mediates the pro-regenerative response seen in both mammalian PNS and in *C. elegans* (110, 120). In both cases DLK also seems to mediate an increase in axonal transport of mitochondria to the injured proximal axonal segment, suggesting that increased metabolic capacity might be important for regeneration (75, 76). Thus, since the MAPK pathway is involved in both death and regenerative responses, it is believed to convey an injury "alert" to the soma, rather than directly determining whether a cell dies or regenerates.

Axonal and somal death mechanisms are separable: WLDs and NMAT

While both somal and axonal loss occur in the same injured neurons, distinct mechanisms control the self-destruction of cell bodies and their still-connected proximal axonal segments versus the distal disconnected side of axons. For example, BAX itself, while highly protective to the RGC soma, is only slightly neuroprotective of the distal axon segments (94, 121). Much of the understanding of the axonal-specific degeneration comes from study of a mouse mutant termed Wallerian Degeneration Slow (WLDs), which exhibits a tenfold delay in axon

degeneration, accompanied by delayed macrophage recruitment, and delayed clearance of axon and myelin debris. However, WLDs mice display no somal protection in acute injury and variable protection in glaucoma models (70, 122-124), demonstrating (like the Bax results) that somal and axonal self-destruction programs are distinct. WLDs is a fusion of the NMAT1 gene with the ubiquitin ligase UBE4B (125, 126). All NMAT isoforms catalyze NAD+ synthesis, and overexpression of any NMAT isoform, or other enzymes that make NAD+, delays axonal degeneration (70). Typically, both Nmat2 and NAD+ levels are rapidly depleted following an injury, but WLDs protects from this NAD+ depletion (127) (128). As such, the current model holds that the WLDs fusion protein substitutes for the rapidly-lost Nmat2 to confer axonal neuroprotection (reviewed in (70)). The toll-like receptor adaptor protein Sarm1 (sterile alpha and TIR motif containing 1) has also been linked to Wallerian degeneration, and it degrades NAD+ (129). Activation of Sarm1 promotes axonal degeneration, and deletion protects axons (but not somas) from degeneration after murine ONC (130, 131) Interestingly, inhibiting DLK increases axonal Nmat2 and is thus also neuroprotective of axons; in fact, an in-vitro mouse sensory neuronal model found that DLK may contribute to degradation of both Nmat2 and Scg10 (132, 133). Scg10 (superior cervical ganglion 10) is a microtubule-binding protein which loses its affinity for tubulin when phosphorylated by JNK. In vitro models have also linked Scg10 expression to both axonal protection and preservation of mitochondrial transport (134). Taken together, these data suggest that the crosstalk between Nmat2, Sarm1 and the MAP3Ks are key determinants of whether axons degenerate or not, and are thus highly promising targets for neuroprotective strategies, as reviewed in (135) . However, since it is still unclear whether WLDs itself affects regeneration (136), it remains to be seen whether any of these genes are good targets for neuroregenerative interventions.

Intrinsic Mechanisms: Regeneration

While the axonal injury signal – namely the MAPK (JNK) cascade initiated by DLK and culminating on the phosphorylation of Jun – initiates the decision between cell death or regeneration, distinct molecular pathways control those processes. Several of the most prominent known regenerative mechanisms are discussed below.

Jak/Stat pathway

The Janus kinase/signal transducers of transcription (Jak/Stat) pathway is activated by the binding of extracellular ligands (growth factors, cytokines, and others) and culminates in various Stats binding to specific DNA sequences to alter gene expression (137). Of the four Jak and seven Stat genes found in mammals, Stat3 seems to be particularly critical for regulation of regeneration. AAV-mediated expression of Stat3 in RGCs promotes axonal

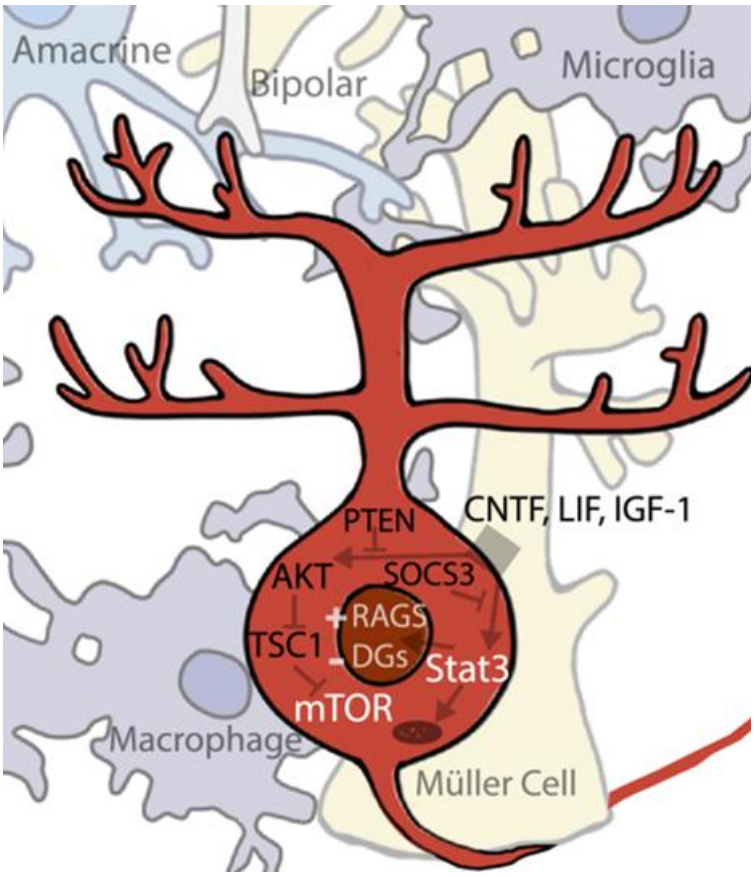

Figure 1.3. **RGC regeneration pathways**. Successful axonal regeneration involves both RGC-intrinsic pathways and factors derived from surrounding cell types. Within RGCs, activation of the mTOR and STAT3 pathways both stimulate axonal regrowth. The mTOR pathway is inhibited by AKT, TSC1, and PTEN, and removal of any of those three genes stimulates pathway activation and regeneration. The STAT3 signaling pathway is partly activated by external factors, including the neurotrophins CNTF, LIF, and IGF-1, all secreted from cells near the RGCs (Müller glia, microglia, and monocyte-derived macrophages). Either application of these neurotrophins, removal of SOCS3 (a Stat3 inhibitor), or other methods of activating the Stat3 signaling pathway induces regeneration. Activated Stat3 localizes to both nucleus and mitochondria and is known to stimulate downstream gene expression changes in the nucleus. Also intrinsic to RGCs, a de-differentiation event occurs involving downregulation of differentiating genes (DGs) and upregulation of regeneration-associated genes (RAGs), involving diverse transcription factors which reprogram RGCs to a growth-capable state.

(From Fague, Liu and Marsh-Armstrong, 2021).

regeneration (138). The growth factor CNTF, among the most potent pro-regenerative stimuli, works in part by activation of Jak/Stat3. CNTF upregulation coincides with Stat3 upregulation, and direct CNTF application to RGCS in vitro activates the Stat3 pathway (Figure 1.3) (139, 140). A long-established observation that inflammatory stimulation, such as that induced by lens injury, is pro-regenerative (141), was eventually connected to IL-6 family cytokines CNTF and LIF, both of which signal through Stat3 (142). Conditional deletion of Socs3, a Jak/Stat negative inhibitor, results in an increase in ON regeneration (143). The Kruppel-like signaling factors (Klfs), transcription factors that regulate the regenerative response, also affect Jak/Stat signaling (144, 145). However, how activation of Jak/Stat3 affects regeneration is not fully understood, but it probably regulates multiple processes. In addition to its own direct modulation of gene expression, Stat3 interacts with c-Jun (downstream of the MAPK (JNK) cascade initiated by DLK) and potentially other transcription factors as well (146, 147). However, there are also some non-nuclear mechanisms through which Stat3 might also affect regeneration. For example, cytoplasmic Stat3 inhibits autophagy in-vitro, (148) and in both cortical neurons and RGCs, it localizes to mitochondria in addition to nuclei, though the significance of this mitochondrial localization is not yet well understood (149). The robustness of the RGC response to CNTF has led to several clinical trials involving CNTF-secreting implants in various retinal diseases. The most promising has been trials involving macular telangiectasia, which have advanced into a current Phase 3 trial; studies of the same implant in glaucoma patients are also ongoing (NCT04577300, NCT02862938).

PI3K/AKT/mTOR

The other pathway known to be critical for the regulation of regeneration is the mammalian target of rapamycin (mTOR) pathway, a node regulating key cellular processes such as translation and metabolism (150). Upregulation of the mTOR pathway has been found to stimulate regeneration in RGCs, though the results are complex. Activation of PI3K by CNTF/LIF may stimulate the pathway in inflammatory retinal injuries, signaling downstream through AKT onto mTOR (140). IGF-1, another growth factor which signals through P13K/AKT, is downregulated after ONC in rat, and IGF-1 application to the rat retina increases neurite outgrowth (151). Deletion of a negative inhibitor of the mTOR pathway, PTEN (phosphatase and tensin homolog), stimulates one of the most significant RGC regenerative responses seen to date, and deletion of a second negative inhibitor, TSC1 (tuberous sclerosis 1), is almost as effective (152, 153). Similarly, pharmacological inhibition of mTOR by rapamycin inhibits inflammation-induced long-distance RGC axonal regeneration *in vivo* (154). Interestingly, downregulation of mTOR has also been linked to dendrite degeneration and retraction, another physiological effect of RGC injury, and insulin application activates the mTOR pathway to promotes robust dendritic regrowth (155). Several clinical studies have targeted the mTOR pathway by various means. Despite one study which was able to increase plasma IGF-l levels in patients, a second study did not find any benefit to IGF-1 injection in ALS patients (NCT00871455, NCT00035815). Another currently active study is testing oral administration of the mTOR inhibitor rapamycin, also in ALS patients (NCT03359538).

Reprogramming factors

A long-standing question regarding regeneration is whether reversion of cells to a fully or partially de-differentiated state is a necessary precursor to regrowth. Two potent transcription

factors, c-MYC and its target P53, are upregulated in successful PNS regeneration, and promote axonal regeneration when overexpressed in CNS neurons, including RGCs (156, 157). As previously mentioned, certain members of the KLF transcription factors are pro-regenerative, while others, including KLF4, seem to act as transcriptional repressors of RGC axon growth (144). Notably, both c-MYC and KLF4 are among the original Yamanaka factors discovered to induce pluripotency by de-differentiating mouse adult fibroblasts (158). Recently, viral-based induction of OCT4, SOX2, and KLF4 (three of the four Yamanaka factors) has been shown to stimulate axonal regrowth and to promote a "youthful" mRNA profile in the treated eyes (159). Another gene that can broadly induce cellular reprogramming, Lin28, an RNA-binding protein that regulates microRNA processing, is typically expressed in undifferentiated cells and thus seems to be a marker of "stem-ness" (160, 161). Lin28 too is upregulated in regenerating PNS neurons after injury, and overexpression of Lin28 in the murine retina enhances regeneration (74, 162), perhaps in an amacrine-dependent manner which enhances RGC responsiveness to IGF (163). The potency of these reprogramming factors in inducing regeneration, coupled to RGC down-regulation of many genes and functions associated with a fully differentiated state, suggest that RGC regeneration may require partial de-differentiation into a more stem-like state. One possibility is that the injury signal conveyed from the axon, mediated by the MAPK (JNK) cascade initiated by DLK, provides such a signal to de-differentiate. Whether that reprogramming leads to death or regeneration, then, might be mediated by the right balance of mTOR and Jak/Stat pathways together with the inhibition of the cell-death pathways.

Combinatorial approaches: successes and challenges

Unless there is a major conceptual breakthrough, combinatorial approaches will almost certainly be necessary for clinically meaningful regeneration. Indeed, such combination treatments often result in improved regrowth in the mouse ONC model. Some examples include: 1) Conditional deletion of both SOCS3 and PTEN enhances regrowth above single deletion of either gene (152); 2) Intraocular application of CNTF yields only limited regeneration, but SOCS3 deletion plus CNTF application strongly increases regrowth (143). 3) Expression of c-MYC, viral-mediated CNTF expression, and dual PTEN/SOCS3 conditional deletion promotes the most extensive axonal growth seen to date even past the optic chiasm for some axons (164, 165) although still a small percentage of all RGCs. 4) Combined lens injury and PTEN deletion allowed for limited brain re-innervation and even reported partial recovery of visually guided behaviors (165, 166). However, sometimes factors improve either survival or regeneration, but inhibit the other – creating a push-pull effect in combinatorial interventions. Some examples of this are as follows. 1) In a conditional PTEN/DLK dual knockdown model, RGC survival was increased but regrowth was decreased compared to a PTEN knockout alone (78). 2) Lens injury combined with BDNF administration enhanced survival but decreased regeneration compared to a lens-injury paradigm alone (167). Such situations illustrate the need to understand not only the role of individual pathways, but the crosstalk between them as well.

RGC heterogeneity and regeneration

As mentioned earlier, RGCs exhibit significant heterogeneity, with over 40 subtypes currently recognized in mice. Different RGCs display different sizes, respond to either increases or decreases in light or motion, receive their innervation at different sub-lamina of the inner plexiform layer, and innervate many different regions of the brain (25, 168). Thus, any

translational strategy should take into consideration the heterogeneity of RGCs and their effects on vision. Translational strategies should also take into consideration that the targets of RGC axons also likely atrophy and re-wire after the degeneration of RGCs (169). Importantly, the vast majority of mouse RGC subtypes have not yet been identified in human or nonhuman primate retinas, though there are a few exceptions (170, 171).

Recent work has made it clear that RGC subtypes respond differently to both injury and regenerative therapies. Two weeks following ONC, some subtypes survive nearly completely, while others are decimated (172). Regarding regeneration, the mouse alpha-RGCs regenerate more successfully in response to PTEN deletion than other subtypes, in large part because of their responsiveness to osteopontin and IGF (173), but those same cells are preferentially killed by Sox11 overexpression, which promotes regeneration of a different RGC subtype (174). Unfortunately, no individual molecular characteristic seems to confer regenerative capacity, and genes which promote survival in one subtype do not reliably translate to other subtypes (172). Interestingly, different RGC subtypes also respond differently to the effect of visual stimulation on regeneration. Subjecting ONC-lesioned mice daily to a high-contrast visual stimulus for several weeks post-injury increases regeneration of alpha-RGCs. Visual stimulus appears to enhance the effect of mTOR pathway elevation, and strikingly, also results in limited target-specific reinnervation of visual targets in the brain and return of simple visual responses, though not the image-forming functions we typically refer to as “vision” (175).

This differential response of RGCs can be viewed either as a positive or a negative. Understanding the differential regenerative response of different mouse RGCs may lead to new genes and pathways to affect regeneration. However, it is difficult to understand how to translate mouse studies to humans, since mice do not appear the have clear midget and parasol RGCs,

corresponding to the parvo- and magno-cellular visual streams, which constitute the grand majority of RGCs of primates, including humans (24, 176, 177). Differential responses of RGCs also make it likely that any simple intervention will have an effect only on some types of RGCs, and may even be deleterious to others. This is yet another reason why we need to understand how is it that some species regenerate all their RGCs (discussed below).

Extrinsic Factors

The intrinsic ability of RGCs to survive insult and regenerate (or not) represents just one piece of the puzzle. Neighboring cells, including astrocytes, Müller glia, microglia, and infiltrating myeloid cells, also play crucial roles. Often, these cells affect both survival and regeneration, and here are discussed separately based on their location, whether those cells affect RGC somas and proximal parts of axons in the retina or their axons in the optic nerve.

Extrinsic Factors: Retina Neurons and Glia

RGCs receive chemical and electrical synaptic inputs from both amacrine and bipolar cells, and recent work suggests that these interactions play a role in the decision as to die or regenerate. For one, amacrine and bipolar input are prime candidates to mediate the light-driven promotion of RGC regeneration (175), though, in principle this effect could be mediated by light-sensing molecules within RGCs (for example, melanopsin or chryptochromes). Another study, however, found that synapses onto RGCs are deleterious. Levels of Zn^{2+} increase in the inner plexiform layer (where amacrines synapse onto RGCs) within 1 day after injury, and is transferred to RGCs by 2-3 days, and this Zn^{2+} elevation negatively affects RGC survival (178). It also remains possible that glutamate excitotoxity contributes to RGC death, though this is no

longer considered the central mechanism of cell death as it once was (179). That the one major RGC neuroprotective clinical trial to take place, which did not reach its end-points (NCT00168350), was based on what is now considered a flawed premise (glutamate excitotoxity as the key driver of RGC death), highlights how much our understanding of RGC's response to injury has evolved in recent years.

In addition to these neuronal connections synapsing with RGCs, two major glial populations, Müller glia and astrocytes, enwrap RGCs and their axons and are a critical source of extrinsic signaling regulating both survival and regeneration. Like the intrinsic pathway previously discussed, the extrinsic apoptotic pathway ultimately converges on caspases which dismantle the cell, but is instead activated by extracellular ligands, including the Fas-associated death domain protein (FADD) and tumor necrosis factor alpha (TNFα) (Figure 1.2) (102, 180). Application of TNFα results in both oligodendrocyte degeneration and RGC death (181). Interestingly, TNFα is upregulated in human glaucoma patients, and in a rat glaucoma model, and Müller glia and microglia/macrophages secrete TNFα upon ocular hypertensive stress (182). Inhibition of either TNFα directly or the calcium-permeable AMPAR receptors, which TNFα typically traffics to the membrane, resulted in substantially improved RGC survival (183).

RGCs also express receptors for many neurotrophins, small trophic factors involved in synapse formation, growth, differentiation, and proliferation within the CNS (184). Of these, BDNF is an astrocyte-secreted factor which is neuroprotective of both RGC axons and soma but does not affect axonal regeneration (167) (185). Transfection of Müller cells with a BDNF encoding construct induced them to secrete BDNF and protected RGCs (186). Interestingly, transport of BDNF to the soma is impaired in several glaucoma mouse models (187) (188). Additionally, the IL-6 family cytokines CNTF and LIF are produced as part of the inflammatory

response to injury by retinal astrocytes, activated microglia, and Müller glia cells in various retinal/axonal injury models. Notably, of all the trophic factors, CNTF/LIF, are the only ones that confer both neuroprotection and axonal pro-regeneration effects on RGCs (139, 140, 189).

Extrinsic factors: Optic Nerve Glia

Unlike CNS neurons, PNS nerves regrow and form functional synapses after injury; and Schwann cells, the myelinating cells of the PNS, are critical to this regeneration (7). Upon injury, Schwann cells de-differentiate into a progenitor-like state with repair-promoting characteristics including neurotrophic factor secretion, proliferation, and debris clearance (190). One of the earliest, and to date most effective, ON regeneration experiments was insertion of a peripheral nerve graft into the region of an ON transection, first done by Ramón y Cajal (191). This crude surgery allows RGCs not only to successfully regrow through the graft, but also to re-innervate central brain targets and even lead to partial restoration of visual function (192-194). While this may somewhat be due to pro-regenerative trophic factors within the graft, it is widely accepted that the CNS environment also actively inhibits regeneration.

In the CNS, it is oligodendrocytes that myelinate axons, and oligodendrocyte-derived myelin blocks regeneration (195). This inhibition is mediated by multiple myelin proteins, including membrane-associated glycoprotein (MAG), Nogo, and oligodendrocyte-myelin glycoprotein (OMgp) – all of which signal through the RGC-expressed NogoR receptor (196-201). While NogoR modulation increases optic nerve regeneration in various paradigms, the results are complex. By itself, viral-mediated NogoR knockdown in the ON is minimally effective; combined with lens injury, it evokes markedly stronger regeneration, and when all 3 isoforms of NogoR are genetically eliminated, moderate regeneration occurs after ONC even

without other interventions (202, 203). Recently, however, a clinical trial testing a NogoR antibody in spinal cord injury (SCI) found good tolerability but no functional recovery in para- or tetraplegic patients (204). Despite this, trials on this particular drug are continuing (NCT0393532). Another trial in SCI patients testing a soluble protein "decoy" or "trap"' which sequesters MAG, Nogo, and OMgp is also underway (NCT03989440).

In addition to CNS myelin inhibition, the ON environment itself becomes regeneration-prohibitive following injury through formation of a glial scar. Astrocytes within the ON lose their ramified morphology, become proliferative and phagocytic, and secrete many extracellular matrix proteins that form a unique and disorganized matrix (205). Together with infiltrating non-resident macrophages (discussed next), a buildup of tissue forms which replaces the dying RGC axons within the ON. This glial scar produces various proteins which inhibit RGC regrowth, including ephrins and chondroitin-sulfate proteoglycans (CSPGs) (206, 207). Degrading these CSPG glycosaminoglycan chains enhances axonal regrowth, at least in a spinal cord injury model (208). However, other data suggests the glial scar may not inhibit CNS regeneration at all. In fact, inhibiting the formation of the glial scar was detrimental to spontaneous regrowth in a mouse SCI model (209).

Both glial-scar signaling and myelin/NogoR-associated inhibition ultimately converge on RhoA (ras-homolog gene A), which binds to its receptor ROCK (Rho-associated protein kinase) and mediates actin cytoskeleton decay and growth cone collapse (210, 211). Since many extrinsic inhibitory factors converge on RhoA/ROCK, several studies, including some clinical trials on a range of neurodegenerative diseases or injuries, have targeted them directly. The results have been mixed. RhoA inhibition resulted in modest axon outgrowth post-injury both *in vitro* and *in vivo*; the effect was greatly increased when combined with lens injury (212) (213).

An active study is investigating the potential of the ROCK inhibitor fasudil to improve outcomes in ALS patients (NCT03792490). On the other hand, in late 2018 a clinical trial testing a third Rho inhibitor in spinal cord injury patients was halted due to futility (NCT02669849). Overall, blocking extrinsic inhibitory effects will likely need to be combined with the promotion of intrinsic pro-regenerative states in order to achieve clinically relevant results.

Extrinsic Factors: Inflammatory cells

The same *C. elegans* developmental screens which discovered the intrinsic apoptotic *ced* pathway genes also discovered several extrinsic *ced* genes which mediate engulfment of apoptotic cells (97, 214). Though *C. elegans* lacks professional (macrophage-like) phagocytes, many extrinsic *ced* genes expressed by engulfing cells in *C. elegans* have orthologs in mammalian phagocytes (215). Two of these are *ced-7*/ABCA1 and *ced-1*/Megf10. *Ced-7* is a cholesterol transporter expressed in both dying and engulfing cells, and loss of *ced-7* in either cell type completely blocks engulfment (214). *ced-1/*Megf10 is a receptor expressed by the infiltrating macrophages that arrive to phagocytose cellular debris (216) (217). Exposed phosphatidylserine molecules, and other cellular components found on the inside of healthy cells, become externalized onto the surface of apoptotic cells, and act as a phagocytic "eat-me" signals which can then be bound by a variety of proteins including ced-1/Megf10, annexin-5, and Mfge8 (215, 217, 218). Indeed, there are trials ongoing to use labeled annexin-5 to visualize dying RGCs, though the broad utility of this method is yet to be determined (219, 220).

Microglia, the myeloid cells that reside within CNS tissues including retina and optic nerve, proliferate following injury (87). Microglia are capable of rapid activation in response to many extracellular changes (13). During development and injury microglia selectively prune

synaptic connections, and after injury, activated microglia become phagocytic and clear RGC debris (221, 222). There is currently lack of consensus as to whether microglia are more beneficial versus harmful after injury, and the answer is likely to be context dependent. In one study, microglia were neuroprotective *during* a prolonged lesion, but microglial presence *following* the injury hindered recovery (223). Suppression of microglial activation using minocycline treatment increased RGC survival in both optic nerve transection and glaucoma murine models (224, 225). However, another study suggested that microglia are not critical for ON degeneration or regeneration (226). The difference may lie in a very specific balance of cytokines and chemokines secreted by activated microglia under different stimuli, but much more work is needed to determine whether these cells are good targets for pro-regenerative interventions (84). In fact, different states and stages of activation, varied molecular mediators, and extensive crosstalk between cell types are characteristic of all inflammatory cells; for a comprehensive review of the inflammatory response to injury in the ON, the reader is referred to Andries et. al. 2020 (84).

Learning from the Peripheral Nervous System: Regeneration is Possible

For reasons that are not fully understood, the peripheral nervous system (PNS) retains some ability to regenerate and heal injuries throughout the animal's lifetime. One possibility, as mentioned earlier, is due to the different cell populations which myelinate CNS and PNS neurons. Though both the central and peripheral nervous system neurons are encased in a myelin sheath, the cells responsible for this myelination are different. Oligodendrocytes, which derive from the ventral neuroepithelium of the neural tube, myelinate the neurons of the central nervous system, while Schwann cells derived from the neural crest myelinate peripheral nervous system

axons (4, 227). Schwann cells, in addition to forming the membranous wraps which become the myelin segments along the nerve analogous to the process followed by oligodendrocytes, also create a basal lamina which separates the intraneural space from the myelination layer. Whether because of this lineage difference or some as-yet unknown factor, the Schwann cells react very differently than do oligodendrocytes in response to axonal injury. However, the difference in the injury response of the myelinating cells is not the only distinction between CNS and PNS neurons. Here we will give a brief overview of the events following PNS nerve injury to highlight these differences.

Following axonal injury to a peripheral nerve, the axon undergoes Wallerian degeneration at the injury site, breaking up into small fragments within 1 day of injury just as CNS neurons do. In the week following injury, the myelin sheath surrounding the nerve has also disintegrated into regular ovoid-shaped accumulations and can continue to be cleared chemically from the nerve proper for 1-2 weeks longer (228). Similarly to what occurs in the CNS, by 2 to 3 days post-injury macrophages arrive and proliferate within the nerve to phagocytose the large amount of axoplasmic and myelin debris generated by the degenerating nerve. Unlike in the CNS, the myelinating Schwann cells are also phagocytic and contribute to this rapid clearance of debris (7, 229). At the same time these Schwann cells, which normally also maintain a basal lamina between the myelination and the axons of the nerve, form a tube which creates a barrier between the disintegrating myelin and the intraneural space (4, 7, 229). Neurite sprouting begins at the proximal stump of the injured nerve as early as day 3, and begin to regrow through this space, eventually reconnecting with their targets and reforming connections. Though the mechanism is not fully understood, it has therefore often been suggested that these multiple

functions of the Schwann cells may be critical for peripheral nervous system regeneration and represent a major difference between CNS mechanisms of regeneration (7, 228, 230).

Beyond the difference in response of the myelinating cells, the ability of the PNS to regenerate seems also at least partially dependent upon the activation of intrinsic regeneration-associated factors within RGCs. Sequencing studies have found that lesioned PNS neurons upregulate several genes associated with regenerative capacity, including cJun, ATF3 and Sox11 (230). Intracellular levels of cyclic adenosine monophosphate (cAMP) also increase following peripheral nerve lesion, and injection of cAMP into peripheral nerves has been shown to stimulate nerve growth (7). In addition to signaling molecules such as these, the induction of enzymes and pathways which promote the production of growth-associated proteins, cytoskeletal components, lipids, energy molecules, and axonal transport molecules begins soon after injury to initiate and support the regrowing axon (231). Cell-adhesion molecules and proteins which mediate interaction of the regenerating axon with the surrounding cytoskeletal components have also been found to be upregulated following injury in regenerating peripheral neurons, suggesting that extracellular mechanisms may be important for axonal regrowth in these contexts (231). However, some of these same signaling molecules and proteins are also upregulated in CNS neurons following injury; why this then leads to axonal death in the CNS and axonal regeneration in the PNS is not fully understood (232). Further work will be needed to understand how all of these factors contribute to peripheral nerve regeneration, and how these lessons might be applied to the CNS.

Learning from Regenerative Species

Unlike mammals, other vertebrates possess extraordinary natural regenerative abilities. Two of the more common models used in biomedical research, *Danio rerio* (zebrafish) and *Xenopus laevis* (African clawed frogs), display both compelling similarities and notable differences in their response to axon injury relative to mammals. Given the conservation of retina structure, including all the major cell types in retina and optic nerve, and the high genomic conservation between humans and these species (84% and 79% of known human disease-associated genes have a zebrafish and *Xenopus* homologues, respectively), attaining clinically-relevant regeneration in human RGCs may depend on our first understanding the successful regenerative programs of these other species (233, 234). These species' ability to achieve regeneration is likely a combination of multiple pathways in multiple cells all deployed at the right time, as would be expected for processes maintained through selective pressure.

Time to regrow

Functional studies assessing regeneration in teleosts and amphibians date back to the mid-twentieth century (235-237). Some dismiss studies of regeneration in these species because their retinas include a ciliary marginal zone of cells which continue to divide and differentiate throughout the animal's lifetime, enabling the eye to grow with age (238, 239), and because these species can regenerate all retina cell types after severe injuries from either Muller cells in zebrafish or retinal pigment epithelial cells in Xenopus (240-244), features not present in mammals. These retina regeneration mechanisms notwithstanding, however, most axonal regeneration after ON injury in both species comes from regeneration of existing RGCs, not by the generation of new cells (245). In fact, in fish and frog 20-25% of RGCs do die after axon injury, like their mammalian counterparts; but the remainder survive and regrow their axons

(246) (245). Regrowth begins anywhere from days to weeks post-injury and re-innervation of brain targets occurs within weeks to months, depending on the size of the animals (247-251). While there are likely to be differences not translatable to humans, including some genes carried by these species which are absent in humans, exploring these naturally regenerative RGCs could yield enormous insight.

Morphological/anatomical comparison of post-injury response in mammals versus fish and frogs

The initial progression of axonal injury occurs in *X. laevis* as it does in mammals: the distal axonal segment undergoes Wallerian degeneration, the proximal segment forms a retraction bulb which progressively degenerates towards the soma, and full brain denervation occurs (250, 252). Two weeks following injury, the proximal stump shows near-complete demyelination, advanced degeneration of remaining axons, and major changes to the glial and astrocytic architecture. However, distinct growth cones have re-formed within the demyelinated fibers within weeks following injury, and fully regrown axons are largely re-myelinated and have successfully re-innervated their brain targets within months (252).

Interestingly, in both fish and frog, regenerating RGC axons make many pathfinding mistakes (253) and when the regenerating fibers initially reach their general target locations in the brain they do not exhibit precise connection patterns (254, 255). The initial retinotopic "map" then undergoes an activity-dependent refinement process which recalls the developmental process of synaptic refinement (256, 257). Also importantly, both mammalian and fish neurons can regrow *in vitro* alongside either fish oligodendrocytes or fish-conditioned media, indicative of a growth-permissive ON environment in these species and underscoring the importance of tracing the contributions of individual cell types within the optic nerve (258).

Perhaps most telling are the classic eye rotation experiments by Roger Sperry that formed the basis of the chemo-affinity hypothesis for neuronal connectivity. When the optic nerve of a newt was transected and the eye rotated 180 degrees, full reinnervation and return of visual function was still achieved, but visual field perception was also exactly rotated (253). This demonstrated that individual RGCs are imprinted developmentally to recognize their specific brain target – and that even when disconnected, they "recall" that location and can return to it. Since similar spatial identity exists in mammals, it renders the quest for regenerative axonal therapies even more urgent, as stem-cell derived RGC transplants may not have the innate 'foreknowledge' of their desired innervation target, posing yet another barrier to clinical deployment.

Molecular comparison of post-injury response in mammals versus fish and frogs

Molecular profiling studies have found regulated pathways after ONC to be largely similar between mammals and pro-regenerative species, but there are also some striking differences. In the ER stress response pathway, Atf3 is strongly upregulated in fish, frogs, and mice, and ddit3/CHOP, Atf4, and a putative downstream gene Chac1 are upregulated in frogs and mice (114, 250, 259). Additionally, c-Jun, upstream of several apoptotic pathways, is highly upregulated in both frogs and mice. However, most other canonical apoptotic players showed no change in frog profiling data (250). Another study revealed that inactivation of CDC42, Rac1, and RhoA by a Wnt-signaling mechanism functions early on in zebrafish optic nerve regeneration, suggesting that de-inhibitory signaling may be as critical as activation of growth machinery (260). Many transcription factor families also show major changes after injury. As aforementioned, Sox11a/b (related to the reprogramming transcription factor Sox2) has been

studied as a pro-regenerative factor in mice, and is markedly increased after injury in both frogs and zebrafish (250, 259). Klf6 and Klf7 are upregulated in RGC-specific profiling studies in zebrafish and *X. laevis* (250, 259) and in mammalian (mouse/rat) retinal profiling studies (114, 115). However, in zebrafish, Sox11a/b knockdown had no effect, and only combined knockdown of Klf6a and Klf7a decreased neurite outgrowth in retinal explants (259). Clearly, functional studies will be required to validate the role of any gene discovered via profiling methods. Work in *Xenopus* found a specific RNA-binding protein was required for optic nerve regeneration, suggesting that post-transcriptional regulation of specific programs may also be critical (246). More recently, several interesting connections between transcription factor binding sites and chromatin accessibility have been discovered in zebrafish; the question of epigenetic mechanisms of regenerative control certainly deserve further exploration (261).

One interesting example of species differences is SOCS3, a negative Jak/Stat inhibitor which enhances regrowth when inhibited in mammalian systems. However, in *Xenopus* and zebrafish, SOCS3 levels increase after injury (250). Additionally, in zebrafish retinal explants knockdown of SOCS3 did not affect neurite outgrowth (259). One study investigated this finding further and found that though SOCS3 mRNA levels were increased in RGCs post-injury, protein levels were increased in axons only. However, both mRNA and protein levels of SOCS2, which degrades SOCS3, were increased in the soma but *not* in axons – all of which suggests that spatial regulation of various signaling factors (in this case, restriction of SOCS3 by SOCS2 to axons-only post-injury) may be as important for regeneration as the presence or absence of the factors themselves (262).

Future directions

In his book *The Abolition of Man,* C.S. Lewis proposed a new Natural Philosophy – one which, "when it explained, it would not explain away. When it spoke of the parts, it would remember the whole" (263). Such has been the intent of this review. The problem of ON regeneration is multifaceted and complex. Regeneration at its core is a race to regrow axons prior to soma death; and both regrowth and survival involve many cell types exerting multiple effects on the overall outcome. Though every contributing element will need to be understood separately, chances are that multiple of them will need to be addressed together for any intervention to be successful clinically.

Clinically, the narrow window between nerve damage and soma death means that acute and traumatic ON injury such as TBI would require immediate treatment initiation. Prolonged, asynchronized neurodegenerative processes such as glaucoma present a longer clinical window, potentially optimal for chronic pro-regenerative therapies. However, the still-unclear pathophysiology of glaucoma, slow progression and sub-optimal means of tracking disease progression, make it a sub-optimal candidate for RGC regeneration clinical trials, which are better conducted in acute scenarios. In addition, different types of diseases may end up requiring different types of therapies. Those which strike at the ONH, such as ischemic optic neuropathies and glaucoma, may need additional strategies to deal with a restructured optic nerve head and lamina cribosa or constricted vasculature; and congenital disorders which affect mitochondria may never be successful unless the underlying mitochondrial dysfunction is addressed concurrent to administration of axonal regrowth therapies.

Regenerative experiments habitually report success by distances or numbers of regenerating axons. However, the only clinically meaningful measure is restoration of visual function. By any metric, no experimental treatment in mammals to date has achieved much

success. A truly successful intervention will likely require understanding what evolution has deemed necessary for the process, information that can only be gained from studying species with intrinsic regenerative capacity. Such understanding could hold the key to finally creating functionally significant regeneration in mammals. Using these insights to achieve success in optic axonal regeneration will not only enable life-altering improvements for millions of vision-impaired patients, but would also likely lead to treatments for a wide range of other diseases and injuries to the CNS.

Chapter II: Novel Live Imaging-Based Assay in *Xenopus laevis* Tadpoles Shows that Dual Leucine Zipper Kinase is Necessary for Retinal Ganglion Cell Axonal Regeneration

Introduction

In mammalian species, the central nervous system (CNS) is incapable of axonal regeneration, and injury to axons typically results in not only the rapid degeneration of the injured axons but also subsequent cell death. As the visual system comprises part of the CNS, optic neuropathies which affect the axons of retinal ganglion cells (RGCs), the sole projecting neurons of the eye, eventually result in partial or complete irreversible vision loss. In acute situations of traumatic brain injury (TBI) or ischemic optic neuropathies (e.g. NAION or AION), this vision loss can occur very quickly, over days or weeks (47, 264, 265). In more chronic optic neuropathies such as glaucoma, which remains the leading cause of irreversible blindness worldwide, insult to RGC axons is more focal and asynchronous, resulting in vision loss which is asymmetric and progressive, unfolding over many years (33, 34). In both the acute and chronic blinding diseases, once the RGC axonal injury has occurred, no neuroprotective therapy yet exists to preserve or regenerate the RGCs and their axons.

By contrast, many non-amniotic species possess the ability to regenerate injured RGC axons, successfully reinnervate appropriate brain targets, and regain functional vision. Roger Sperry's classic eye rotation experiments in newts (266) and forced nerve uncrossing experiments in anuran amphibian species (267) long ago showed that fully disconnected RGC cell axons are able to reconnect and drive visually driven behaviors. Given that the genome of *Xenopus laevis* bears significant sequence identity to that of humans (79% of disease-causing genes in humans have clear homologues in *Xenopus* (233, 268)), it is likely that the molecular

pathways responsible for the RGC axonal regeneration of anurans remains extant in the human genome. As such, understanding the key genetic pathways essential for this successful RGC axonal regeneration in *X. laevis* may lead the way to attaining RGC axonal regeneration in clinical settings, which could have immense impact on patients suffering from glaucoma and other diseases or injuries that affect RGCs.

Here, we have developed an optic nerve crush (ONC) model in young *X. laevis* tadpoles that is suitable to perform a moderate-throughput CRISPR-based knockout (KO) screen of genes involved in RGC axonal regeneration. Using this screen, we report that a gene previously shown to be important in the response of neurons to injury, Dual leucine zipper kinase (*dlk)* is essential for RGC axonal regrowth in *Xenopus laevis* and for the restoration of vision after injury. We find that Dlk seems to function largely cell-autonomously within the RGCs, and that loss of Dlk blocks the regeneration of RGC axons without affecting axon growth by non-injured RGCs. We further find that while ONC affects mitochondrial movement along RGC axons soon after axon injury, loss of Dlk has no measurable effect on this acute injury response. However, Dlk loss completely eliminates the injury induced activation of the transcription factor cJun within RGCs that occurs days later, suggesting that the ability of RGCs to successfully regenerate their axons instead of undergoing programmed cell death is driven largely by a transcriptional program.

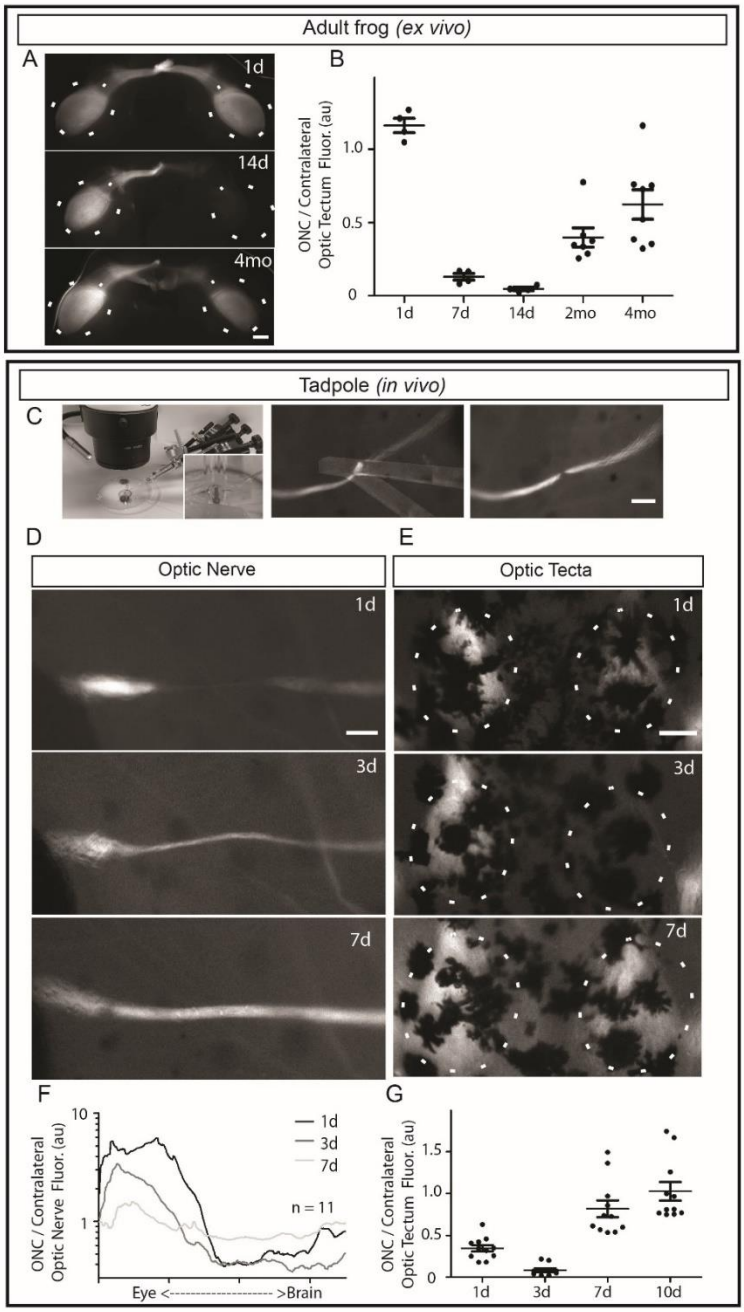

Figure 2.1. A novel ONC assay in young *X. laevis* tadpoles has a fast timecourse and enables live imaging of degeneration and regeneration in both optic nerves and optic tecta. A-B, In adults, regeneration is slow and must be measured *ex vivo*. A. Dissected flattened brain preparations showing GFP driven by RGC-specific promoter. 4mo image has what appears to be a doubled optic chiasm due to a dissection artifact. Scalebar = 1 mm. B. Timecourse of regeneration in adult frogs. C-G. Novel surgical and live-imaging/quantification assays in young tadpoles. C. Young tadpole ONC surgical procedure. Micromanipulator-mounted pulled and beveled glass needles, visualized mid-surgery along with the GFP-labeled fluorescent optic nerves, are used to crush the optic nerve in 8-day old tadpoles. Contrast settings for the needles in the middle panel were non-uniformly lightened to better show their placement. D-E. The optic nerves and optic tecta of the same animals can be live imaged over the course of axonal degeneration and regeneration. Scalebars = 100 μm. F. Measures of fluorescence along the injured optic nerve, normalized to equivalent positions along the uninjured contralateral nerve show the transient large increase in fluorescence proximal to the injury (note the logarithmic scale) and that regeneration of axons is largely complete by 7d post-ONC. G. Measures of fluorescence in crushed optic tecta relative to contralateral tecta similarly show that denervation is complete by 3d and innervation is largely restored by 7d post-ONC.

Results

A tadpole ONC model

The ON was crushed in adult *X. laevis* as previously done by us and others (235, 269, 270) but in transgenic animals in which the RGCs express a membrane-localized GFP under the control of the zebrafish Isl2b RGC-specific promoter (Isl2b: mem-GFP) (271). Comparison of the fluorescence intensity in the tecta connected to the crushed nerve to the fluorescence intensity in the contralateral (uninjured) tecta in the same animal enables rapid estimation of the extent of denervation and reinnervation, as we have previously showed (15). In contrast to the lateral geniculate nucleus which receives binocular input starting at metamorphosis (272), innervation to the optic tecta in *X. laevis* is largely if not exclusively monocular (273). In the case of adult frogs, where the dermis is entirely opaque and the brain fully encased in the skull, tectal fluorescence had to be assessed *ex vivo* in a dissected partially hemisected and flattened brain preparation to visualize the optic tecta and other RGC innervation targets. Using a relative fluorescence measure, we find that after ONC the injured optic tecta becomes completely de-innervated by 14 days, and only becomes largely reinnervated by 2-4 months post-ONC (Figure 2.1A-B). Notably, even by 4 months post-ONC the tecta corresponding to the crushed nerve display a lower fluorescence intensity compared to the contralateral tecta, similar to what we previously showed using a cytoplasmic rather than membrane GFP reporter in animals, where it took 7 months to reach near-full tectal reinnervation (270).

Since RGC axonal regeneration in adult frogs is slow and must be assessed *ex vivo*, we sought to develop a separate assay that might be better suited for assessment of genes involved in axonal regeneration. To this end, we designed a novel ONC technique that can be performed on

8-day old transgenic *X. laevis* tadpoles, in which micromanipulator-mounted glass needles are visualized under a fluorescence stereomicroscope to create a highly focal and reproducible ONC injury to the fluorescent optic nerve (Figure 2.1C). Given the transparent dermis and relatively few melanophores of young *X. laevis* tadpoles, this simple preparation allows for repeated *in vivo* imaging of the optic nerves and optic tecta within individual animals, enabling for *in vivo* monitoring of both denervation and reinnervation. Comparing the fluorescence intensities of the injured versus contralateral tecta (Figure 2.1E and G) revealed that, as expected for these much smaller animals, both the denervation and reinnervation were much faster than in adults; denervation is complete by 3d and reinnervation near maximal by 7d post-ONC. To quantitatively measure the axonal degeneration and reinnervation in the optic nerves, crushed and contralateral nerves were delineated, scaled to equal lengths, and fluorescence values compared across the length of the crushed nerve to equivalent positions along the contralateral nerve (Figure 2.1D and F). Consistent with the tectal measures, the optic nerve measures showed axonal degeneration to be maximal at 3d and axonal regrowth near complete by 7d post-ONC. At 1d post-ONC, the axonal degeneration is largely confined to the center of the optic nerve near the ONC, while by 3d post-ONC the distal portions of RGC axons have been largely removed, presumably by Wallerian degeneration (70). Notably, as soon as 1d post-ONC and still evident by 3d post-ONC, there is a prominent increase in fluorescence proximal to injury, nearer to the eye, likely representing the retraction of axons away from the injury site and towards the soma commonly observed after ONC injuries (69, 274). Thus, a novel assay was developed using animals that are about 1 week old, in which axon degeneration and regeneration can be live imaged and quantified in individual animals over the timecourse of an additional

week, properties that facilitate the scaleable interrogation of genes involved in axonal degeneration and regeneration in vertebrate RGCs.

Tadpole ONC model shows little to no RGC death after injury and involves true axonal regeneration

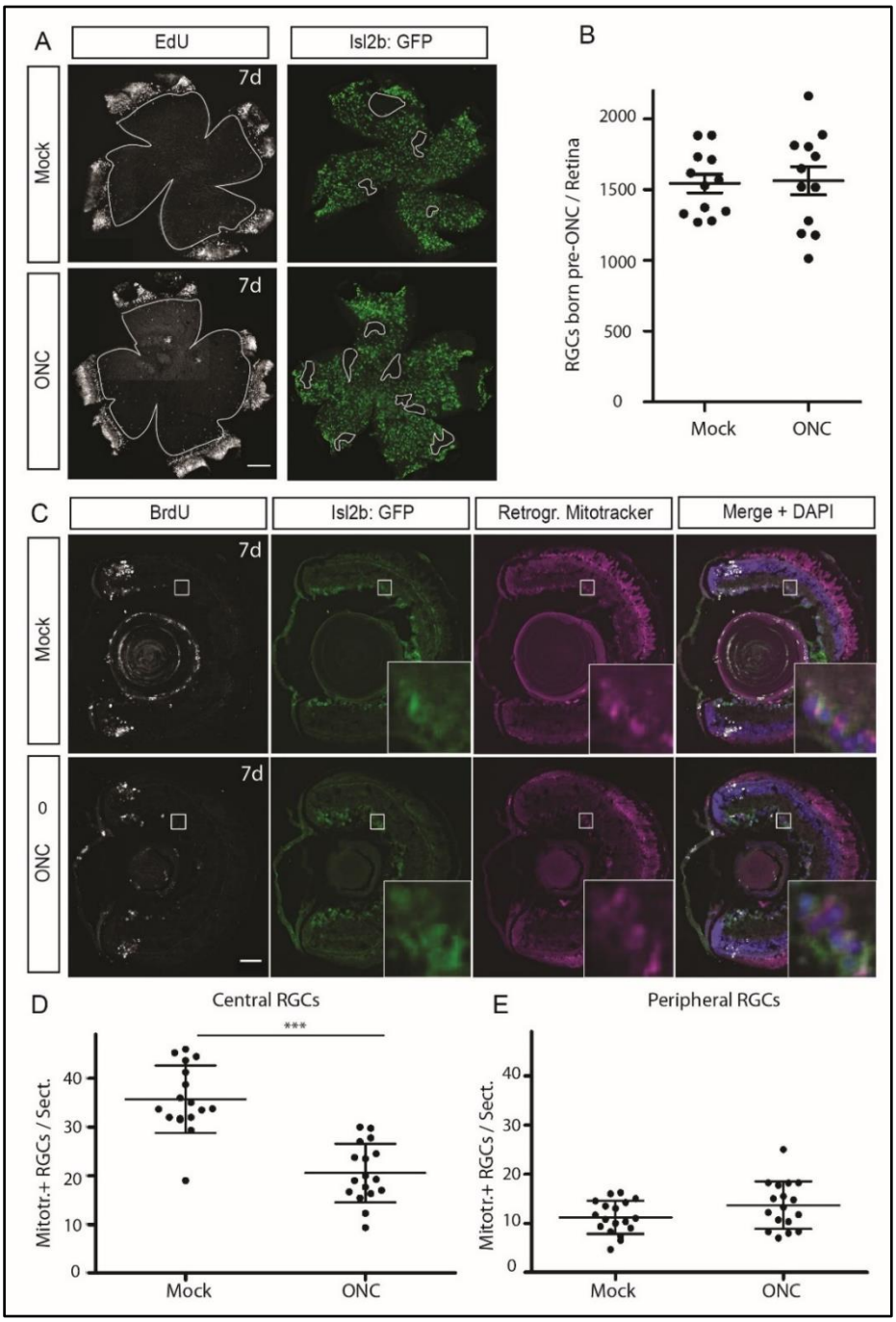

In adult *X. laevis*, up to 20% of RGCs die in the several weeks following ONC (246), similar to what has been reported after ONC in adult zebrafish (245). Additionally, the retinas of *X. laevis* continuously grow at the periphery via continuous addition of all retinal cell types at the ciliary marginal zone (CMZ), also similar to zebrafish (238, 243, 244), and this CMZ

Figure 2.2. In young tadpoles, the RGCs whose axons were crushed do not die, and provide the majority of the tectal innervation 7d after ONC. A-B. RGCs present in the retina prior to the ONC survive and remain at comparable numbers to mock-crushed retinas 7d post-ONC. A. An EdU pulse administered in tadpoles which express cytoplasmic GFP in their RGCs on the day of ONC distinguishes central RGCs born prior to ONC from peripheral RGCs born after ONC. Contours in the GFP images show dissection artifacts that were excluded from the cell counting. Scale bar = 100 μm. B. Automated cell counts of central RGCs numbers show that by d7 post-ONC, there is no significant death of the injured RGCs. N = 12 retinas each for mock and ONC retinas. C. BrdU labeling on the day of ONC to delineate RGCs born prior to ONC from RGCs born after ONC is combined with retrograde tracing by Mitotracker at d6 to label those RGCs which have successfully connected to the optic tectum. Scale bar = 50 μm. D-E. Manual counts of those RGC soma which are retrogradely labeled 24 hours after retrograde tracer application find that the majority of the tectal innervation 7d post-ONC derives from the injured central RGCs. N = 15 mock and 18 ONC retinas, with a minimum of 4 cryosections counted per retina.

addition is most robust at young pre-metamorphic stages (275). Thus, it was possible that the reinnervation of the tectum after ONC in the young tadpoles might not be due to axonal regeneration, as the central RGCs might die, but rather to just the addition of new RGCs born at the CMZ post-injury. To determine whether there was significant RGC death post-ONC, we administered an EdU pulse just after the ONC or mock injury in *X. laevis* tadpoles whose RGCs expressed cytoplasmic GFP (Isl2b: GFP, previously described in (270), as this transgene allows for visualization of RGC soma in the retina. Flatmount *ex vivo* preparation of the EdU labeled retinas enabled clear demarcation of the RGC cells interior to the EdU pulse, which represent the RGCs born prior to ONC whose axons would have been affected by the crush injury. Cell counts using an automated cell-counting algorithm (276) found no significant difference in numbers of central RGCs between ONC and mock-crush retinas (Figure 2.2A-B), demonstrating that most if not all RGCs survive the injury.

The more critical question was whether the majority of the tectal innervation observed at 7d post-ONC came from the axonal regeneration of RGGs disconnected from the brain by ONC, or rather from the newly born RGCs whose axons were innervating the tectum for the first time. To answer this question, we administered a BrdU pulse alongside either ONC or mock-crush on

Isl2b: GFP transgenic tadpoles 8dpf, then followed this by insertion of a small Mitotracker-soaked piece of Gelfoam into the optic tectum connected to the crushed ON at 6d post-ONC (14 dpf) to retrogradely trace RGC axons which had successfully innervated the optic tectum. In this case, retinas were analyzed in sections rather than wholemounts, as the peripheral-most newly born RGCs are difficult to visualize in wholemounts because of curling of the flatmounted tissue. When we quantified the number of RGC soma labeled by Mitotracker which were colocalized with or peripheral to the BrdU labeling (representing RGCs born after ONC), we find no significant difference in numbers between ONC or mock-crushed retinas (Figure 2.2C-E), suggesting that RGC axon injury does not lead to either an alteration in the generation of new RGCs from the ciliary marginal zone or the brain innervation by these new RGCs. Importantly, in both the retinas subjected to ONC and those subjected to mock-crush, the majority of RGCs that were connected to the optic tectum were central to the BrdU pulse, demonstrating that the injured RGCs not only survive but are also able to successfully re-establish connections with the optic tectum. Notably, there were fewer retrogradely-labeled RGC soma interior to the BrdU pulse in ONC retinas compared to the mock-crushed retinas, suggesting that some injured RGCs may either not reconnect with the brain at all, or that the regeneration of RGC axons may take longer to complete than initial innervation of the optic tectum by newly-born RGCs.

To confirm the tectal innervation after ONC derives from both older injured and newer non-injured RGCs, we developed an inducible reporter system based on the expression of two transgenes, FZD5(CSA): rtTA and TetOP:mCherry, which upon application of doxycycline to the tadpole media, induces expression of cytoplasmic mCherry in all newly-born cells in the retina. The regulatory regions for this construct derive from a conserved non-coding sequence approximately 40kb upstream of the human Frizzled 5 gene, and it has been previously been

used to express transgenes in retina progenitors in *X. laevis* (277). To confirm correct transgene expression and activation timing, we bred animals carrying both FZD5(CSA): rtTA TetOP-mCherry inserted into the same genomic location, to animals carrying the Isl2b: GFP transgene. After an EdU pulse on the first day of doxycline administration, in both retina flatmounts and cryosections, all cells labeled with mCherry signal are positioned either peripheral to or colocalized with the EdU pulse (Figure 2.3A-B) Live imaging of the optic nerve of animals expressing this transgene (Figure 2.3D) show that by 7d post-ONC, many of the RGC axons that have grown past the crush site and into the optic tectum are indeed newly born, and further demonstrates that these new RGC axons grow on the periphery of the nerve, corresponding with to localization of these new RGC soma at the periphery of the retina (Figure 2.3A-B). Furthermore, the extent of GFP labeling in both tecta and optic nerve both fully overlapped with and exceeded the region covered by the mCherry labeling, demonstrating that the majority of the RGC axons which grow past the injury are mCherry negative, and therefore the RGCs that existed prior to the ONC. Thus, both the retrograde tracing and the transgene labeling methods concur in showing that in the young tadpoles innervation of the optic tectum after ONC does involve a significant baseline due to innervation by newly born RGCs that were not injured, but that the majority of the tectal innervation derives from the axons from the damaged RGCs, thus making the assay suitable for the interrogation of RGC axonal regeneration genes.

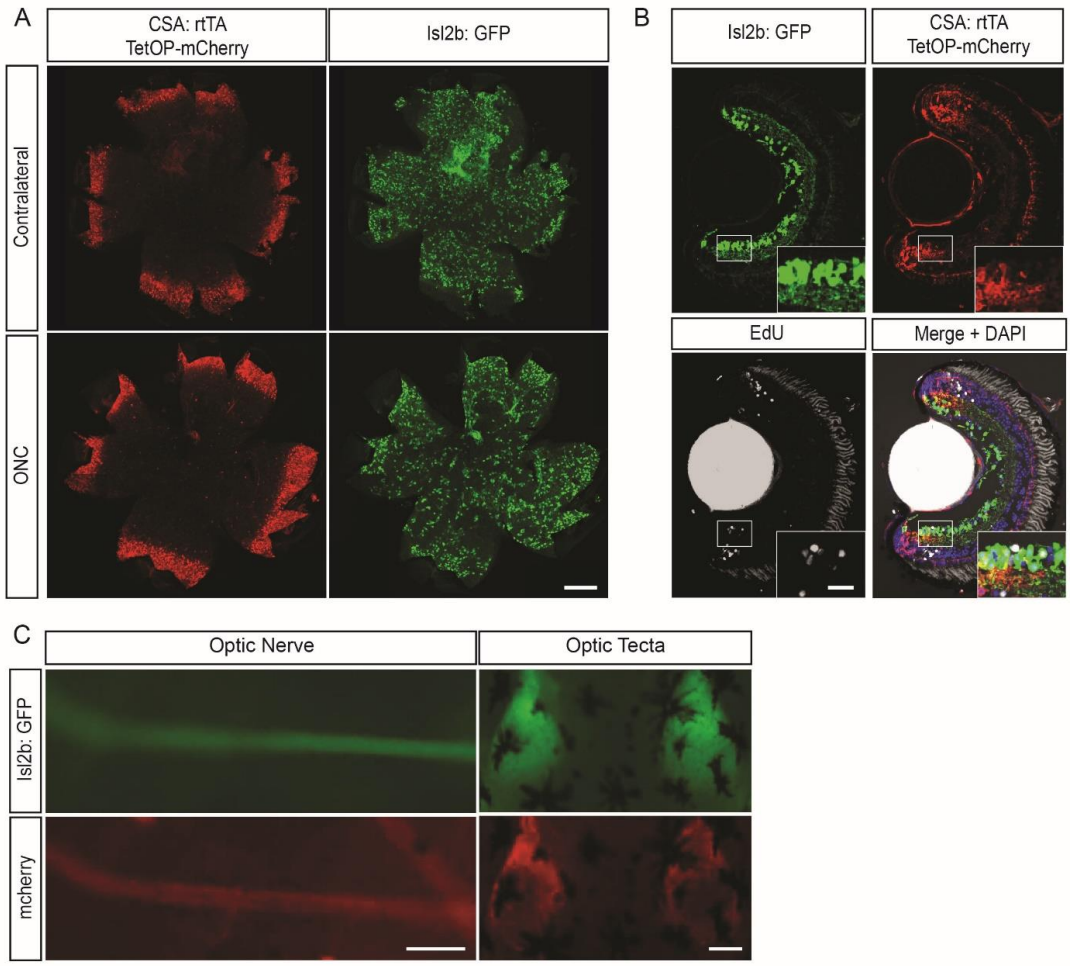

Figure 2.3. Novel *X. laevis* transgenic line enables fluorescent labeling of newly-born RGCs. A. A. Expression of CSA:rtTA2 and tetOP:mCherry together enables new retinal cells to be distinguished after application of doxycycline. Retinal flatmounts from 15-day-old tadpoles also carrying an RGC-expressed GFP transgene show mCherry fluorescence in only the most peripheral (newly born) cells, including RGCs. Scalebar = 100 μm. B. Expression of the CSA: rtTA / TetOP:mCherry transgene after doxycycline induction correlates well with the EdU localization. Scalebar = 50 μm. C. 7d after transgene induction, *in vivo* imaging reveals that mCherry expression is confined to the periphery of both optic nerve and optic tectum. Scalebars = 100 μm.

FO loss-of-function screen shows that Dlk functions in tectal reinnervation after ONC

CRISPR/Cas9 injection at the one or two cell stage has previously been used in *X. laevis* to conduct moderate throughput screens (278, 279), despite this species being allotetraploid and therefore requiring loci of interest often to be targeted in two separate chromosomes. To query the function of regeneration associated genes in our novel ONC regeneration assay by a

CRISPR/Cas9 approach, we developed a genetic screen in the progeny of Isl2b:GFP transgenic frogs (Figure 2.4A). Cas9 protein sgRNAs designed using ChopChop (280) were injected into about 50 eggs per sgRNA at the one-cell stage within 30 minutes of fertilization; two separately targeting sgRNAs were designed and injected per embryo if one sgRNA could not be designed which targeted both chromosomes. At 1d, genomic DNA from pooled (n=5) embryos were extracted, and 500-1000 bp amplicons centered around the sgRNA consensus sequence were PCR amplified and sequenced. TIDE (Tracking of Indels by Decomposition) (281), which compares the mixed population of indels created by the F0 CRISPR microinjection to a homogenous control amplicon from the same region was used to determine the targeting efficiency (Figure 2.4B-C). We set a minimum threshold of 80% overall indels and 50% frameshift indels for sgRNAs to be of sufficient efficiency to progress into the tadpole ONC assay. Once sgRNAs were validated in this manner, 10-15 injected animals per sgRNA which expressed the RGC-localized GFP transgene in their RGCs were selected and subjected to a unilateral ONC at 8d post-fertilization. One, three and seven days later, the optic tecta and optic nerves were live imaged in anesthetized animals. Any animals with an incomplete crush or a complete transection at 9d post-fertilization (1d post-ONC) was excluded from further analyses; this was typically less than 10% of animals subjected to ONC. The extent of axonal degeneration was assessed at 3d post-ONC (11 dpf overall), and the extent of regeneration assessed at 6 or 7d post-ONC (13 or 14 dpf overall), dependent of when the control group had reached approximately half tectal innervation. Thus, from microinjection to assessment of denervation and reinnervation, the screening time for a new sgRNA could be as little as 15 days.

What follows is the description of the first hit in the screen to affect regeneration: dual leucine zipper kinase or *dlk.* Dual leucine zipper kinase (Dlk) is a MAP3K which functions in the mitogen-activated protein kinase pathway upstream of known cell-death regulator Janus Kinase (JNK) (79). This was among the first genes tested as it is thought to be part of the mechanism by which the injury to the axon is conveyed back to the soma (77-80, 282, 283). The sgRNA eventually chosen, which targets the first coding exon of *dlk* (Figure 2.4B), produced a high incidence of mutations near the target site (Figure 3C), and was determined by TIDER analysis (281) to have 90% KO efficiency and >50% frequency of frameshift mutations in both the S and L chromosomes of *X. laevis* F0 embryos (Figure 2.4D-E). The vast majority of indels produced were frameshift deletions, with the frequency of a -7 deletion being particularly high on both S and L chromosomes, but other in-frame deletions and some out-of-frame insertions were also produced. When transgenic Isl2b: mem-GFP/*dlk* sgRNA-injected F0 animals were subjected to ONC, these animals displayed a significant defect in innervation of the injured optic tectum 6d post-ONC compared to uninjected WT control embryos from the same in vitro fertilization (Figure 2.4F). Furthermore, the mean fluorescence across the crushed nerve normalized to equivalent positions across the contralateral nerve (n=5 wildtype, n=9 *dlk* gRNA injected) showed that the *dlk* CRISPR injected animals on average still had at 6d post-ONC the thicker proximal nerve phenotype characteristic in WT animals at 3d post-ONC (Figure 2.4G), suggesting that the axons had degenerated back towards the eye but had a defect in axonal regeneration. The qualitative assay in the nerve and the quantitative assay of the optic tectum in the F0 screen, thus suggested that Dlk function could be required for RGC axonal regeneration in *X. laevis.*

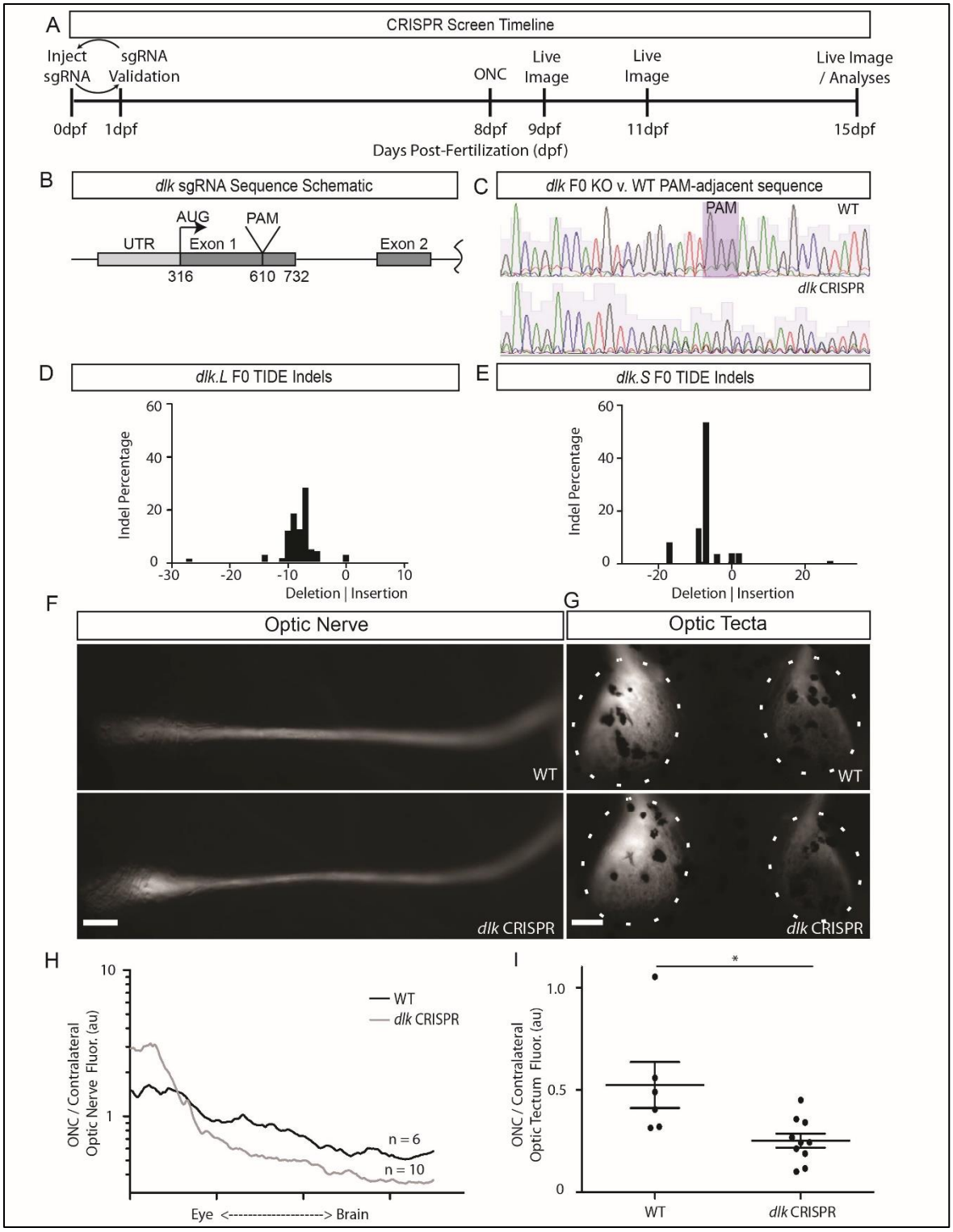

To confirm and expand upon the F0 results, we raised gRNA injected animals to sexual maturity and repeated the tadpole ONC assay in F1 progeny created by breeding together two

Figure 2.4. F0 CRISPR and the young tadpole ONC-assay demonstrate that Dlk function is involved in RGC axon tectal innervation after ONC. A. CRISPR screen timeline. F0 knockout animals were generated in the background of a transgenic line in which RGCs express GFP. sgRNA + Cas9 protein were injected within 30 min of fertilization. One day later, DNA was obtained from pools of 5 embryos to assess KO efficiency by TIDER analyses of PCR products. At day 8, GFP+ tadpoles were subjected to ONC, followed by three days of imaging (1d, 3d, and 7d post-ONC) and then tissue harvesting. B. Schematic of first 2 exons of *dlk* showing the location of the sgRNA PAM within exon 1. C. Sample sequencing traces from uninjected (top) and Dlk gRNA injected (bottom) embryos near predicted CRISPR cut site. D-E. *dlk* F0 indel efficiency was >90% for Dlk alleles on both L and S chromosomes. F-G. Representative live images at 6d post-ONC; nerve and optic tecta images are from the same animals. F. Live imaging of the optic nerves shows that *dlk* gRNA injected animals have a phenotype consistent with an inhibition or delay of RGC axon growth after ONC: thinner ON distally and thicker ON proximally relative to the ONC site. Image shown is at 6d post-ONC, and is of a moderately affected animal (near the mean for the experiment). Scalebars = 100 μm. G. Live imaging of the optic tecta shows that *dlk* gRNA injected animals have on average a diminished tectal innervation after ONC. Image shown is at 6d post-ONC and is of a moderately affected animal (near the mean for the experiment); in some animals the phenotype was far more pronounced. H. Measures of fluorescence across the crushed nerve normalized to equivalent positions along the uninjured contralateral nerve (mean of 6 and 10 animals for WT and *dlk* gRNA injected, respectively) show that, compared to WT the nerves of *dlk* gRNA injected animals at 6d post-ONC have a nerve fluorescence profile consistent with an inhibition or delay of RGC axon growth after ONC. Measures of fluorescence comparing tectal fluorescence in injured tecta denervated after ONC to contralateral tecta in the same animals show a significantly decreased GFP signal.

KO animals, of which one also carried the Isl2: mem-GFP transgene. Since in *X. laevis* multiple cells contribute to the germline and sgRNA/Cas9 injection at the 1-cell stage still results in mosaic animals, in individual F1 animals there could be as many as 4 different *dlk* alleles, with different combinations of alleles in different siblings, as was confirmed by TIDER analyses (Figure 2.5A). As such, analyses using F1s required genotyping of every animal used to identify those that only carry only frameshift alleles (hereafter referred to as *dlk* KO); an advantage of such approach, though, is that it can reveal dosage effects. Thus, by breeding two founders which carried no WT alleles and high frequency of frameshift alleles, we obtained animals that

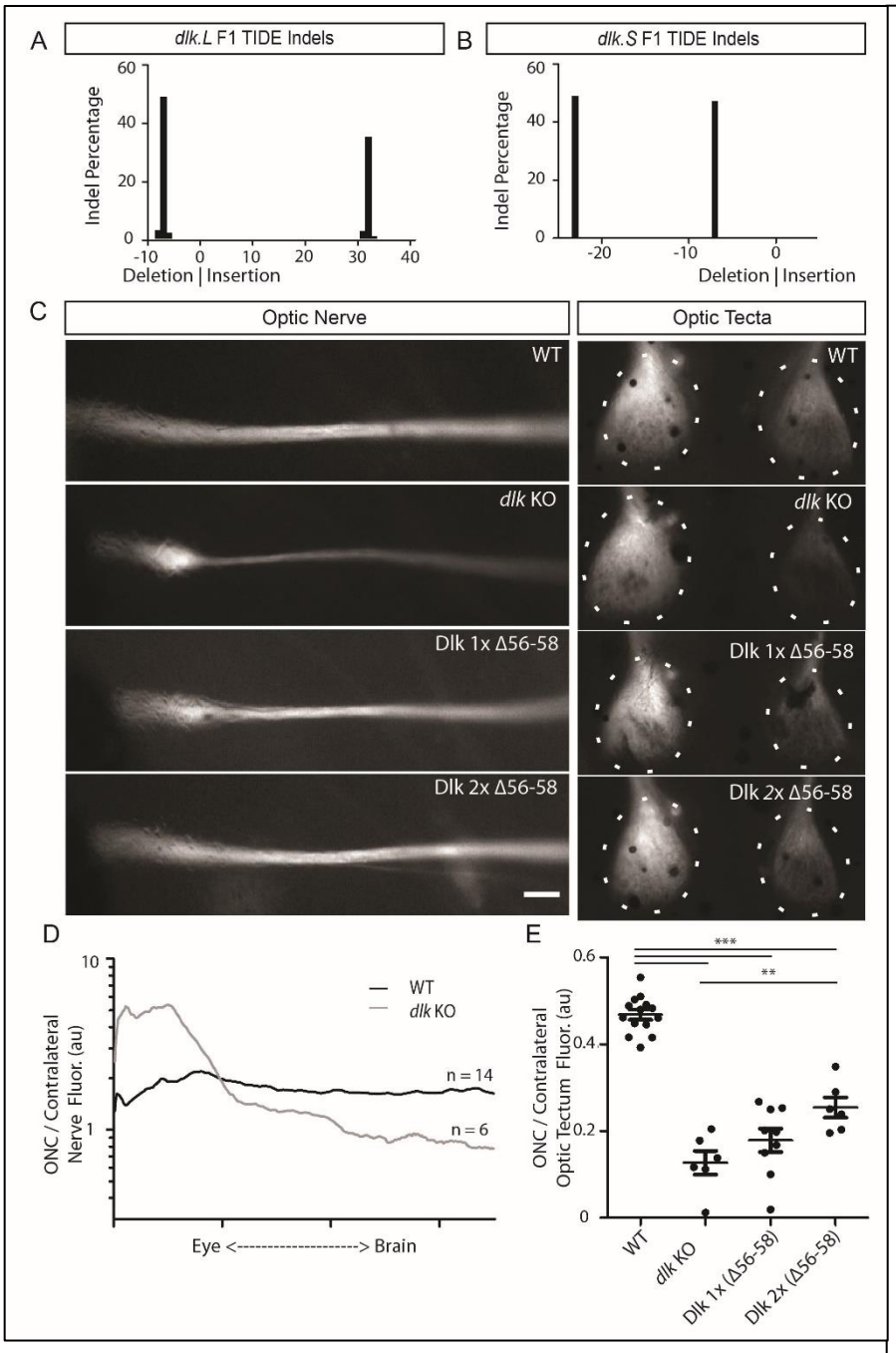

Figure 2.5. Analyses of F1 animals derived from the original F0 screen demonstrate that the effect of Dlk on RGC-axonal regeneration is dose-dependent. A-B. Example TIDE genotyping traces of dual frameshift mutations in the S and L chromosome. A, TIDE trace from a F1 animal carrying a -7 deletion and a +32 insertion in its L chromosome. B. TIDE trace from a different F1 animal carrying a -23 and a -7 deletion in its S chromosome. C. A small in-frame deletion that eliminates 3 amino acids, Dlk Δ56-58, occurred in both S and L chromosomes of F1 animals. Two copies of Dlk Δ56-58 resulted in the least severe phenotype, while having only frameshift alleles (*dlk* KO) resulted in the most severe phenotype. Scalebar = 100 μm. D. Measures of fluorescence across the crushed nerve normalized to equivalent positions along the uninjured contralateral nerve show that, compared to WT crushed nerves, in F1 *dlk* full KO animals the proximal nerve remains enlarged while the distal nerve fluorescence is attenuated at 6d post-ONC. E. Measures of fluorescence comparing the crushed to the uninjured contralateral optic tecta show an allelic series in which rising copy number of the Dlk Δ56-58 mutation results in progressively less severe axonal regeneration defects.

genotyping revealed were an allelic series: carrying either only frameshift mutations in *dlk* on both the S and L chromosomes, one copy (L chromosome) of an in-frame *dlk* -9 mutation, predicted to delete amino acids 56 to 58 (Dlk Δ56-58), or two copies (S and L chromosomes) of this Dlk Δ56-58 allele (Figure 2.5D-E). While the thicker

proximal nerve phenotype was consistent across groups, the more quantitative tectal innervation measures showed the degree of tectal reinnervation varied depending on the dosage of Dlk. Tadpoles carrying two frameshift mutations and therefore which presumably possess no functional Dlk showed the most severe tectal innervation defects as well as the most severe nerve phenotypes, while those with one or two copies of Dlk Δ56-58 had intermediate phenotypes (Figure 2.5C-D). To confirm the dosage dependence, using separate founders we compared animals with 4 WT *dlk* alleles to ones where half of the alleles were WT, and the other half carried frameshift alleles. From this, we find that 50% loss of Dlk also results in an inhibition or slowing of tectal innervation after ONC (Figure 2.6).

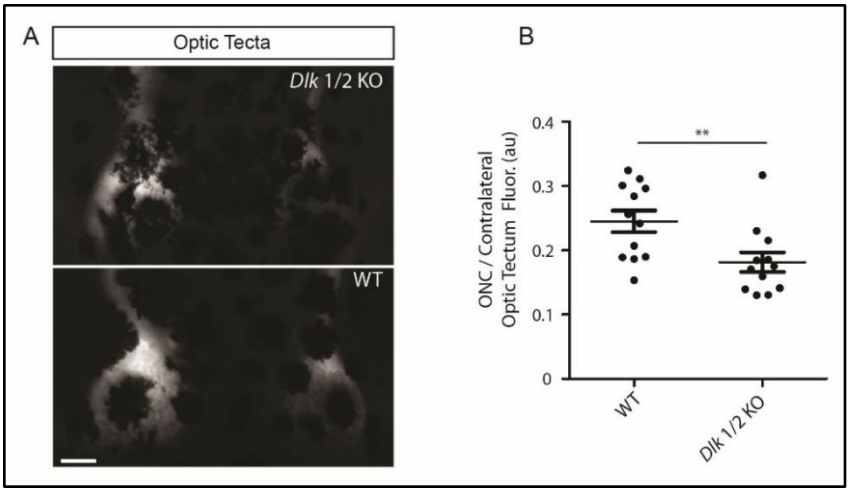

Figure 2.6. Animals with half the complement of Dlk show a defect in tectal reinnervation at 6d post-ONC. A. Representative images. B. Measures of fluorescence. Scalebar = 100 µm..

Loss of Dlk does not affect either the innervation of the optic tectum during development or an optic tectum-dependent visually driven behavior but does affect the recovery of this behavior after ONC.

In order to determine whether Dlk absence might be affecting RGC axonal regeneration indirectly, either by more generally affecting RGC axon outgrowth or by making the RGCs generally dysfunctional, we assessed both the initial innervation of the optic tectum during

development and a behavior that depends on innervation of the optic tectum by RGC axons. To assess whether Dlk affects RGC axon growth in general, we compared Isl2b: mem-GFP embryos with only frame-shift alleles of *dlk* (*dlk* KOs) to WT embryos expressing the same transgene at Nieuwkoop and Faber stage 41, which is the earliest stage at which retinal projections have been documented to innervate the brain (284). In terms of morphology and tectal innervation, *dlk* KOs were indistinguishable from WT embryos (Figure 2.7A). To assess whether RGCs and the rest of the visual pathway were functionally affected by Dlk loss, we employed a behavioral collision-avoidance assay previously validated in *Xenopus laevis* tadpoles of this age (285), which relies specifically on optic tectum innervation (286, 287). In this assay, tadpoles are placed in glass-bottomed bowls atop an LED screen on which a black-dot stimulus is displayed. The user then directs the black dot stimulus to move towards the location of either a static tadpole, or on a collision course with a slowly swimming tadpole; ten trials of "collisions" (judged by partial or complete overlap of the stimulus with the tadpole head) are recorded and every trial in which the tadpole responds by darting away from the black dot stimulus is graded as a "response" (Figure 2.7B). First, to determine the effect of the ONC on this behavior, we selected Isl2b: mem-GFP WT animals with over 60% response rates and then performed bilateral ONCs on half of those animals; such preselection of animals has been deemed necessary to exclude non-responders (see (285, 287) and methods). Crushed and naïve animals were then "scrambled" by one investigator, and then the behavioral assay was repeated on the same animals at 3d post-ONC by a second investigator blinded to which animals had received the surgery. This was followed by live-imaging to confirm complete bilateral crushes on the crushed cohort, by confirming that all transgene fluorescence in both optic tecta had been lost. At this timepoint, the tadpoles had lost the ability to respond to the visual stimulus (Figure 2.7C). By 6d post-ONC, at which point the

fluorescence intensity of the optic tecta had begun to return, the majority of these animals were once again able to respond to and avoid the visual stimulus. We also interpret these results to mean that the 50-70% tectal innervation typically observed by 6d after ONC is sufficient to drive this visually-guided behavior.

We then repeated this behavioral assay on the F1 progeny of *dlk* Crispr-Cas9 F0 and found that the overall response in the trials was indistinguishable between WT and the *dlk* Crispr-Cas9 F1s (Figure 2.7D), demonstrating that *dlk* knockout does not affect the overall function of RGCs or the circuits needed for this visually-guided behavior. Then, *dlk* Crispr-Cas9 F1 animals with greater than 50% response prior to ONC were divided into two cohorts, subjecting only one to bilateral ONC on one cohort and reserving the other to ensure that *dlk* knockout did not lead to loss of the avoidance behavior over the course of the experiment. We found that *dlk* KO tadpoles (individually confirmed by TIDE genotyping as carrying only frameshift alleles) subjected to bilateral ONC also lost the ability to respond to the black-dot stimulus at d3 post-ONC, but unlike WT tadpoles, did not recover this response at 6d post-ONC (Figure 2.7E). Taken together, these results indicate that Dlk does not affect RGC axon outgrowth or the initial innervation of the optic tectum nor does it affect basic cellular processes within RGCs which control their ability to drive vision, but that it acts specifically in vision recovery after axonal injury.

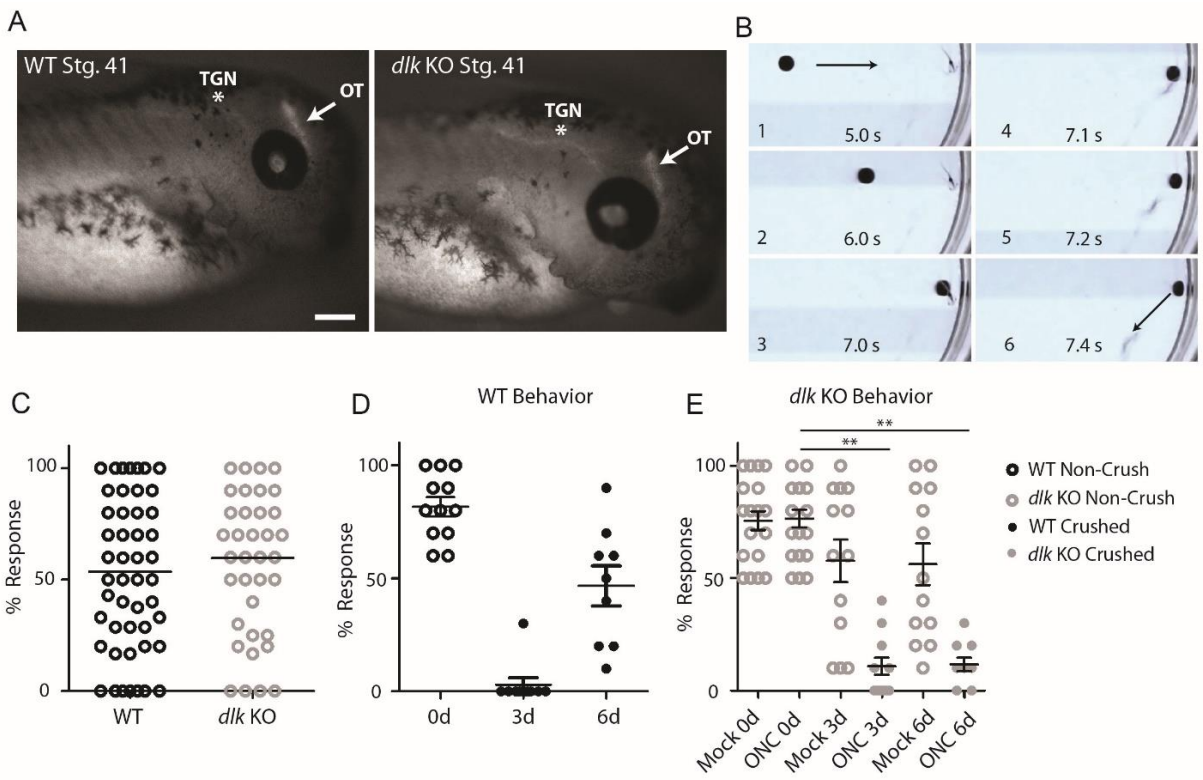

Figure 2.7. Absence of Dlk does not affect developmental optic tectum innervation by RGC axons or a visually guided behavior dependent on optic tectum innervation, but does block the restoration of the visually guided behavior after ONC. A. *dlk* KO animals show normal optic tectum innervation at NF stage 41. Both *dlk* KO and WT animals express an Isl2b: mem-GFP transgene. Note that Isl2b promoter expresses also in trigeminal neurons and sparse neurons in hindbrain and spinal cord, which also were not affected by loss of Dlk. OT = optic tectum, TGN = trigeminal nucleus. B. A behavioral test of vision in *X. laevis* tadpoles. A black dot stimulus projected from an LED screen beneath glass-bottomed bowl is manually directed at the tadpole (still frames 1-3); if tadpole immediately darts away from stimulus, trail is counted as a "response" (still frames 4-6); percent response is then calculated after ten mock-collisions. C. Both WT and *dlk* KO animals show a similar range of responses to behavioral assay during preselection screening. Only animals which responded in 50% or more of trials were included in subsequent ONC experiments. D. WT tadpoles subjected to bilateral ONC lose the dot-avoidance response by 3d post-ONC, but largely regain it by 6d after ONC. E. *dlk* KO animals subjected to bilateral ONC but not mock-crush lose the dot-avoidance behavior 3 days post-ONC and do not recover it by 6d post-ONC. Non-Crush animals at 3d and 6d were subjected to a mock crush following pre-screening at 0d.

dlk KO specifically affects the regenerating axons of the injured RGCs

Since the innervation of the optic tectum 7d post-ONC derives from a mix of axons from the injured RGCs and more recently generated RGCs (see Fig. 2.2D-E), it is possible that the impairment observed in the *dlk* KOs in tectal innervation (see Fig. 2.5E) and tectum innervation dependent behavior (see Fig. 2.7E) could be due to the lack of Dlk in the new RGCs, in the injured RGCs, or both. To determine whether both cohorts of RGCs were equally affected by the loss of Dlk, we administered a BrdU to *dlk* KO and WT tadpoles at 8 dpf immediately following ONC. At 6d post-ONC, at which point live imaging confirmed that the injured optic tecta of WT tadpoles had reached approximately half the level of innervation of the uninjured control tecta,

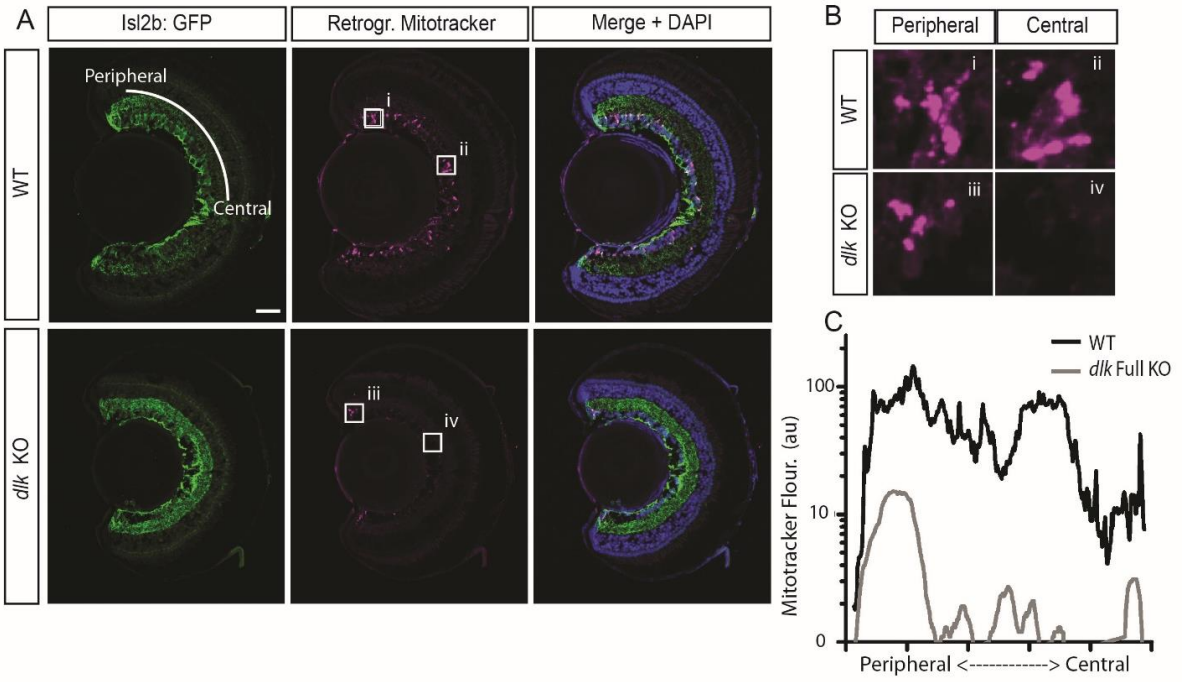

Figure 2.8. Dlk is necessary for the optic tectum reinnervation by the RGCs whose axons have been injured but is dispensable for the optic tectum innervation by new RGCs born after the injury. A-B. Tectal innervation assessed at 7d post-ONC after implantation of Mitotracker dye into the optic tecta connected to the crushed nerve 6d post-ONC. Retina sections (A) and insets shown magnified (B) show that in WT animals the tectal innervation 7d post-ONC derives from throughout the retina, but in the *dlk* KO animals only from the peripheral-most RGCs. C. Average Mitotracker fluorescence in the ganglion cell layer as a function of location within the retina (from periphery to center) shows that in the retinas of *dlk* KOs (confirmed by genotyping), unlike in WT retinas, the Mitotracker signal is confined to only the peripherally located, more recently born, RGCs. N = 10 *dlk* KO and 12 WT retinas. Scalebar = 50 μm.

we again performed retrograde tracing by insertion of a small Mitotracker-soaked fragment of Gelfoam into the injured optic tecta (Figure 2.8). We found that in the WT retinas, both the centrally-located RGCs that were present in the retina prior to injury and the peripheral RGCs that correspond to the newly-born RGCs were retrogradely labeled, suggesting that both groups of RGCs were both able to innervate the optic tectum post-injury. However, in the *dlk* KO animals, the Mitotracker signal was limited almost entirely to the peripheral RGCs, indicating that Dlk absence disproportionally affects the regeneration of the injured RGC axons. Note that the fluorescence intensity of Mitotracker labeling in the periphery of the Dlk KO animals was lower than in the WT animals; thus, Dlk loss may be affecting all RGCs to some extent, directly or indirectly, or at least their ability to be retrogradely labeled by Mitotracker, a possibility we directly tested below.

Dlk likely functions autonomously within X. laevis RGCs

Because our CRISPR injection and F0 interbreeding process creates global KOs, it is possible that the observed effect of Dlk loss on RGC regeneration is not cell-autonomous and is instead the result of perturbation of extrinsic factors derived from neighboring cells. The most likely sources for such intrinsic factors are cells within the optic nerve, such as oligodendrocytes, astrocytes, or resident microglia, all of which would also be devoid of Dlk on our F1 tadpoles and could potentially affect axonal regeneration. Thus, to address whether Dlk acts on RGC axonal regeneration via a cell-intrinsic or a cell-extrinsic mechanism, we transplanted small groups of retinal progenitor cells from the eye anlage of early *dlk* KO embryos into that of wildtype embryos. Transplantations were done at a stage prior to RGC genesis, but donor cells carried a transgene that marked the progenitor cell-derived RGCs with two transgenes: a membrane-localized GFP and membrane-localized mCherry (Isl2b: mem-GFP/mem-mCherry).

The hosts carried a transgene (Isl2b:GFP) such that their RGC axons expressed only one fluorescent protein, a cytoplasmic GFP. We then subjected these animals to ONC at 8d post-fertilization and live-imaged the crushed nerves of each of 8 animals at 1, 3, and 7 days later, this time using a spinning disc confocal microscope, where the entire visible nerve was imaged in

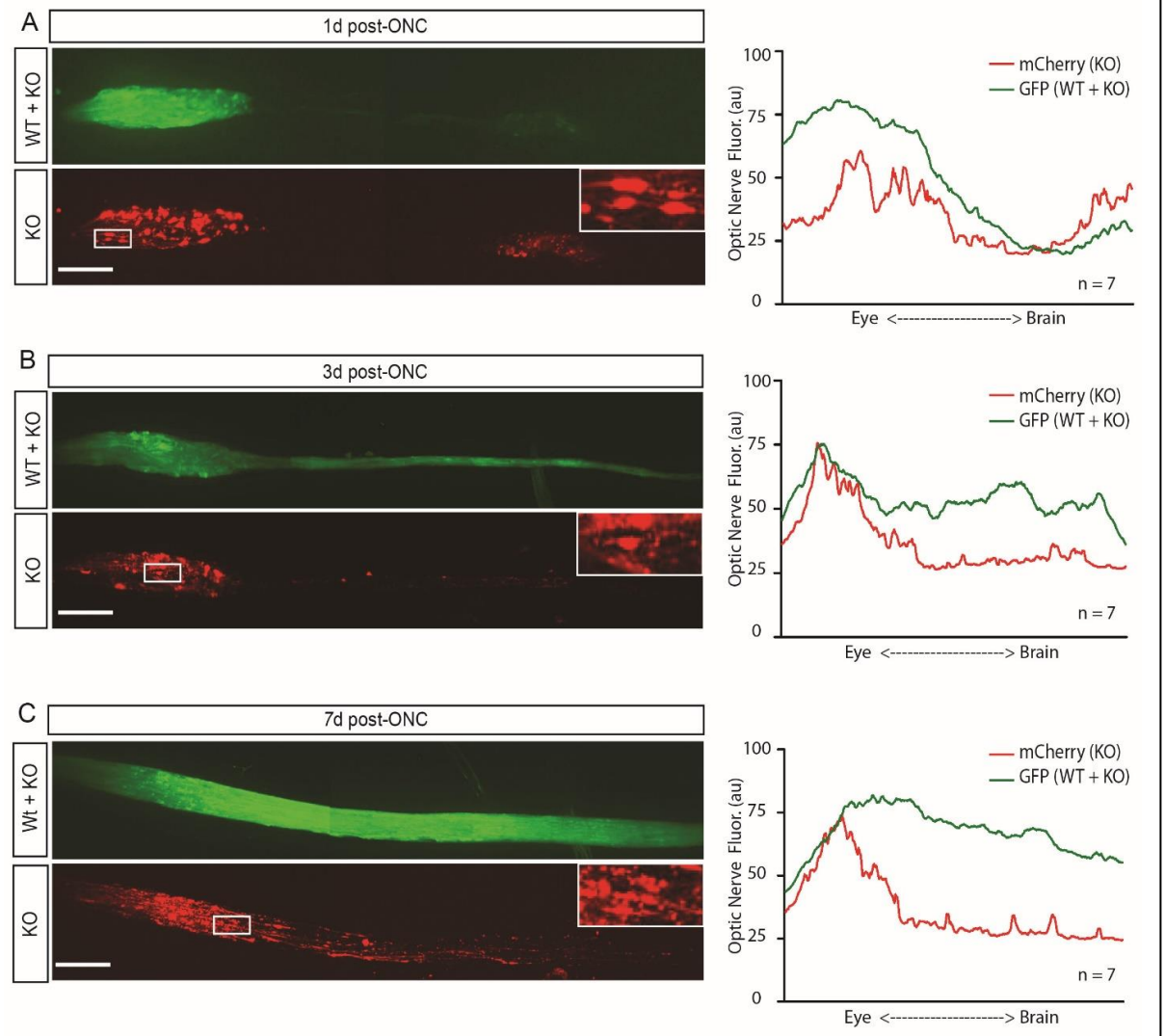

Figure 2.9. **Axons of *Dlk* KO RGCs fail to regrow after crush in Wt optic nerve surrounded by regenerating Wt RGC axons.** A-C. Sparse *dlk* KO donor-derived RGC axons expressing membrane GFP and membrane mCherry reporters amid host RGC axons expressing a cytoplasmic GFP reporter. A. By 1d post-ONC, both donor and host axons have similarly degenerated past the crush site. Inset shows retraction bulb in mCherry-labeled *dlk* KO axons. B. By 3d post-ONC, the GFP-labeled WT axons but not the mCherry-labeled *dlk* KO axons have begun to grow past the crush site. C-D. By 6d post-ONC, even when large numbers of WT RGC axons have extensively regrown, most *dlk* KO axons remain proximal to the crush site. Note that some *dlk* KO axons do grow across the crush site; these likely represent axons from RGCs derived born after the crush also derived from the transplanted RGC progenitor cells. Scalebars = 50 μm.

overlapping regions, each spanning the entire thickness of the nerve, so as to image the entire nerve with single axon resolution. At 1d post-ONC, the GFP fluorescence was largely confined to regions of the optic nerve proximal to the injury site, with much weaker GFP fluorescence distal to the injury (Figure 2.9A); the majority of this signal derives from the WT host axons. At this same time, the donor *dlk* KO axons, uniquely labeled by the mem-mCherry reporter, were also largely confined to proximal to the injury site, with somewhat more residual fluorescence distally, consistent with the predicted slower loss of fluorescence of mCherry vs. GFP. Proximal to the injury site, *dlk* KO axons had prominent retraction bulbs of consistent morphology similar to what has been reported in the literature for damaged axons (71, 72), suggesting that Dlk absence has little if any effect on the initial morphological response to axon injury or on Wallerian degeneration. At 3d post-ONC, these retraction bulbs were less prominent, but there was little if any regrowth of axons from the RGCs lacking Dlk, especially as compared to the GFP fluorescence distal to the ONC site derived from the WT axons, which also was markedly higher than at 1d (Figure 2.9B). By d7 post-ONC, the GFP fluorescence was uniform across the nerve, indicating very extensive axonal regeneration of WT axons within the ON. However, the mCherry-labeled *dlk* KO axons showed very little regrowth across the injury site (Figure 2.9C). While a small number of mCherry labeled axons grew past the site of injury, their small number suggest that those axons likely originated from newly-born RGCs generated from the RGC progenitor cells grafted into the WT nerve as opposed to axonal regeneration from the injured population of RGCs. These experiments do not rule the possibility that Dlk might be acting in other cells within the retina derived from those progenitors, for example amacrine cells known to affect the regeneration capacity of RGCs (93, 163), or in the progenitor cells themselves.

However, the simplest explanation is that in *Xenopus* RGCs, the pro-regenerative mechanism by which Dlk acts occurs within the injured RGCs themselves, as has been suggested in other contexts where Dlk affects the response of cells to injury (77-79, 110, 120, 135).

Dlk does not affect changes in mitochondrial movement within RGC axons acutely induced by injury

In *C. elegans* motor neurons and in murine spinal cord, Dlk as been proposed to act immediately and locally within the axon following injury by helping recruit mitochondria to the injury site (76, 77, 282). First, to test

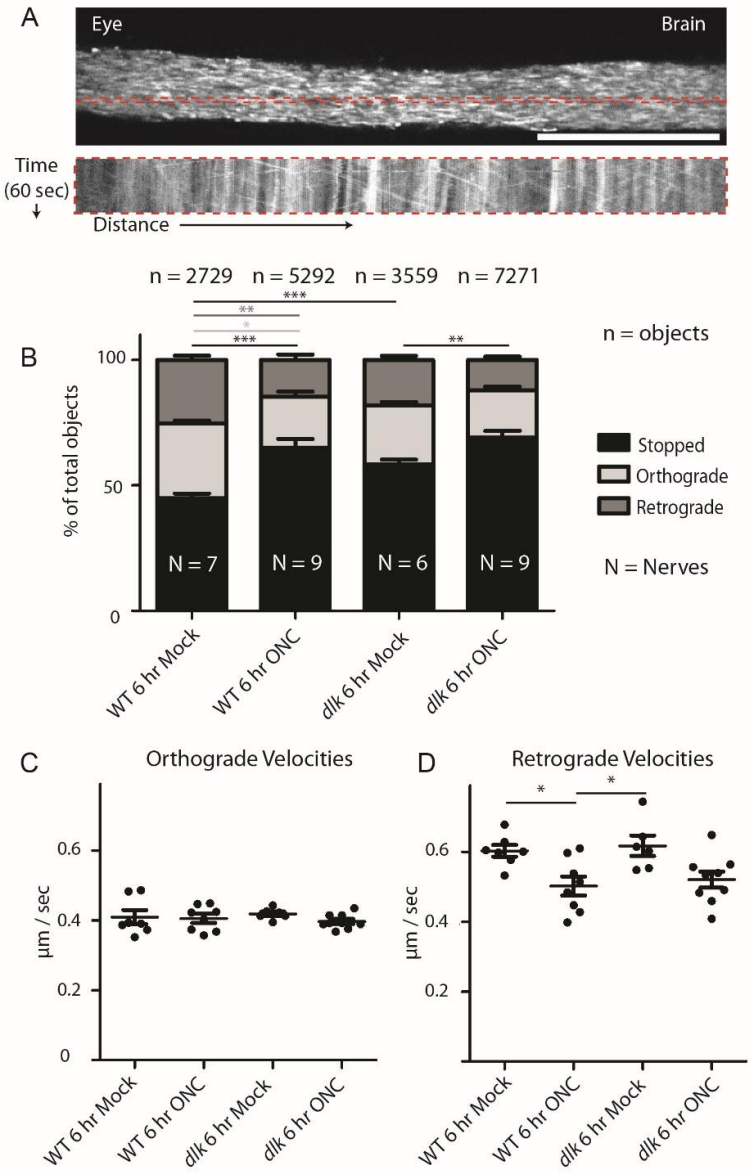

Figure 2.10 Absence of Dlk does not affect the ONC-induced change in mitochondria movement behavior proximal to the crush site 6hr after injury. A. Single frame from 60s live imaging of Mitotracker-labeled RGC axonal mitochondria. Red dotted box indicates one of many region of interests (ROIs) per nerve analyzed through kymographs; the corresponding kymograph for that ROI shown below. Scalebar = 100 µm. B. In both WT and *dlk* KO nerves, ONC increases the percentage of stopped mitochondria relative to mock-crushed nerves at the expense of retrogradely-moving mitochondria. *dlk* KO has no effect on the relative percentage of mitochondria moving in either direction. N = number of nerves per group; n = number of total objects in all nerves per group. C-D. *dlk* KO does not affect either ortho- or retro-grade velocities. C. Axon injury does not affect orthograde velocities (C) Axon injury does decrease retrograde velocities.

whether axon injury affects the behavior of axonal mitochondria, RGC axonal mitochondria were labeled by intravitreal injection of Mitotracker one day prior to ONC, and the region of the optic nerve proximal to the injury site was imaged by spinning disc confocal microscopy 1 and 6 hrs after the ONC. In WT animals, the ONC resulted in a small increase in the number of immobile (stopped) mitochondria at the expense of mitochondria moving retrogradely along the nerve (from brain to soma) at both 1hr and 6hr after ONC (Figure 2.10 and Figure 2.11), consistent with previous studies of axonal injury (288, 289). ONC also resulted in a decrease in the velocity of retrogradely-transiting mitochondria at 6 hr post-ONC (Figure 2.10). To test whether Dlk absence affected this transient change in the behavior of axonal mitochondria, *dlk* KO animals were similarly analyzed at 1 and 6 hr post-ONC. The increase in stopped mitochondria at both timepoints post-ONC and the decrease in the velocity of retrograde movement at 6 hour post ONC occurred equally even in the absence of Dlk (Figure 2.10 and Figure 2.11) While Dlk appeared to have a small effect on the velocity of retrograde movement after a mock ONC at 1 hr post-surgery (Figure 2.11), this effect was not observed at 6 hr post-ONC (Figure 2.10). Importantly, there was no significant effect of Dlk on the velocity of moving mitochondria after injury in either direction nor on the fraction of stopped mitochondria. Thus, while the live assay reliably detects a consistent effect of ONC on mitochondria behavior, an increase in stopped mitochondria, this effect is not altered in the *dlk* KO.

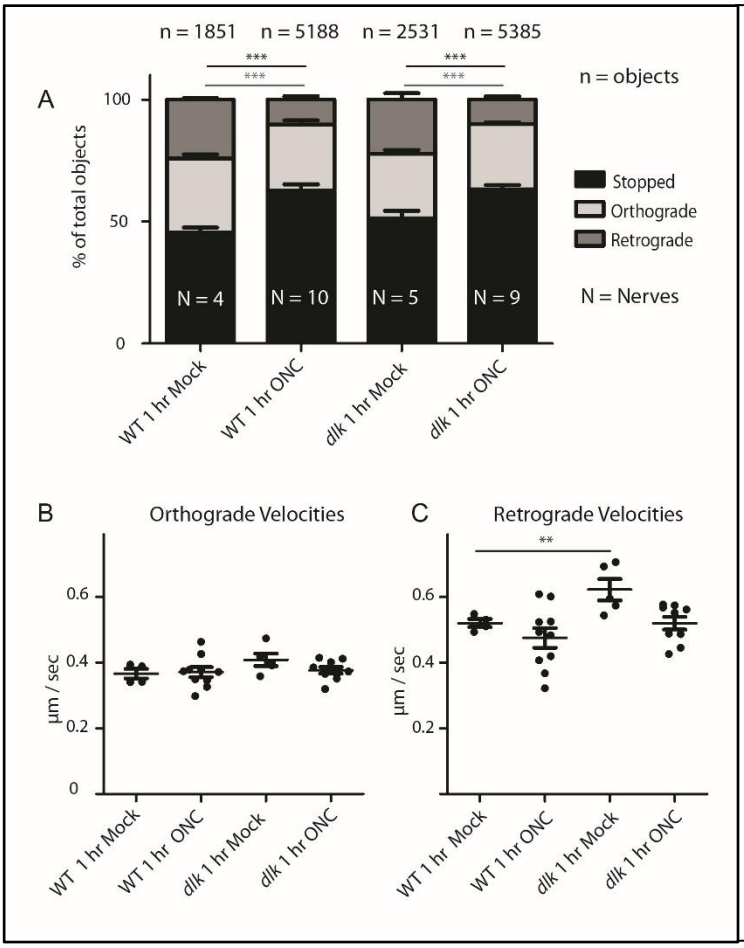

Figure 2.11. At 1-hour post-injury, absence of Dlk does not affect the ONC-induced change in mitochondria movement behavior proximal to the crush site. A. In both WT and *dlk* KO nerves, ONC increases the percentage of stopped mitochondria relative to mock-crushed nerves at the expense of retrogradely-moving mitochondria; percentages of stopped mitochondria 1-hour post-ONC are slightly lower than at 6 hours post-ONC. *dlk* KO has no effect on the relative percentage of mitochondria moving in either direction. N = number of nerves per group; n = number of total mitochondria measured in all nerves per group. B. Neither injury nor *dlk* KO affects orthograde velocities at 1-hour post-ONC. C. *dlk* KO may have a small effect on retrograde velocities of mock-crushed animals 1 hr post-ONC.

Dlk knockout eliminates the activation of c-Jun in RGCs after ONC

The effects of Dlk on axonal degeneration and regeneration in other species have been shown to be mediated by a set of sequential phosphorylation events that lead to the phosphorylation and nuclear translocation of the transcription factor cJun, part of the AP1 complex, that then transcriptionally regulates many downstream genes (77, 78, 110, 120). To determine whether and when c-Jun is phosphorylated following injury in our tadpole ONC model, we performed ONC on WT tadpoles and examined retina sections at various timepoints post-ONC for the presence of phosphorylated c-Jun (pJun) in RGC nuclei. We find a large increase in RGC nucleic pJun as early as 2d post-ONC, with the peak of cJun phosphorylation

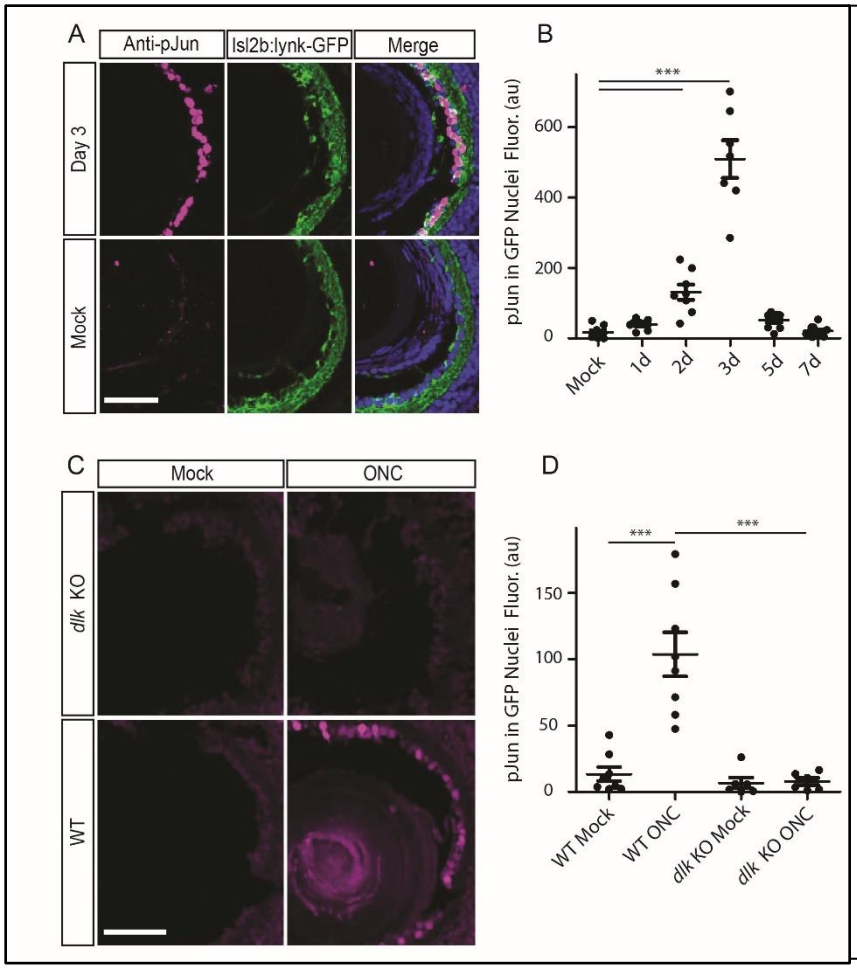

Figure 2.12. Dlk is essential for any activation of the transcription factor c-Jun in RGCs after ONC. A-B. A large increase in phosphorylation and nuclear translocation of c-Jun within RGCs peaks at 3d post-ONC. N = 7-11 retinas per timepoint, with a minimum of 3 cryosections averaged per retina. Merge includes nuclear labeling with Dapi. All significant timepoints relative to Mock are shown. C-D. *dlk* KO tadpoles display no nuclear pJun at 2d post-ONC. N = 6 each for Dlk Mock and ONC retinas, 9 Wt Mock retinas and 8 Wt ONC retinas, with a minimum of 3 cryosections averaged per retina.

occurring at 3d post-ONC and levels of phosphorylated c-Jun then returning to near-baseline levels by 7d (Figure 2.12A-B).

Given that by 2d post-ONC, phosphorylated c-Jun is still actively accumulating in the retina but there is already a significant level of activation, we then tested *Dlk* KO and WT retinas collected 2d following either mock crush or ONC for levels of cJun phosphorylation. We find that in *Dlk* knockout retinas, there is essentially no RGC nuclear pJun at 2d post-ONC (Figure 2.12C-D), suggesting that Dlk is necessary to activate c-Jun and, presumably, its downstream targets following axonal injury. This positions Dlk as the sole upstream activator of c-Jun after

ONC and makes Dlk an essential component of the RGC axonal injury response in a species which can regrow and functionally reconnect RGC axons after injury.

Discussion

In this study we report the development of a novel RGC axon regeneration assay in *Xenopus laevis* tadpoles which enables moderate-throughput screening of CRISPR-mediated F0 knockouts in just weeks and minimally-invasive *in vivo* imaging of axons within the optic nerve and tectum, as well as of mitochondria within those RGC axons. Using a CRISPR KO approach, we find that in this regeneration capable vertebrate Dlk is essential for the regeneration of RGC axons after injury, and that it functions largely cell-autonomously. We further find that Dlk is dispensable for the initial axonal outgrowth and tectal innervation of RGCs innervation during development, and dispensable for the axonal outgrowth and tectal innervation by new RGCs generated from retinal progenitors within the retina following the optic nerve crush. Collectively, these findings position *dlk* as a regeneration-specific gene. Finally, we find that activation of c-Jun post-ONC, as monitored by its phosphorylation and nuclear translocation, is completely dependent on Dlk, which positions Dlk as the sole axonal injury signal in *X. laevis* RGCs. This last point stands in contrast to mammalian species, in which both Dlk and the closely related leucine zipper kinase (*lzk*) seem to function as early axonal injury signals (80, 132).

Much is known about molecular pathways activated in neurons after axonal injury (reviewed in (290)). In particular, Dlk has been found to be a key mediator of cell death and regeneration in both central and peripheral system neurons after injury (79). Following injury in either system, Dlk is produced at the injury site and then retrogradely transported back to the soma, where it activates the JNK1-3 pathways (77, 78). In *C. elegans, dlk* is required for

regeneration in sensory motor neurons; (120, 282) similarly, Dlk initiates a pro-regenerative transcriptional response after sciatic nerve injury (110). Additionally, the *Drosophila* homolog of *dlk*, Wallenda, functions as part of the injury-signaling cascade upstream of JNK/Fos, and this signaling pathway is necessary for axonal regrowth following motor neuron injury (283). All of these involve peripheral nervous system neurons, which, like *Xenopus*, possess an intrinsic capacity for regrowth following injury. In the murine central nervous system, which is regeneration-incapable, Dlk has been found to activate both proapoptotic and pro-regenerative factors following injury by broad alteration of the transcriptional response to injury; and loss of *dlk* abrogates even the small amount of RGC axonal regeneration induced by *PTEN* deletion (78). However, Dlk has also been found to induce RGC cell death in immunopanned primary murine RGCs by activation of a JNK/MKK signaling cascade; and in cultured human stem-cell derived RGCs, inhibition of DLK is neuroprotective of RGCs (80). Our studies interpreted in the context of these previous studies show that in the vertebrate CNS, Dlk helps convey a signal from the injury site in the axon back to the nucleus to trigger the appropriate transcriptional response, and that without conveyance of this injury signal successful axonal regeneration cannot occur.

Several points raised by our own data will require further investigation. The overall lack of effect of Dlk on mitochondrial movement after ONC stands in contrast to its reported effect on mitochondrial movement in other studies. It is possible that the effect of Dlk may have been missed by the assays we employed. Alternatively, it could be that in the vertebrate CNS, any effect of Dlk on mitochondria behavior is of little consequence as to whether or not a successful regenerative response is mounted. Of great interest and worthy of future study is the dose dependence of the Dlk effect, suggesting that boosting Dlk activity might be therapeutic.

However, it will be critical to determine when and where Dlk action exerts this dose dependence, as MAPK pathways typically exhibit tight spatiotemporal control (94). In regards to the in-frame deletion of *dlk* we reported, Dlk Δ56-58, if this variant produces a fully functional protein then the intermediate phenotypes we observed in our allelic series were achieved based solely on rising copy number of full *dlk* knockout. Alternately, this mutant could also be a hypomorph, in which case careful dissection of the functional domains of *dlk* around this small deletion could yield insights as to the overall mechanism of Dlk action within RGCs.

Overall, our results indicate a key role for *Dlk* as a conserved early axonal injury signal which activates RGC-intrinsic pathways to initiate axonal regeneration. As the targets of Dlk are incompletely known at present, comprehensive profiling studies to map which key genes lie downstream of *dlk* and *cJun* in frog RGCS hold great potential to uncover new gene candidates that could be leveraged to develop regenerative therapeutic interventions. Our *dlk* KO model also highlights the efficacy of our novel ONC assay to both rapidly screen new putative regeneration-associated genes and to determine their mechanism of action. The key to achieving clinically-relevant axonal regeneration may well depend upon careful and thorough deconstruction of an evolutionarily conserved successful RGC axonal regeneration response.

Methods

Animals

Wild-type and genetically modified *X. laevis* lines were housed in an investigator-maintained facility at UC Davis, and all work was carried out in accordance with protocols approved by the

local IACUC. Xenopus 2-wks and older were maintained in a drip-through *Xenopus* facility, and younger animals were maintained in 0.1X MMR in static glass containers.

Transgenic lines were created by restriction enzyme mediated integration (REMI) as first described in (291). Transgenic constructs and lines to express a cytoplasmic GFP in RGCs, Tg(Isl2b:GFP), and a membrane localized mCherry in RGCs, Tg(Isl2b:Mett7l-mCherry) here referred to as Tg(Isl2b:mem-mCherry), have been previously described (250) and (1). To be able to optimally label RGC axons with a membrane localized GFP, a four-step cloning strategy was used. First, an early version of GFP that fluoresces brightly in transgenic *Xenopus*, GFP3, where Kozak and ATG sequences were replaced by HindII-EcoRV-NheI sequences, was cloned into the HindIII and XhoI sites of a pCS2 backbone using primers AAGGAGAAGCTTGATATCGCTAGCAGTAAAGGAGAAGAACTTTT and CGCTCGAG TTATTTGTATAGTTCATCCATGCC. Then, a 9 amino acid membrane localization sequence from lyn kinase was cloned into the HindIII and NheI sites using annealed kinased oligos AGCTTGCCACCATGGGATGTATAAAATCAAAAACAGACAATG and CTAGCATTGTCTGTTTTTGATTTTATACATCCCATGGTGGCA. This cDNA encoding lynk-GFP3 was then moved using the unique HindIII and XhoI sites into an intermediate that was then used to create the final construct pCS2(zf_Isl2b 20kb):lynk-GFP3 by recombineering, essentially as previously described (1); animals expressing this construct are here referred to as Tg(Isl2):mem-GFP. Since the line used for most regeneration studies has a mem-GFP and mem-mCherry transgenes inserted into the same locus, these animals are here referred to as Tg(Isl2b:mem-GFP/mem-mCherry).

To create a construct to express in retina progenitors, a 307bp highly conserved sequence 44kb upstream of the human FZD5 was amplified from a BAC, RP11-161I22, using primers

ACGCCAGTCGACTCTCTATCAGGAACCTGGGCCTC and AAGGACGGATCCGTCCGGGCTAACTCCTGAATAGC, digested with SalI and BamHI, and cloned into the SalI and BglII sites of pG1-TOP-GFP construct that has a minimal cFos promoter driving GFP, in order to create pCS2(FzD5CSA):GFP. A BclII-NotI fragment containing rtTA2-pA from pCS2(Blbp):rtTA2 (1) was cloned into BamHI-NotI of pCS2(FZD5CSA):GFP to create pCS2(FZD5):rtTA2. To make pCS2(TetOP):mem-mCherry, the mem-mCherry-pA of pCS2(Blbp):mCherry-Gap43 (1) was swapped in for the GFP-pA of pCS(TetOP):GFP (292). Adult *Xenopus* ONC: For adult frog ONC, the procedure was carried out as previously described (250, 269, 270). In brief, animals were anaesthetized in 0.5 g/L tricaine solution (MS222). A small incision was made in the roof of the mouth using a sharp scalpel blade, followed by blunt dissection of the muscle and tissue layers using forceps to access the optic nerve, taking care to avoid injuring major blood vessels. The optic nerve was crushed for 4 seconds using #2 forceps. Animals were then allowed to recover in filtered 0.1x Modified Marc's Ringer (MMR) solution for 1 day before being returned to the drip-through tanks until day of euthanasia.

Young tadpole *Xenopus* ONC: For tadpole ONC, two glass needles were pulled and then broken to 50-75 µm thickness, beveled to a 20-degree angle and mounted on micromanipulators. Tadpoles were anaesthetized in 0.2 g/L MS222 in filter sterilized 0.1x MMR solution and mounted on a custom stability plate (two glass rods affixed to the plate using modeling clay near parallel to one another; this shape supports the tadpole head on the rods with tail allowed to rest between the rods). Animals were positioned beneath a small fragment of Kimwipe dipped in the same anesthetic solution to prevent drying and to maintain adequate anesthesia for the duration of the surgery, with another small anesthetic-soaked fragment of Kimwipe placed just above the

head across the glass stability rods to prevent drift. Surgery was performed using a Leica MZ10F fluorescent stereomicroscope to visualize the fluorescent ON. ONC was performed by inserting the two glass needles dorsally just adjacent to the ON and crushing by pressing the needles together. ONC were done monocularly except for animals to be used for behavioral assays of vision, in which case ONC was binocular. Tadpoles were allowed to recover in filtered 0.1x MMR + 20 mM HEPES + 50 µg/mL gentamicin at 16 degrees for 12-15 hours. Following imaging 1d post-ONC, tadpoles were then kept at room temperature on a 12/12-hour light-dark cycle for the duration of the experiment. In most experiments, tadpoles were kept in plastic boxes with dividers, with approximately 5ml per cubicle to monitor the reinnervation response of every animal over time. In the case of the animals to be use in the behavioral assay, animals were housed together after ONC, as we find that schooling affects the robustness of the dot-avoidance response.

Live imaging: For lower resolution *in vivo* assessment of optic tecta and optic nerve denervation and reinnervation tadpoles were anaesthetized with 0.2 g/L MS-222 in 0.1x MMR and positioned in the same setup described above for tadpole ONC surgery. The same Leica MZ10F fluorescent stereomicroscope equipped with a PlanApo 1.0x lens (Leica, Wetzlar, Germany). that used for the surgery was used again, this time along with custom iVision-Mac scripts (BioVision, Exton, PA) to capture images using a Qimaging Retiga-Exi Monochrome Cooled 12-Bit camera (RET-EXI-F-M-12-C) (Teledyne Photometrics, Tuscon, AZ). These scripts prompted operators to focus and photograph each nerve and tecta individually using both GFP and mCherry filter sets. For the high-resolution imaging of RGC mitochondrial movement within axons and analyses of sparsely labeled axons, animals were also anesthetized with 0.2 g/L MS-222 in 0.1x MMR and

then immobilized in 30 x 15 mm plastic dishes with custom Sylgard silicone molds previously created using gluteraldehyde fixed animals. These molds, with the addition of round 12mm glass coverslips atop the animal and mold for stability, oriented the animals in such a way that the left nerve was parallel to the focal plane of the objective. Nerves were imaged using a Dragonfly spinning disc confocal microscope (Dragonfly 503 multimodal imaging system, Andor Technology, Belfast, UK) fitted with an 40x/1.1 (magnification/numerical aperture) HC PL APO water immersion objective and a Leica DMi8 inverted microscope (Leica, Wetzlar, Germany). Images were captured using an iXon Ultra 888 EMCCD camera and Fusion Software (both from Andor Technology, Belfast, UK) and laser lines of 50 mW 488 nm, 50 mW 561 nm, and 100 mW 643 nm. T-stack images for each animal recorded for 1 min at 1 Hz. Z-stack images scanned the entire length of visible nerves in 3-4 overlapping sections, scanning the entire thickness of the ON at each location at 1 µm steps, and using 2-frame averaging to increase resolution.

Retrograde tracing: For retrograde tracing, small Gelfoam® (Pfizer) strands visible only under the dissection microscope were soaked with 1µL of Mitotracker DeepRed FM (Cell Signaling #8778S) at a concentration of 50 µg/µl until all Mitotracker solution was absorbed. Once dried, the Gelfoam® strands were further broken into smaller pieces of 5-15 µm diameter using forceps. Anesthetized tadpoles were placed in triangular notches carved into poured paraffin, removing most solution to anchor the animals sufficiently for the surgery. A small piece of Kimwipe soaked in anesthetic was used to cover tadpole to prevent drying and maintain adequate level of anesthesia. A pulled solid glass rod (Harvard Apparatus GR100-15) broken blunt and mounted on a micromanipulator was used to pierce the skin overlaying the rostral optic tectum contralateral to the ONC. Using a 00 insect pin, the Mitotracker soaked Gelfoam fragments were

placed overtop the created holes, followed by their insertion into the tectal neuropils with the aid of the solid glass rods. After surgeries, tadpoles were allowed to recover in filter sterilized 0.1X MMR at 16 ^{o}C for 12 hours and then kept at room temperature for 6 hours prior to euthanasia and tissue collection for cryosectioning.

Axonal mitochondria labeling and live imaging: For live-imaging of mitochondria movement within RGC axons in the optic nerve, Deep-Red Mitotracker at a concentration of 200 µM diluted in filter sterilized 0.5x MMR was injected intravitreally using a Narishige IM 300 Microinjector fitted with glass needles pulled and cut to approximately 1µm diameter. 40-80 nL of solution was injected per eye, as calibrated by comparing droplet sizes injected into mineral oil compared to those injected using a Nanodrop II piezo-controlled injector. Successful injections were verified by observing a small swelling of the eye. Animals were allowed to recover in filter sterilized 0.1X MMR for 24 hours at room temperature prior to ONC. Live imaging was carried out 1 hr and 6hr post-ONC using the same Leica Andor dragonfly confocal microscope with 40x/1.1 N.A. water immersion objective as described above.

sgRNA design and synthesis: sgRNA design and CRISPR KO creation was based on protocols previously described for *X. laevis* (278, 279) with the following modifications. For sgRNA design, short sequence regions of *dlk* with 100% conservation between S and L chromosome were selected for input into CRISPR sgRNA design machine at https://chopchop.cbu.uib.no/ and candidate sgRNAs to test were selected based on low number of predicted potential off target sequences (0 targets predicted to have 1 mismatch, and maximum of 1-3 off-targets predicted to have 2-3 bp of mismatch). sgRNA consensus regions in which all mismatches occurred within

the 5 base pairs at the 5' most end were excluded, as this has been suggested to decrease specificity and increase off target cuts (293). sgRNAs were ordered and synthesized as described in (279) except at the last step, sgRNAs were diluted to 800 ng/uL and snap-frozen on dry ice in single-use aliquots for injection. Final *dlk* sgRNA consensus sequence region chosen for this study was 5'-GACAGACCATGTCGGGCATTGGG-3'.

CRISPR microinjections: For sgRNA injection, *X. laevis* eggs were fertilized by overlaying them with macerated testes for 5 minutes prior followed by immediate dejellying with 25 g/L cysteine at pH8. Eggs were quickly immobilized in custom mesh-inlaid 30 x 14 mM dishes in 0.1X MMR + 0.4% Ficoll + 20 mM HEPES + 50 µg/mL gentamicin. 0.5 µL of Cas9-NLS protein at 6.3 mg/mL (Macrolab; UC Berkeley) and 2.5 µL of 800 ng/µL sgRNA were mixed together and 20-40 nL of this mix injected into each embryo through 1-2µm tip diameter pulled glass needles controlled by a Narishige IM 300 Microinjector, with injection volume calibrated as above. Injected embryos were then removed into 0.1X MMR + 0.4% Ficoll + 20 mM HEPES + 50 µg/mL gentamycin and placed at 16 ^{o}C overnight to recover. Injections were done in small batches so that all were complete within 30 minutes of fertilization.

***Xenopus* genotyping:** For genotyping F0 sgRNA-injected embryos, 5 embryos were pooled together at NF stages 10-11.5 (approx. 24 hpf). For genotyping of F0 or F1 tadpoles, animals were euthanized by MS-222 overdose and 0.25-0.4 cm of tail tissue collected separately for each embryo. For genotyping of frogs, animals were fully anaesthetized and a 2mm fragment of webbing tissue was taken from one hindlimb using an Integra Miltex 2mm biopsy punch (8-MIL-33-31-EA). Following tissue collection, tissues were snap-frozen on dry ice if genomic

DNA extraction could not proceed on the day of tissue collection. In all cases, genomic DNA was prepared from tissue samples using Qiagen DNEasy Blood and Tissue Kit. A ~600 bp region was then PCR amplified around the predicted PAM site using the following primers: L chromosome, 5'-CTTGATGAGTACCTGGTAATACTCTTGGTAGG-3' and 5'-GCTAATGACTTCAGCTTGGGATTTAGGGAAGG-3' ; S chromosome, 5'-CCTTGATGCCTGGTAATACTTGTGGTACTTTC-3' and 5'-GGCCTCAGAAGCTGCTATTAGGATTTTAGCT-3'. PCR products were then sequenced using primers 5'-CTTGATGAGTACCTGGTAATACTCTTGGTAGG-3' for L chromosome and 5'-GGTACTTTCCTTGACTTGCAC-3' for S chromosome. Sequencing returned .ab1 files which were then analyzed by TIDE (Tracking of Indels by Decomposition) analysis (281) via comparison to an unmixed control (no indel) sample from uninjected WT embryos amplified using the same primer sets.

Behavior assay: Software used to drive the tadpole visual avoidance assay was as previously described in (285). Dish radius was set at 210-235 px, background set to 160, travel time at 2500 px/sec and dot radius at 15 px. Monitor used for projection of the visual stimuli onto the tadpoles was a LiteMax 10.4" LED Backlight Monitor with brightness of 800 cd/m^2 monitor (model SLD1055-ENA-B01-02, 10.4" TFT LCD, LED Backlight, 800nits, XGA). Recording of each trial was done using a Logitech HD Pro Webcam C920, 1080p Camera. Prior to behavioral experiments, all tadpoles were kept in groups so that animals could school and were maintained on a 12/12 light-dark cycle with daily feeding. For the behavioral assay, an individual tadpole was transferred into a 60 mm straight-sided glass dish with approximately 1.5 cm of 0.1X MMR depth placed atop the monitor on which software projecting the visual stimulation was displayed.

Room lights were darkened during trials to ensure maximum contrast between the backlit monitor and the visual dot stimuli displayed. For each trail, user manually tracked tadpole movement and directed movement of a black dot stimuli onto the stationary tadpole or onto the path of a slowly swimming tadpoles. A trial was recorded as "response" if tadpole immediately changed speed/direction and moved away from dot upon overlap; if the velocity or direction of tadpole travel showed no change upon dot collision the trail was recorded as "no response". Ambiguous trials were not counted. Ten informative trials were performed for each tadpole with a minimum time of 20 seconds between each trial. In the case of comparing Wt to Dlk KO animals in the absence of any insult, the behavior of all animals assayed was counted. For animals that were to be used in an ONC experiment, an initial screening was carried out prior to ONC. Tadpoles with a 50% or higher rate of "response" were retained for later experimentation, to exclude possible non-responders. Following such selection, tadpoles were subjected to bilateral ONC and allowed to recover in 0.1x MMR + 50 µg/mL gentamicin + 20 mM HEPES overnight at 16 ^{o}C, then moved back into 12/12 light-dark cycle at room temperature. At d3 post-ONC, tadpoles were examined for complete ONC and any tadpoles with incomplete tectal de-innervation were excluded. Tadpoles with complete bilateral ONC were re-assayed using visual dot avoidance behavioral assay and moved into singly-housed 15 x 30 mm dishes for individual tracking. Tadpoles were maintained singly housed on 12/12 light-dark cycle and fed daily until final behavioral assay was performed again at 6d post-ONC.

***Ex vivo* analyses.** For adult tissue dissections, animals were euthanized by MS-222 overdose followed by decapitation. Brain was removed and flat-mounted by a partial-width incision along the tectal midline to open out both optic tectum lobes for imaging. Tecta were immediately

imaged upon dissection. For tadpole tissue dissections, animals were euthanized by tricaine overdose and fixed in 4% PFA for 4 hours at 4 ^{o}C for cryosectioning or 1 hour at 4 ^{o}C for retinal flatmounts. After fixation, eyes were removed from brain using 00 insect pins and placed in sucrose overnight at 4 ^{o}C (for cryosectioning) or in methanol overnight or longer at -20 ^{o}C (for flatmounts). For tadpole retinal flatmounts, the lens was removed and eye flattened using 4-8 scalpel blade cuts placed symmetrically around the eye perimeter, then pressed open between a coverslip and glass slide in Aquamount mounting media. For cryosectioning, eyes were embedded in OCT, frozen in dry ice, and then sectioned in 10 µm sections onto gelatin-coated slides. Slides were blocked for 30 min in 10% normal goat serum (NGS) in phosphate buffered serum with 0.1% BSA and 0.1% TritonX-100 (PBT), then incubated ON at 4 ^{o}C in primary antibodies diluted in PBT with 5%NGS, washed in PBT, followed by 4 hrs at RT in secondaries in PBT, additional PBT washes and counterstaining with DAPI. Primary antibodies included: Aves GFP #GFP-1020 (1:500), BD Pharmingen anti-BrdU #555627 (1:500), Clontech Living Colors mCherry #632543 (1:500), Cell Signaling Technologies P-c-Jun #9261S (1:200), and Abcam mCherry #ab167453 (1:500). Secondary antibodies included: Jackson ImmunoResearch Cy3 anti-mouse IgG #115-165-146, Jackson ImmunoResearch AlexaFluor 488 anti-chicken #103-547-008, Jackson ImmunoResearch AlexaFluor 647 anti-rabbit #111-605-144, Jackson ImmunoResearch Cy5 anti-mouse #115-175-146, and Jackson Immunoresearch Cy3 anti-rabbit IgG #111-165-144. All secondary antibodies were used at 1:250 and passed through a 0.2µm filter before use. For birthdating experiments with BrdU, 250 nL BrdU was injected into tadpoles intraperitonally at a concentration of 20 mM. For birthdating experiments with EdU, tadpoles were immersed (non-anaesthetized, free-swimming) in a solution of 0.1X MMR + 20 µM EdU for 20 minutes.

Script to quantify optic nerve and optic tecta axon degeneration and regeneration: A custom IPlab (Biovision, Exton, PA) script was created in which both tecta (crushed and contralateral) are individually traced and then their fluorescence normalized by a background subtraction step using an area of the tadpole head immediately adjacent to the tecta that lacked any melanocytes. Each tecta's fluorescence values 10% above background were subjected to a subsequent auto segmentation step which excludes all pixel values within the traced region which fall below 10% below background and thus likely represent melanocytes within the traced regions. Following this normalization, both area and mean fluorescence measurements were taken for each tecta, and the values for crushed tecta divided by the values for the contralateral tecta to return a measure of relative fluorescence of crushed tecta compared to the fluorescence of control. Lines were then manually drawn over crushed and contralateral nerves and then thickened to about two nerve diameters, normalized in length to an arbitrary value of 600, and then used to extract the fluorescence intensity values across the central 400; values at either end were excluded to account for the out-of-focus regions nearest the head and the eye which are unavoidable in live-imaging the *X. laevis* optic nerve at this stage. This was then followed by a two-step normalization. First, background subtractions are done individually for each nerve using a background location selected by user adjacent to each nerve and free of melanocytes. Next, every value on either crushed or contralateral nerve is set to a minimum value of 10 to account for any values of 0 which might have been returned from the background subtraction due to melanocytes in the ROI; this avoids division by 0 and infinitely high values in following step. Finally, the values along each of the 400 points along the nerve were divided by the value of the contralateral nerve at the equivalent location. In the case of the sparse labeling experiments, analyses were

carried out on maximal intensity projections of composites aligned manually or through the Stitching Fiji plugin. In order to compensate for large endbulbs or myeloid cells that produce sharp maxima that skewed analyses, small artifacts were manually excluded and compensated for, and histograms were smoothened by presenting all values as the average of the surrounding 50 points.

Analyses of pJun and retrograde tracer in retina sections: Custom IPlab scripts were used to analyze maximum intensity projections of 10µm retina sections. For quantifying RGC nuclear pJun, three to six sections were analyzed per retina, and the RGC area was automatically segmented using the GFP color channel, followed by autosegmentation of DAPI, to isolate the RGC nuclei. Within these RGC nuclei, and in order to avoid introduce subjective choices that could bias results, the far-red (pJun) signal was then measured as the signal above 20 different stepwise thresholds, and while results were significant at most of these and changes in magnitude larger in different ones, the ones presented are the central threshold of those that attained above $p<0.01$ significance between any two groups, similar to what we have previously done (294). In the case of Mitotracker retrograde tracing, four to six sections were analyzed per retina. In this case the GFP and Dapi were not autosegmented but were used to manually draw a line through the entire ganglion cell layer. After automatically thickening the line to approximately 2 cell diameters, the Mitotracker associated AlexaFluor signal was plotted as a function of distance from the retina periphery; to compensate for the very punctate nature of the Mitotracker signal, the histograms were smoothened by presenting all values as the average of the surrounding 50 points.

Statistical analysis: GraphPad Prism was used for graphing data and determine statistical significance for all experiments. Mean comparisons were tested for significance using a two-way ANOVA with Mann-Whitney post-test for all multi-group comparisons and a students' T-test for all two-group comparisons. For all tests, a p-value less than 0.05 was considered significant.

Data and code availability: All scripts used for image analysis are available from the Lead Contact upon request. Python cell-counting code previously published in (276) is available at https://github.com/jbmiesfeld/Atoh7-remote-enhancer.

Chapter III – Immune Cells are Essential for both Degeneration and Regeneration of Retinal Ganglion Cells in *Xenopus laevis*

Introduction

In mammalian species, the axons of retinal ganglion cells (RGCs), the sole projecting cells of the retina, are incapable of regeneration. Injuries or neuropathies which affect the optic nerve (ON) and retina therefore lead to permanent loss of RGCs and their axons, resulting in irreversible vision loss. Over the past century and a half much work has endeavored to discover ways to confer a regenerative capacity upon RGCs, and a large amount of these studies have focused upon the intrinsic molecular programming of RGCs themselves. Some factors intrinsic to RGCs seem to be neuroprotective; in studies involving experimental damage to the optic nerve, overexpression of these factors significantly enhances post-injury survival of RGC somas and axon (142, 189, 295-297). Other RGC-intrinsic factors have been found to enhance the ability of the injured axons to regrow past the injury site (152, 259). However, the regrowth seen in these instances falls far short of a full recovery. In most cases, only a few percent of axons are able to grow millimeters father than controls; and only a few rare cases have seen evidence of some axons reinnervating their targets within the brain (175, 232). Without effective regenerative therapies to regrow RGC axons, even neuroprotective factors found to increase RGC survival for several months following axonal injury are therefore ultimately futile in restoring functional vision (106).

While the molecular program of RGCs is seemingly an important factor contributing to survival and regeneration, the optic nerve environment may be just as important to regeneration, if not more so, than the intrinsic regenerative programming of the RGCs themselves. Indeed, the

most successful report of increasing RGC regeneration to date involved the grafting in of peripheral nerve fragments, which necessarily include astrocytic and myeloid cell types, grafted into the injured ON; these nerve grafts allowed full-length axonal regeneration along the ON tract and quite extensive re-innervation of brain targets (192-194). This discovery strongly suggests that the different PNS environment is permissive to axon regrowth in a way that the typical environment in the ON is not. Many later studies have investigated the question of whether immune cells within the ON in particular may play a key role in regeneration. Under healthy conditions, the ON harbors relatively few resident microglia in a ramified, non-activated state (89, 298). Following injury, however, both molecular and histological studies show a distinct increase in microglia number at the injury site (87, 298). In addition, non-resident macrophages activate, proliferate, and invade the injured area (89, 298). Importantly, classic work which found that the induction of a lens injury concurrent to optic nerve crush results in a higher degree of regeneration than with ONC alone also necessarily involves a large inflammatory response as a result of the lens injury (141). Some evidence suggests that such activated myeloid cells have little to no effect on axon regeneration (226). However, studies in the African spiny mouse (an unusual mammalian species with high regenerative capacity) and in the salamander found that depletion of macrophages compromises axonal regeneration (299, 300). In addition, there is little is known about the role of myeloid cells in axonal regeneration in regeneration-capable species. One recent study found that immune cells are important to regeneration of the retinal pigment epithelium (RPE) in zebrafish (301); but another found that the immune cell response is actually detrimental to RGC survival after optic nerve transection (302). As such, new data is needed to resolve these differing opinions regarding the role of myeloid cells in regeneration.

Here we utilize a newly-reported tadpole optic nerve crush (ONC) assay and find that immune cells mount a robust response within the tadpole optic nerve and brain within just 24 hours of injury. We find that this increase in immune cell number correlates well with the timing of accumulation and then removal of axonal debris. Most importantly, we find that ablation of the immune cell response after injury results in not only a failure to clear axonal debris, but a distinct delay in reinnervation of the optic tectum by regenerating RGCs

Results

Myeloid cells increase in the adult ON after crush

In mice, neutrophils begin to infiltrate injured CNS neurons around one day following injury, and then both infiltrating monocyte-derived macrophages and resident microglia proliferate and migrate to the site of injury within the next two days (81, 82, 84, 85). The purpose of this immune cell presence within the optic nerve is believed to be at least in part for the clearance of the large amount of membrane and myelin debris associated with both the acute injury and the subsequent degeneration of the RGCs. To determine whether a similar influx of inflammatory cells occurs in adult *X. laevis* following ONC and whether this correlates with buildup and removal of RGC axonal debris, ONs were collected at various timepoints post-ONC from adult frogs whose RGCs express dual membrane-localized GFP and mCherry transgenes (Isl2b: mem-GFP/mem-mCherry) (Figure 3.1A). Since GFP loses both fluorescence and antigenicity quickly following incorporation into acidic lysosomes, but mCherry retains these properties even at low pH, mCherry-based transgenes have previously been used by our lab as

cellular debris markers (1). Conversely, GFP transgenes can be utilized to visualize intact axons. By quantifying the sum of GFP fluorescence within the optic nerve, we demonstrate that a sharp decline in intact axons occurs at 5d post-ONC (Figure 3.1B). When we used measures of sum mCherry fluorescence within the nerve to quantify the amount of cellular debris, we found that axonal debris within the axonal parenchyma peaked at 5d post-ONC and had begun to slightly decline by 7d, thought this decline was not significant (Figure 3.1C) By contrast, axonal debris in the optic nerve sheath, defined as the region exterior to the green-labeled axons, steadily declined in the week following injury (Figure 3.1D). While further work will be needed to explore this phenomena, other studies in the lab suggest that the debris in the optic nerve sheath is a read-out for glymphatic clearance (303), and these results would suggest that upon injury the debris clearance mechanism may shift from glymphatic based to myeloid cell based.

When we looked at the density of *Bandeiraea simplicifolia (Griffonia simplicifolia)* isolectin B4 (IB4)-positive myeloid cells (microglia and macrophages) as assessed by sum fluorescence intensity measures, we find that myeloid cell presence within the nerve parenchyma is increased by 3d post-ONC and peaks at 5d post-ONC, beginning to decline again at 7d (Figure 3.1E). Furthermore, colocalization analysis of the overlap between the red and far-red signals reveals that the peak of cellular debris within myeloid cells in the parenchyma occurs at the same times, around 5d and 7d post-ONC (Figure 3.1C). Taken together, this information suggests that immune cell presence within the ON increases with increasing amounts of cellular debris and deterioration of healthy RGC axons, consistent with a phagocytic role for these infiltrating macrophages at these times.

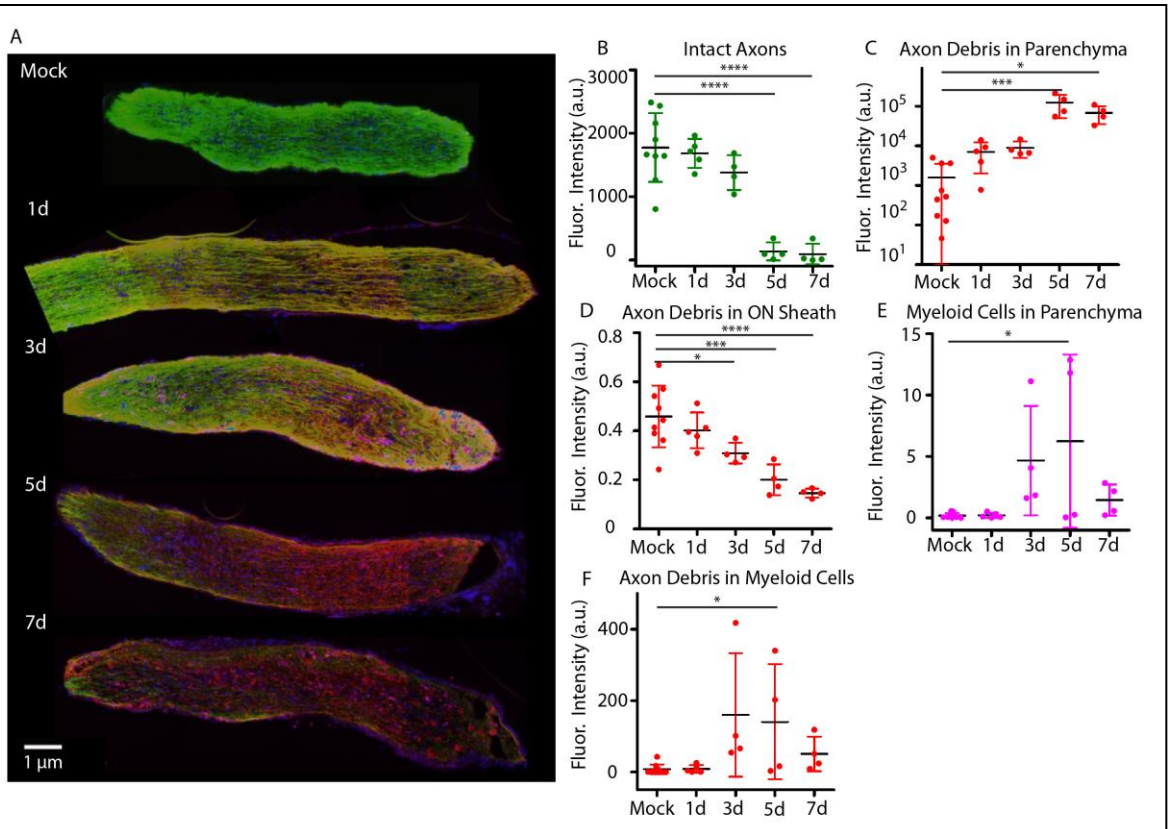

Figure 3.1. ONC results in axonal degeneration, debris accumulation and removal, and myeloid cell influx within the first week post-injury in adult *X. laevis*. A. Cryosections of adult optic nerves at various timepoints after ONC. B. Intact RGC axons as measured by GFP fluorescence have begun to degenerate by 5d post-ONC. C. The amount of RGC axonal debris within the optic nerve parenchyma, as measured by mCherry fluorescence, peaks at 5d post-ONC and is similarly elevated at 7d post-ONC. D. RGC axonal debris in the optic nerve sheath (exterior to the limits of GFP fluorescence) steadily decreases in the week following injury. E-F. Both myeloid cell presence within the parenchyma (measured by fluorescence intensity of Ib4-Cy5 labeling) and the amount of axonal debris signal colocalized with myeloid cells are highest at 3d and 5d post-ONC and declining by 7d. N = 4-8 nerves per timepoint.

Myeloid cell presence within the tadpole optic tectum also correlates with amount of axonal debris

In our previous work, we described the establishment of a novel ONC assay to study RGC axonal regeneration in the young *X. laevis* tadpole which offers both a condensed time course of regeneration compared to adult frogs and the capacity for live-imaging both the optic tectum and the optic nerve. Previously, we had determined that at 3d post-ONC, the innervation

of the optic tectum by RGC axons in the injured ON has fully disappeared, and that by 7d post-ONC, and that the tectum has become re-innervated to a level which supports functional restoration (see Chapter 2, Figure 2.1 and 2.7). However, the previous study had focused mainly on the innervation of the tectum and regeneration of the optic nerve, and not the process of degeneration itself. Work in other models has revealed that upon ON injury, RGC axons begin to fragment via Wallerian degeneration, a process which results in the production of a large amount of cellular debris (70, 274); this buildup of axonal debris was visible in our adult ONC model. To understand how axonal debris is produced and cleared in the tadpole visual system, we performed ONC in tadpoles expressing the same dual membrane-mCherry and membrane-GFP transgenes as the animals used for our adult assay (Isl2b: mem-mCherry/mem-GFP). We compared measures of mCherry fluorescence in the optic tectum connected to the crushed optic to that of the uninjured contralateral tectum to estimate the amount of axonal debris remaining in the injured tectum at various timepoints post-ONC. We found that the amount of mCherry signal steadily decreased from 1d to 3d post-ONC, and begins to increase again by 5d post-ONC, a timepoint at which our mCherry marker ceases to be a reliable measure of axonal debris, since the optic tecta is beginning to become re-innervated by regenerating RGC axons expressing newly synthesized mem-mCherry (Figure 3.2A-B).

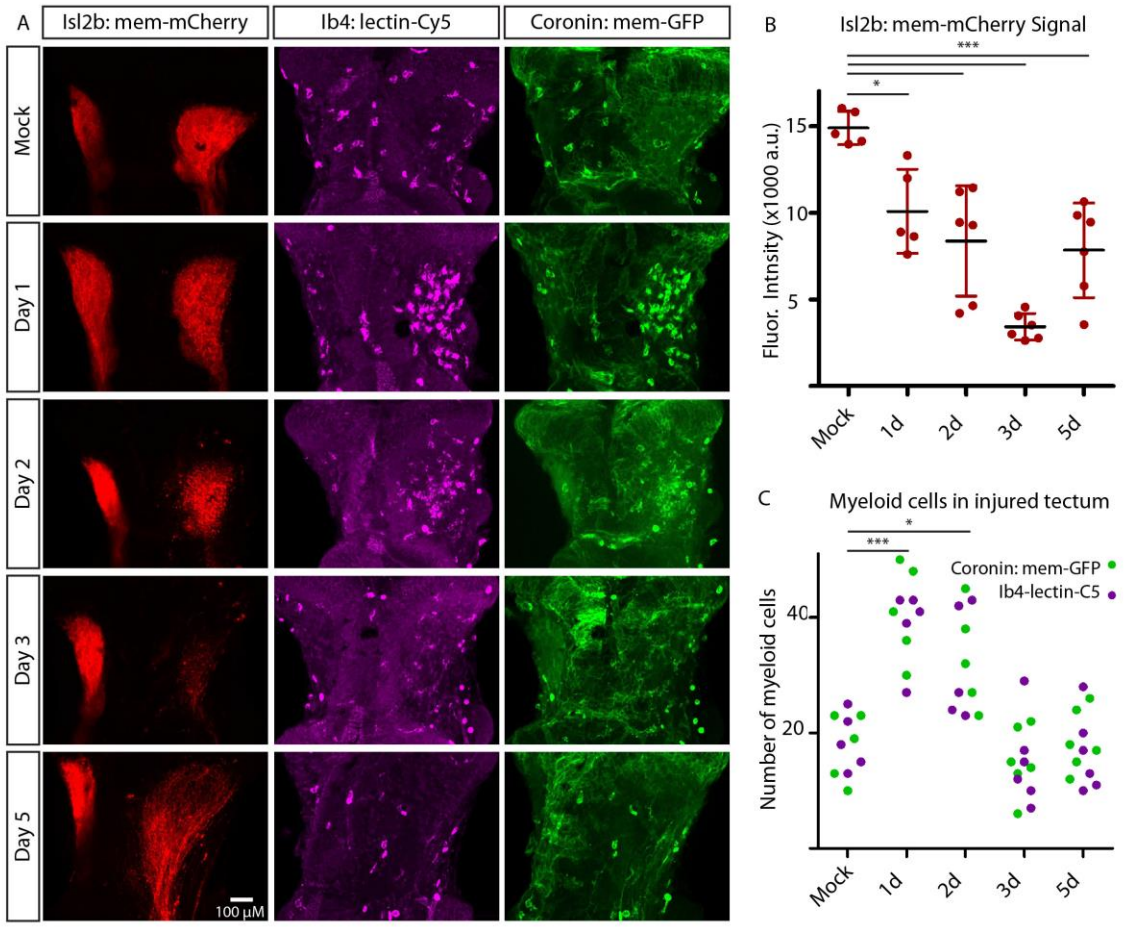

Figure 3.2. Debris accumulation and clearance correlates with myeloid cell influx into the tadpole optic tectum following ONC. A-B. Red-labeled RGC axons are cleared from the optic tectum by 3d post-ONC, and regenerating axons have begun to re-innervate the tectum at 5d post-ONC. A, C. A novel transgene to label myeloid cells with GFP labels the same population as those visualized by Ib4-Cy5 staining of *ex vivo* flatmounted optic tectum. The peak of myeloid cell presence within the injured optic tectum occurs at 1d post-ONC and by 3d post-ONC the number of myeloid cells within the injured tecta is indistinguishable from mock-crushed animals. N = 5 tecta per timepoint.

Given that in the adult model, the accumulation of cellular debris in the parenchyma (but not the ON sheath) correlates well with myeloid cell influx into the ON parenchyma, we next examined how myeloid cell influx correlates with clearance of degenerating RGC axons in the tadpole ON. In order to visualize myeloid cell presence into the tadpole visual *in vivo* as well as *ex vivo*, we developed a novel transgenic line in which the myeloid cells express a membrane-localized GFP transgene (Coronin1a: mem-GFP) and bred this to our RGCs expressing a second

membrane-localized mCherry transgene (Isl2b: mem2-mCherry) to visualize debris accumulation and clearance alongside myeloid cell presence. *Ex vivo* visualization of the optic tecta and retinas confirmed the correct localization of our transgene to the same population of myeloid cells labeled by Ib4-Cy5 staining (Figure 3.2A). Crushed optic tecta displayed a significant increase in the number of myeloid cells at 1d post-ONC, an effect that decreased over time until by 5d post-ONC, the number of myeloid cells in the tecta were indistinguishable from controls (Figure 3.2C). Thus, the amount of RGC axonal debris in the injured tectum decreases following the arrival of the myeloid cells, which supports that a major purpose of these myeloid cells within the optic tectum at this time may be to phagocytose and remove degenerating axons. Future analysis using Imaris image processing software will quantify the percentage of the axonal debris that is contained within the myeloid cells.

Myeloid cells in the retina increase, but only in small numbers and only after axonal regeneration is underway

Given the large increase in myeloid cells within the optic tectum, it was possible that the retina might experience a similar increase in immune presence in the weeks following crush. To address this, we examined the retinas of Coronin1a: mem-GFP/Isl2b:mem-mCherry tadpoles at various times after the connected optic nerve had been crushed. In contrast to the large numbers of immune cells present within the tectum within 24 hours of injury, myeloid cells were scarce in the entire week following ONC, and only by 5d post-ONC were there significantly more myeloid cells in crushed retinas than in mock-crushed retinas (Figure 3.3). That this increase occurs several days following the peak of both myeloid cell presence within the tectum and the clearance of the majority of axonal debris suggests that these myeloid cells may not be

phagocytosing dying RGCs within the retina. Indeed, given that our previous observations (see Chapter 2, Figure 2.2) suggest that little to no RGC death occurs following ONC in our tadpole model, it is likely that little debris has been produced from dying RGC cells which would require removal by immune cells. Additionally, we have previously observed morphological changes to the dendritic arborization of RGCs in cryosections of tadpole retinas which express our membrane-localized mCherry transgene in the week following injury (unpublished observations). Since at 5d post-ONC, RGC axons are again beginning to regenerate and reinnervate the optic tectum (Figure 3.2A), the increased immune cell presence at this time may be carrying out dendritic pruning of newly-established synapses created in the process of axonal regeneration, though this hypothesis will require further investigation in future.

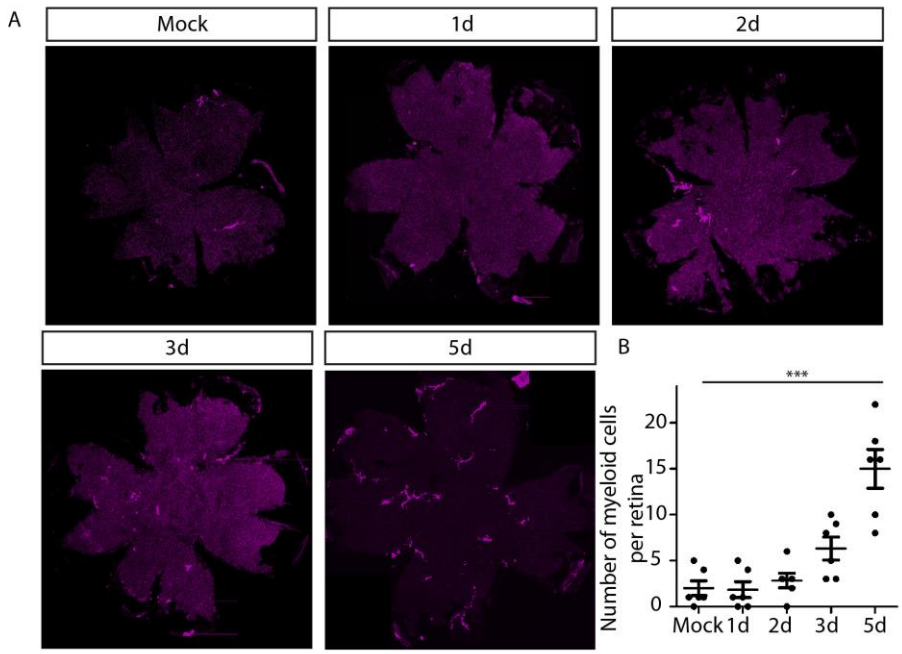

Figure 3.3. Immune cells in the retina after injury. The number of IB4-Cy5 labeled myeloid cells in the tadpole retina are significantly increased compared to mock-crushed retinas at 5d post-ONC. N = 5 retinas per timepoint.

Because our novel transgene enables live imaging of myeloid cells, we also examined the optic nerve *in vivo* and found a large increase in myeloid cells surrounding the crushed region of the ON at 1d post-ONC, an effect that had largely faded by 3d post-ONC (Figure 4). However, because the tadpole ONC surgery involves injury to the dermis and surrounding tissue of the ON as well as to the ON itself, this effect is poorly studied with our *in vivo* wholemount imaging, and the question of immune cell action within the ON will need to be re-examined in either an imaging modality capable of isolating the nerve from surrounding tissue, or in the context of a chemical or optogenetic injury context which does not damage surrounding tissue.

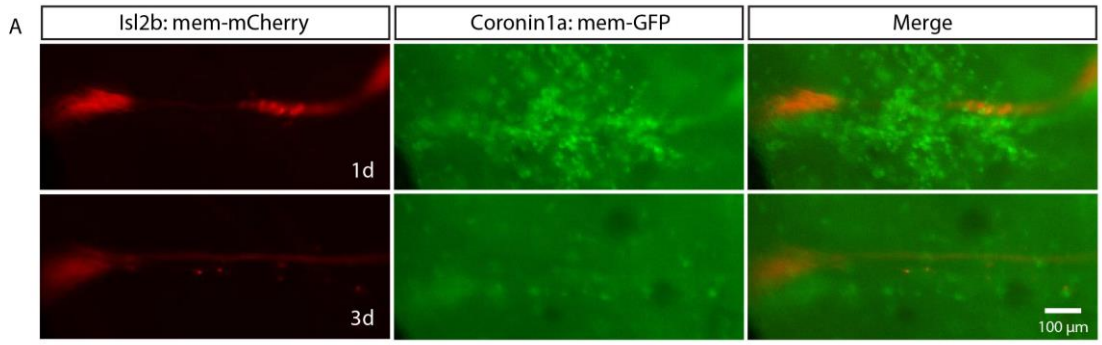

Figure 3.4 Novel transgenic line enables *in vivo* visualization of myeloid cell accumulation at the site of ONC injury. At 1d post-injury in a transgenic line in which RGCs express a membrane-localized mCherry (Isl2b: mem-mCherry) and myeloid cells express a membrane-localized GFP (Coronin1a: lynk-GFP3), myeloid cells are visible clustering in large numbers immediately proximal to the site of injury. By 3d post-injury, these clustered cells are largely absent, though small numbers remain visible along what seems to be a vascular channel immediately proximal to the optic nerve. Due to the disruption of dermis and surrounding tissue in the course of ONC surgery, disambiguation of myeloid cells responding to the damage in the ON vs. the surround environment is not possible.

Myeloid cells are present within the tadpole ON even under non-injury conditions and seem to enter the ON to clear axonal debris

Alongside the large increase in myeloid cells in the tadpole OT and retina following optic nerve injury, we noticed that a small number of myeloid cells were present within both the tectum and retina even under non-injury conditions. We thus questioned whether myeloid cells

were similarly present within the tadpole ON under non-injury conditions. Because of the very small size of the optic nerve at this age (< 50 µm in diameter), *ex vivo* methods to visualize the nerve which would be directly analogous to our flatmount preparations of the tadpole tecta and retina were not be possible. We therefore utilized live-imaging to visualize myeloid cell movement in the naïve optic nerve in a triply-transgenic line in which immune cells express membrane-localized GFP (Coronin1a: mem-GFP) and astrocytes express both membrane-localized BFP (Blbp: mem-BFP) and an mCherry-tagged, dominant-negative version of the astrocyte-secreted debris marker Milk Fat Globule EGF And Factor V/VIII Domain Containing, Mfge8 (Blbp: Mfge8DN-mCherry), which reports the presence of membranous debris as this protein binds extracellular phosphatidylserine (1). We found that myeloid cells are present both adjacent to the nerve, presumably in vascular tissue, and within the nerve itself. Moreover, these immune cells within the nerve frequently colocalize with accumulations of mCherry signal,

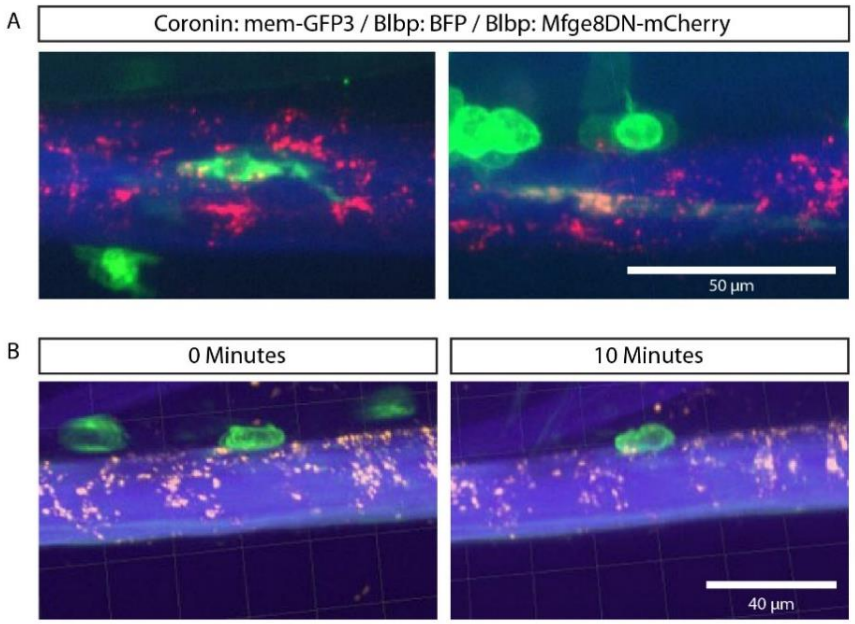

Figure 3.5. Myeloid cells are visible within the tadpole optic nerve even in uninjured state and seem to move and engulf mCherry-tagged debris. A. A triple-transgenic line in which astrocytes express cytoplasmic BFP (Blbp: BFP) and a dominant-negative version of the astrocytic-secreted phagocytic marker Mfge8 (Blbp: Mfge8DN-mCherry (1)), and immune cells express a membrane-localized GFP (Coronin: lynk-GFP3), myeloid cells are seen within the ON (as delineated by BFP fluorescence) and colocalized with large deposits of debris. B. When visualized over time, individual myeloid cells within the optic nerve can be seen migrating towards and overlapping with debris deposits.

suggesting that they may be actively phagocytosing cellular debris produced within the nerve (Figure 3.5A) In addition, time-lapse imaging shows that myeloid cells within the nerve move over time and overlap with accumulations of mCherry-labeled debris at later timepoints, further pointing towards an active phagocytic role (Figure 3.5B). While further time-lapse and 3D colocalization analysis is needed to confirm these impressions, these data suggest that even under naïve conditions myeloid cells will enter the nerve to phagocytose and clear debris.

Novel transgene enables inducible ablation of myeloid cells

The increased immune cell presence within the visual system at times and locations in which disconnected axonal segments are degenerating into cellular debris suggests that myeloid cells play a major role in the process of degeneration and potentially regeneration of RGC axons following injury. Thus, to determine the role of immune cells within the visual system following injury, we developed a novel transgenic line to inducibly ablate myeloid cells by expression of an optimized bacterial nitroreductase (epNTR) under the control of the same myeloid cell-specific promoter utilized previously (Coronin1a: mCerulean-epNTR) (304). When metronidazole is added to the tadpole media, it is cleaved by epNTR into a toxin that then kills the expressing cells. However, metronidazole when administered at the standard concentration of 10 mM has been found to be toxic when used for prolonged periods in transgenic zebrafish carrying the NTR transgene in various cell types (305). To address this issue, previous work had found that a second compound, nifropirinol, may be more effective and less toxic than metronidazole, and can be administered at concentrations orders of magnitude lower than metronidazole (306). We thus tested the relative toxicity of metronidazole and nifropirinol to young tadpoles when administered continuously through the second week post-fertilization (8-15

dpf). Metronidazole at 5 mM and nifropirinol at 1 uM both resulted in 10-30% attrition of Coronin: mem-GFP tadpoles by 4 days of administration, which reached 50% attrition of tadpoles at the 7 day endpoint (Figure 3.6A). Wt tadpoles showed no attrition when subjected to either drug, suggesting that the toxicity was due not to the drug itself, but rather stemmed from either the systemic loss of immune cell presence, or a byproduct resulting from myeloid cell death which proves toxic to surrounding cells. Administration of either drug at lower doses did not affect survival; however, lower doses took 48-72 rather than 24 hours of administration hours to observe a near-compete level of myeloid cell ablation (data not shown).

A

Animals Remaining with Continous Nifropirinol or Metronidazole for 7d

	0d	1d	2d	3d	4d	5d	6d	7d	% Survival at 7d
Coronin: NTR +Nifropirinol 1uM	10	10	10	10	9	7	6	5	50%
Wt +Nifropirinol 1uM	10	10	10	10	10	10	10	10	100%
Coro +Nif 0.1 uM	10	10	10	10	10	10	10	10	100%
Wt +Nif 0.1 uM	10	10	10	10	10	10	10	10	100%
Coronin: NTR +Metronidazole 5 mM	10	10	10	10	10	6	6	5	50%
Coronin: NTR +Metronidazole 1mM	10	10	10	10	10	10	10	10	100%
Wt +Metronidazole 5mM	10	10	10	10	10	10	10	10	100%
Coronin: NTR No Drug	10	10	10	10	10	10	10	10	100%

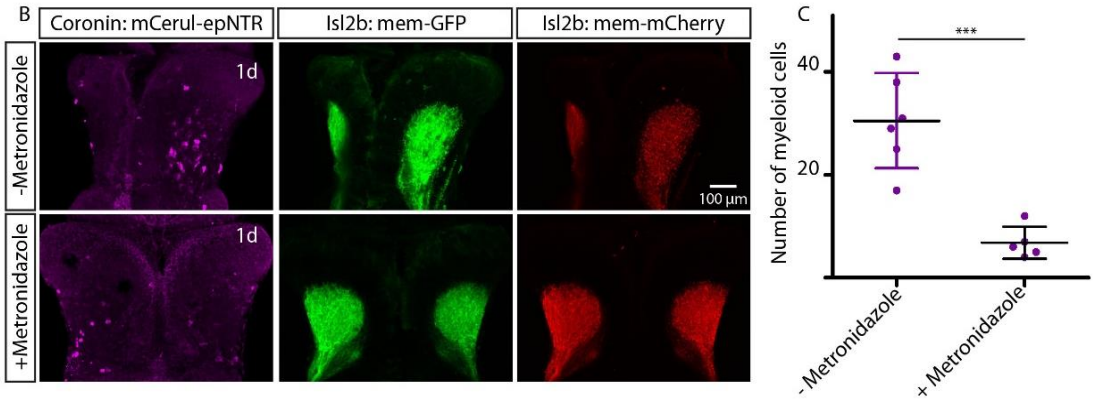

Figure 3.6. Novel transgene enables inducible ablation of myeloid cells. A. A novel transgene line in which myeloid cells constitutively express a fluorescently-tagged nitroreductase (Coronin1a: mCerulean-epNTR) addition of either metronidazole or nifropirinol to the tadpole media kills immune cells as the NTR is cleaved into a cellular toxin. Pilot experiments to determine the relative toxicity of metronidazole and nifropirinol to *X. laevis* tadpoles find that either drug at high concentrations (5 mM metronidazole or 1 uM nifropirinol) results in 50% attrition with 7 days of drug application. B-C. Addition of 5 mM metronidazole to rearing media blocks the usual influx of myeloid cells into the tadpole optic tectum 1d post-ONC in *X. laevis* tadpoles whose RGCs express membrane-localized GFP and membrane-localized mCherry (Isl2b: mem-mGFP/mem-mCherry). N = 5 metronidzole-treated and 6 untreated tecta.

Given the lack of improvement in attrition with nifropirinol treatment and the more established precedent for usage of metronidazole in such experiments, we selected 5 mM metronidazole to achieve ablation of immune cells in our model. To quantitatively measure our ability to ablate myeloid cells with this treatment *in vivo,* we generated tadpoles carrying both the myeloid-cell expressed NTR transgene and also expressing dual membrane-localized mCherry and membrane-localized GFP in their RGCs (Coronin1a: mem-GFP/Isl2b: mem-mCherry/mem-GFP). We pre-treated tadpoles with either 5 mM metronidazole or vehicle for 24 hours pre-ONC, and then examined the optic tecta *ex vivo* at 1d post-ONC for IB4-lectin labeled myeloid cells. The treated tadpoles displayed significantly lower levels of myeloid cells in the injured tecta compared to untreated tadpoles at 1d post-ONC, demonstrating that the NTR transgene is capable of virtually completely eliminating myeloid cell influx at this timepoint (Figure 3.6B). Interestingly, the appearance of the mCherry signal in treated tadpoles was less granular than in untreated tadpoles, suggesting that there may already be a difference in the degeneration of the RGC axons at this early stage.

Elimination of myeloid cells inhibits both degeneration and regeneration of the optic tectum and optic nerve following ONC

Given the ability of our novel transgenic line to block immune cell infiltration into the tadpole optic tectum, we could determine whether loss of myeloid cells resulted in either a degeneration or a reinnervation defect in the optic tectum. For these experiments, we again utilized triply-transgenic (Coronin1a: mem-GFP/Isl2b: mem-mCherry/mem-GFP) animals and at 7dpf treated tadpoles with either 5 mM metronidazole or control media for 24 hours pre-ONC to ablate myeloid cells. We then imaged the optic tectum and nerve *in vivo* at 1d, 2d, 3d, 5d, and 7d

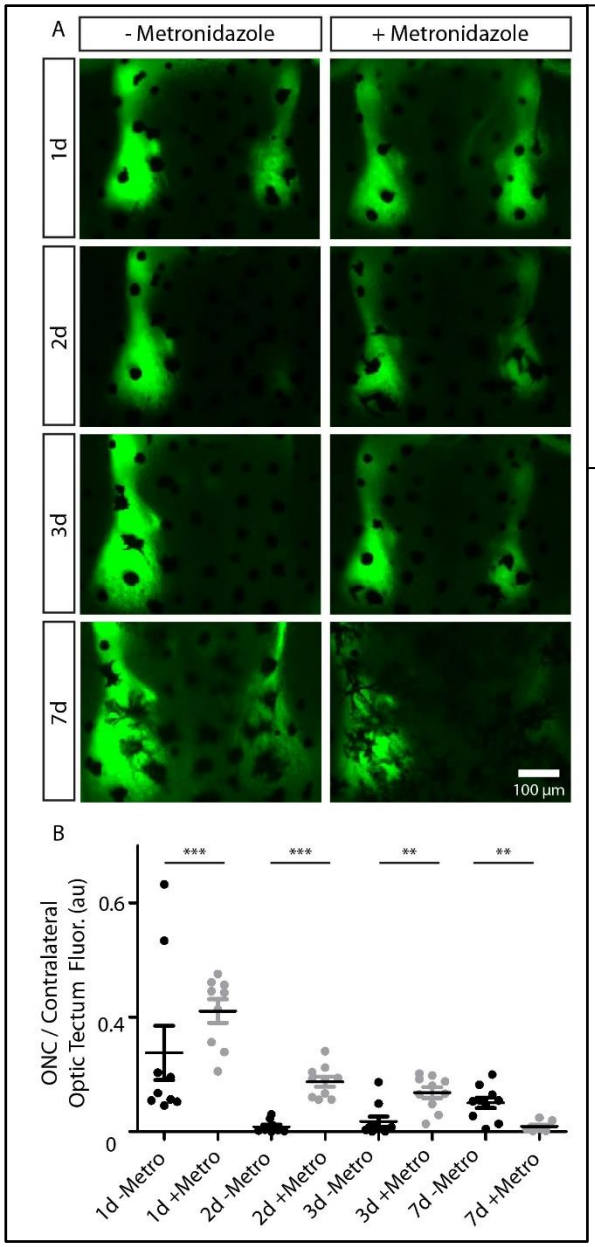

Figure 3.7. Loss of myeloid cells delays both denervation and reinnervation of the optic tectum. A-B. Ablation of myeloid cells in Coronin: mCerulean3-epNTR/Isl2b: mem-GFP/mem-mCherry tadpoles by addition of Metronidazole from 7dpf to 11 dpf (1 day prior to ONC and up until 3d post-ONC) results in delayed degeneration of the optic tectum connected to the crushed optic nerve at 2d and 3d post-ONC. At 7d post-ONC, the injured optic tectum of metronidazole-treated animals has received significantly less reinnervation from regenerating RGCs than has the optic tectum of tadpoles which have never received metronidazole. N = 8-10 tadpoles per

post-ONC to visualize both degradation of intact RGC membranes in the optic tectum and optic nerve (GFP signal) and the accumulation and clearance of cellular debris from the optic nerve (mCherry signal). We discontinued metronidazole treatment immediately following the 3d imaging collection series due to the attrition observed in our early pilot experiments; however, despite this, *in vivo* imaging showed total lack of myeloid cells in treated animals even up through the 7d timepoint (data not shown).

At 2d post-ONC, the metronidazole-treated tadpoles displayed significantly higher GFP fluorescence in the injured optic tecta compared to the contralateral uninjured tectum than did the control tadpoles (Figure 3.7). At 3d post-ONC, the injured optic tecta of the untreated tadpoles was almost completely devoid of GFP signal, indicative of RGC axonal degeneration, but the injured optic tecta of treated tadpoles still retained 40% of the fluorescence intensity of the contralateral tectum. Strikingly, by 7d post-ONC, while the untreated tadpoles had begun to re-

innervate the optic tectum, with the injured optic tectum averaging a relative fluorescence intensity of 30% compared to the uninjured contralateral tectum, there was little to no re-innervation apparent in treated tadpoles, with the relative fluorescence intensity of the injured tecta only 5-10% that of the contralateral. Thus, it seems that the loss of myeloid cells impairs the removal of RGC axonal remnants from the injured tecta, as well as reinnervation of the tecta by regenerating RGC axons (Figure 3.7). The experiment is currently being repeated at the time of thesis submission.

To assess whether a similar delay in regeneration or degeneration was evident in the optic nerve, we utilized our previously reported optic nerve tracing quantification process. In brief, first the crushed and contralateral nerves were each traced and scaled to equal lengths, and then fluorescence values compared across the length of the crushed nerve to equivalent positions along the contralateral nerve. In this case, we then demarcated a single consistent region of each nerve which corresponded to an area directly distal of the crush site and calculated a single average fluorescence intensity of the 50 crushed/control values (or 1/8 of total nerve length) in this area to enable direct comparison of the same nerve region metronidazole-treated to untreated tadpoles. When we compared these measures at 2d post-ONC, the crushed/control GFP fluorescence ratio of untreated tadpoles was significantly lower than that of metronidazole-treated tadpoles (Figure 3.8A). This same retention of GFP signal in the crushed nerve of treated tadpoles was retained at 3d, though at slightly lower significance, which we predict may be due to the loss of GFP protein levels over time as the severed axonal segments are expected to be compromised in their ability to synthesize new GFP, rather than due to clearance of degenerating RGC axons. At 7d post-ONC, the ratio of crushed/control GFP fluorescence was similar in treated and untreated tadpoles; however, overall fluorescence levels were lower in the treated

animals, suggesting a possible systemic health effect to the metronidazole treatment (data not shown).

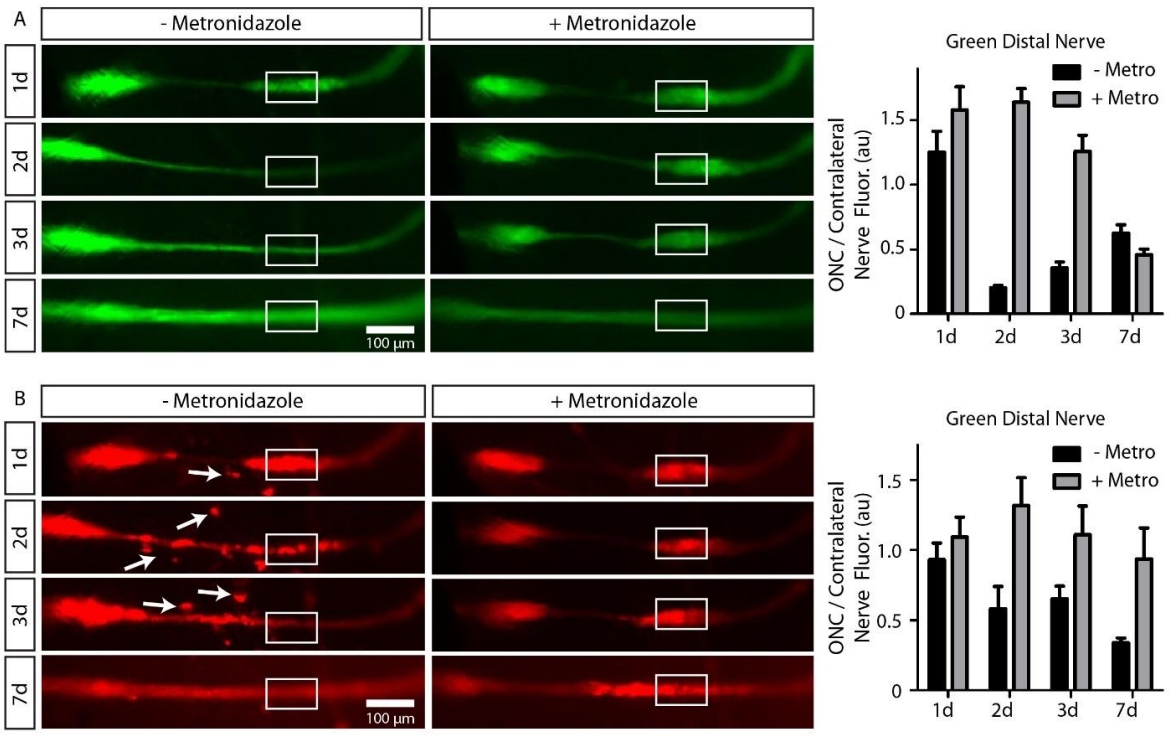

Figure 3.8. Ablation of myeloid cells delays optic nerve degeneration and removal of axonal debris after ONC in *X. laevis* tadpoles. A-B. Intact axons, as measured by the ratio of GFP fluorescence of the crushed/contralateral nerves in a region immediately distal to the crush injury (white boxes), are not removed by 3d post-ONC in metronidazole-treated tadpoles as they are in untreated controls. C-D. Significantly more mCherry signal remains in the distal portion of the crushed nerve of metronidazole-treated tadpoles at 7d post-ONC. Further, treated tadpoles do not display the focal highly bright accumulations of mCherry signal along the nerve at 2d and 3d post-ONC that untreated tadpoles do. N = 8-10 tadpoles per timepoint.

When we used the same measure to compare mCherry fluorescence in the same location, the ratio of crushed/control mCherry fluorescence treated tadpoles was again higher at 2d and 3d post-ONC, and this difference persisted at 7d post-ONC, suggesting that even at this late timepoint, removal of axonal debris had been unable to proceed to completion (Figure 3.8B). Furthermore, in the untreated tadpoles, distinct bright deposits of mCherry signal were visible along the attenuated distal and middle regions of the ON at 2d and 3d post-ONC, with other focal

accumulations of mCherry signal nearby the nerve. These bright focal deposits were not seen at any timepoint in the metronidazole-treated tadpoles. We hypothesize that these mCherry accumulations are likely debris contained within myeloid cells, and without immune cells present to collect and phagocytose debris these aggregations are not seen. Taken together, our results indicate that immune cells are necessary to phagocytose and clear RGC axonal debris following an injury, and that the lack of these cells impairs the ability of RGCs to regenerate their axons and to reinnervate the optic tectum.

Discussion

Whether a robust immune response is essential to mount an effective axonal regeneration response is an important and still incompletely answered question regarding optic nerve injury and disease. Here we report that in the regeneration-capable model *Xenopus laevis*, immune cells proliferate or infiltrate within the optic tectum within just 24 hours of injury and are largely absent one week following. We further find that this immune cell response is necessary for both the degeneration and removal of RGC axonal fragments in the optic tectum and optic nerve post-ONC and for the reinnervation by RGC axons of their targets within the optic tectum.

Although the removal of cellular debris by phagocytosis is a major functional role of both infiltrating monocyte-derived macrophages and resident microglia within the PNS and the CNS (13, 16, 229), other cell types and processes may contribute to debris clearance alongside or in the absence of immune cell action. For example, previous work in the lab found that during metamorphosis, astrocytes rather than Ib4+ cells are responsible for the majority of debris clearance from the optic nerve (1). However, the long persistence of intact RGC axonal fragments for days following ONC (as indicated by GFP fluorescence) in both the optic tectum

and the optic nerve of young *X. laevis* tadpoles in the absence of myeloid cells suggest that after injury immune cell action is the primary process by which cellular debris is removed. In the adult nerve, there was a decrease in the amount of debris in the optic nerve sheath concomitant with the increase in debris and myeloid cells within the optic nerve parenchyma. This suggests that maybe the role of the astrocytes, under non-injury conditions, is to mobilize debris out towards the optic nerve sheath, were myeloid cells reside, but that after injury that pathway is no longer active as the myeloid cells themselves invade into the parenchyma to fetch the debris themselves. Most importantly, the observed defect in tectal reinnervation in the absence of myeloid cells at 7d post-ONC suggests myeloid cells are also essential for RGC axonal regeneration, something which has been widely assumed or implied but not formally demonstrated.

Two possibilities for this mechanism are suggested here. One, because RGC axonal regeneration seems to initiate after the majority of tectal and axonal debris has been cleared and myeloid cell numbers have dropped to baseline levels, it is possible that regeneration cannot be achieved until cellular debris has been cleared, and that myeloid cells are necessary only for this removal. However, the presence of a large amount of axonal debris in the proximal nerve segment even at 7d post-ONC (Figure 3.8B), at which timepoint there is no significant difference between GFP fluorescence of the distal portion of myeloid-deficient tadpoles compared to myeloid-competent controls, does suggest that this debris may not be significantly inhibiting regrowth of RGC axons through the optic nerve per se. Thus, the other possibility is that the myeloid cells themselves may be performing a critical signaling function to induce RGC axonal regeneration. In fact, neutrophils, the first infiltrating monocyte-derived macrophages to arrive at the optic nerve following injury in mammals, are known to release oncomodulin to recruit

further immune cells to the injury site (82). This oncomodulin signal, or some as-yet unknown signaling molecule, could be a critical component of RGC axonal regeneration initiation. Future work will focus on dissecting the mechanism for the necessity of immune cells to degeneration and regeneration of RGC axons.

Methods

Animals

Wild-type and genetically modified *Xenopus laevis* lines were housed in an investigator-maintained facility at UC Davis, and all work was carried out in accordance to protocols approved by the local IACUC. Transgenic *Xenopus* lines were created by restriction enzyme mediated integration (REMI) as first described in (291). Transgenic constructs and lines to express a cytoplasmic GFP in RGCs, Tg(Isl2b:GFP), and a membrane localized mCherry in RGCs, Tg(Isl2b:Mett7l-mCherry) here referred to as Tg(Isl2:mem-mCherry), have been previously described (250) and (1). Transgenic constructs and lines to create a dominant-negative, mCherry-tagged version of the astrocyte-secreted protein Mfge8 (Milk Fat Globule EGF And Factor V/VIII Domain Containing) within astrocytes (Blbp: Mfge8DN-mCherry) have been previously described (1). Transgenic lines to optimally label RGC axons with a membrane-localized GFP, here referred to as Tg(Isl2):mem-GFP, are described in the Methods for Chapter 2. As in those Methods, since the line used for most regeneration studies has a mem-GFP and mem-mCherry transgenes inserted into the same locus, these animals are here referred to as Tg(Isl2b:mem-GFP/mem-mCherry).

To create a second transgenic line which expresses membrane-localized mCherry in RGCs, Tg(Isl2b: Gap43-mCherry (here referred to as Tg(Isl2b:mem2-mCherry), the Blbp promoter of

pCS2(Blbp):mCherry-Gap43 (1) was replaced with the Isl2b RGC promoter (250) previously published.

To transgenic line which expresses membrane-localized GFP in myeloid cells (pCS2(Coronin1a): lynk-GFP, here referred to as Tg(Coronin1a): mem-GFP), a 7115 bp sequence was amplified from zebrafish genomic DNA using primers acgacgctcgagAGCAACAACGTTCTAAGAGA and acgacgggatccGATGACCTGAGGAAAGACA, and TA cloned into using the pGEM-T Easy kit. This sequence was then amplified from pGEM-T: zfCoronin1a using primers GCTATTACGCCAgtcgacAGCAACAACGTTCTAAGAG and cccatggtggcAAGCTTGATGACCTGAGGAAAGAC. pCS2 (Blbp): lynk-GFP3 was digested with HindIII and SalI to remove the Blbp promoter and the amplified Coronin-promoter containing fragment ligated into its place using Gibson assembly (307).

To create a construct to ablate myeloid cells by expression of a bacterial nitroreductase, Addgene plasmid #62213 (pCS2-epNTR) (304) was amplified using primers ggaggaggaggaagtagtATGGATATTATTAGTGTGGC and GGTGGCGGATCCTGCAAAAAGAAC. A 783-bp fragment was then amplified around mCerulean3 from pCS2(CA600): mCerulean3 using primers GTTCTTTTTGCAGGATCCGCCACCATGGTGAGCAAGGGC and actacttcctcctcctccCTTGTACAGCTCGTCCATG. These two fragments were ligated together using Gibson assembly to create pCS2(CMV): mCerulean3-epNTR. The CMV promoter of this construct was then exchanged for the zfCoronin1a promoter using BamHI/Sal to digest the vector pCS2(CMV):mCerulean3-epNTR and XhoI/SalI to excise the zfCoronin1a promoter from pGEMT: zfCoronin1a.

To create a transgenic line in which astrocytes express cytoplasmic BFP (pCS2(Blbp): BFP-Ras), pCS2(xtFapb7):mTagBFP2-Ras: BFP from pBAD-mTagBFP2 (Addgene plasmid #34632; http://n2t.net/addgene:34632 ; RRID:Addgene_34632) (Subach et al., 2011), was amplified using FK99 and FK96 and cloned into HindIII and BglII sites of a pCS2 vector. The oligonucleotides encoding BglII-Ras farnesylation sequence (AAGCTGAACCCTCCTGATGAGAGTGGCCCCGGCTGCATGAGCTGCAAGTGTGTGCT CTCCTGA) -XbaI was inserted into BglII and XbaI sites of the vector by using complementary oligonucleotides. Then the full cDNA of mTagBFP2-Ras and SV40 polyadenylation sequence was placed in between HindIII and NotI sites of pCS2(xtFabp7) vector.

Method Details

***Xenopus* husbandry, breeding and egg/embryo collection:** All *Xenopus* work was carried out as previously described in the Methods for Chapter II.

Adult *Xenopus* ONC: For adult frog ONC, the procedure was carried out as previously described (250, 269, 270). In brief, animals were anaesthetized in 0.5 g/L tricaine solution (MS222). A small incision was made in the roof of the mouth using a sharp scalpel blade, followed by blunt dissection of the muscle and tissue layers using forceps to access the optic nerve, taking care to avoid injuring major blood vessels. The optic nerve was crushed for 4 seconds using #2 forceps. Animals were then allowed to recover in filtered 0.1x Modified Marc's Ringer (MMR) solution for 1 day before being returned to the drip-through tanks until day of euthanasia.

Young tadpole *Xenopus* ONC: Tadpole ONC assay was performed as previously described in the Methods of Chapter 2. In brief, tadpole was anaesthetized with 0.2 g/L tricaine in filter-sterilized 0.1x MMR solution and mounted on a custom stability plate beneath and between two small fragment of anesthetic-soaked Kimwipe for stability and to prevent drying. ONC was performed using a fluorescent Leica stereomicroscope to visualize the fluorescent ON. Two glass needles pulled and cut to 50-75 µm thickness and beveled to a 20 degree angle were mounted on micromanipulators to perform the crush. Tadpoles were allowed to recover in filtered 0.1x MMR + 20 mM HEPES + 50 mg/mL Gentamicin at 16 degrees for 12-15 hours. Following imaging 1d post-ONC, tadpoles were then kept at room temperature on a 12/12 hour light-dark cycle for the duration of the experiment.

Drug treatments: To ablate immune cells with Metronidazole in the Coronin1a: mCerulean-epNTR transgenic line, tadpoles were kept in filtered 0.1x MMR + 0.1% DMSO plus addition of either 5 mM Metronidazole or 1 mM Metronidazole. Control animals were kept in in filtered 0.1x MMR + 0.1% DMSO from 8dpf until 7 dpf. To ablate immune cells with nifropirinol, a stock solution of 1 mM nifropirinol was prepared in DMSO and then diluted to appropriate working concentration of either 1 µM or 0.1 µM in filtered 0.1x MMR. All solutions and glass bowls were changed daily. For experiments involving ONC in the Coronin1a: mCerulean-epNTR transgenic line, metronidazole-treated tadpoles were kept in filter-sterilized 0.1x MMR + 5 mM Metronidazole + 0.1% DMSO + 2 mM HEPES + 50 µg/mL from 1 day pre-ONC to 3d post-ONC, and then moved into filter-sterilized 0.1x MMR + 2 mM HEPES + 50 µg/mL gentamycin for the remainder of the experiment. Control animals were kept in filter-sterilized

0.1x MMR + 0.1% DMSO + 2 mM HEPES + 50 µg/mL Gentamicin from 1d pre-ONC to 3d post-ONC and then moved to 0.1x MMR + 2 mM HEPES + 50 µg/mL Gentamicin for the remainder of the experiment.

Live imaging: For lower resolution *in vivo* assessment of optic tecta and optic nerve denervation and reinnervation tadpoles were anaesthetized with 0.2 g/L MS-222 in 0.1x MMR and positioned in the same setup described above for tadpole ONC surgery. A Leica MZ10F fluorescent stereomicroscope was used with a PlanApo 1.0x lens with custom iVision scripts to capture images using a Qimaging Retiga-Exi Monochrome Cooled 12-Bit camera (RET-EXI-F-M-12-C). These scripts prompted operators to focus and photograph each nerve and tecta individually using both GFP and mCherry filtersets. For the high-resolution imaging of myeloid cells within axons, animals were also anesthetized with 0.2 g/L MS-222 in 0.1x MMR and then immobilized in 30 x 15 mM plastic dishes with custom Sylgard silicone molds previously created using gluteraldehyde fixed animals and extensively washed. These molds, with the addition of round 12mm glass coverslips atop the animal and mold for stability, oriented the animals in such a way that the left nerve was parallel to the focal plane of a 40x/1.1 N.A. water immersion objective on a Dragonfly spinning disc confocal microscope (Andor, model DMi8 automated). T-stack images for each animal recorded for 1 min at 1 Hz. Z-stack images scanned the entire length of visible nerves in 3-4 overlapping sections, scanning the entire thickness of the ON at each location at 1 µm steps, and using 2-frame averaging to increase resolution.

Slide imaging. For imaging of cryosectioned adult optic nerves, a minimum of 3 and an average of 4 sections were imaged per optic nerve at 20x magnification using an Axiovision fluorescent

microscope using custom IPlab scripts. An average of 4 images were taken of each ON to visualize the entire length and then stitched into composites.

Ex vivo analyses. For adult optic nerve dissections, animals were euthanized by tricaine overdose followed by decapitation. Optic nerves were removed and fixed in 4% PFA overnight at 4 ^{o}C, then moved into 30% sucrose solution in PBS. For cryosectioning, the nerves were embedded in OCT, frozen in dry ice, and then sectioned in 10 µm sections onto gelatin-coated slides. Slides were blocked for 30 min in 10% normal goat serum (NGS) in phosphate buffered serum with 0.1% BSA and 0.1% TritonX-100 (PBT), then incubated ON at 4 ^{o}C in primary antibodies diluted in PBT with 5%NGS, washed in PBT, followed by 4 hrs at RT in secondaries in PBT, additional PBT washes and counterstaining with DAPI. For tadpole tissue dissections, animals were euthanized by tricaine overdose and fixed in 4% PFA for 4 hours at 4 ^{o}C for cryosectioning or 1 hour at 4 ^{o}C for retinal flatmounts. After fixation, eyes and/or brains were removed using 00 insect pins and placed in methanol overnight or longer at -20 ^{o}C (for flatmounts). For tadpole brain flatmounts, glass slides were prepared by using small pieces of waterproof tape with circular cutouts so that tectum could be placed within cutout and allow coverslip to rest slightly above tectum for allow for minimal flattening and distortion. Tadpole was mounted in Aquamount within cutouts beneath a glass coverslip. For tadpole retinal flatmounts, the lens was removed and eye flattened using 4-8 cuts placed symmetrically around the eye perimeter, then pressed open between a coverslip and glass slide in Aquamount mounting media. Primary antibodies included: Aves GFP #GFP-1020 (1:500), BD Pharmingen anti-BrdU #555627 (1:500), Clontech Living Colors mCherry #632543 (1:500), Cell Signaling Technologies P-c-Jun #9261S (1:200), and Abcam mCherry #ab167453 (1:500). Secondary

antibodies included: Jackson ImmunoResearch Cy3 anti-mouse IgG #115-165-146, Jackson ImmunoResearch AlexaFluor 488 anti-chicken #103-547-008, Jackson ImmunoResearch AlexaFluor 647 anti-rabbit #111-605-144, Jackson ImmunoResearch Cy5 anti-mouse #115-175-146, and Jackson Immunoresearch Cy3 anti-rabbit IgG #111-165-144. All secondary antibodies were used at 1:250 and filtered through 0.2 μm before use.

Quantification and Statistical Analysis

Script to quantify tadpole optic nerve and optic tecta axon degeneration and regeneration: These scripts were used as previously described in the Methods for Chapter 2.

Script to quantify adult optic nerve intact axons, axonal debris, and myeloid cell influx: Custom IPlab scripts was created in which each composite image (produced by stitching together of all images per section of a given nerve) was traced around first the limits of all fluorescence signal, and then around the limits of the GFP signal only; the region between the outer limits of the GFP signal and the outer limits of the entire nerve was designated as the optic nerve sheath. Both area and mean measurements were then taken of the red, green, and far- red signal in each area at multiple segmentations (thresholds). Finally, a percentage overlap between the red and far-red signal in the region designated as parenchyma was calculated to estimate the amount of debris contained within myeloid cells. The results per nerve were first averaged across all sections for that nerve using Excel. For simplicity, the data presented are only for the one segmentation value which best approximates the mean fold change of segmentations that revealed significant changes.

Script to quantify myeloid cells and axonal debris in flatmount tadpole tecta and retinas: A custom IPlab script was created in which the tadpole tecta was traced and then normalized with a background subtraction step using a region immediately adjacent to the tecta. Both area and mean measurements were then taken for the red signal within the traced region. The same traced region was then manually counted for myeloid cells in the green and far-red channels separately by drawing small segment circles for each myeloid cell and counting the number of these segments drawn in each channel. Counts of myeloid cells within flatmounted retinas were carried out using a similar script which was identical except in that it did not also include measurement of red fluorescence signal.

Statistical analysis: GraphPad Prism was used for graphing data and determine statistical significance for all experiments. Mean comparisons were tested for significance using a two-way ANOVA with Mann-Whitney post-test for all multi-group comparisons and a students' T-test for all two-group comparisons. For all tests, a p-value less than 0.05 was considered significant.

Appendix I: Translational Profiling Comparison of *Dlk* KO to WT Animals Post-ONC

Forward

Experiments involving translational profiling of RGCs were originally proposed in a different (and admittedly somewhat more ambitious) format for my Qualifying Exam (QE) proposal in the spring of 2017. However, following my QE, we found unexpected success in what was then Aim 2 of my proposal (creation of global CRISPR KO models to allow fast screening of putative regeneration-associated factors), which led us to the discovery that *dlk* is necessary for *X. laevis* optic nerve regeneration and thus the preparation of Chapter II of this dissertation. The findings of that paper strongly suggested that the major mechanism of *dlk* action within RGCs was activation of a transcriptional program intrinsic to RGCs. Thus, translational profiling of RGCs will still be an important part of the future work of the lab, but now requires alteration given this new information about a known regeneration-critical gene which can be leveraged in the work. What follows is a proposal for a project-in-progress which will use translational profiling of RGCs to map out differences in the transcriptional response downstream of the *dlk* axonal injury signal which are likely to be crucial effectors of the regenerative response in *X. laevis.*

Significance and Specific Aims

While humans and other mammals cannot regrow damaged central nervous system (CNS) axons once they are injured, some species, including zebrafish (*Dario renio*) and the African clawed frog (*Xenopus laevis*), exhibit an extraordinary capacity for CNS regeneration. The relatively close evolutionary distance between these species suggests the tantalizing

possibility that the same molecular "blueprint" for regenerating RGCs in fish and frogs may be induced to do the same in mammalian species. The overarching goal of this project is to identify and functionally test the most important molecular factors regulating optic nerve regeneration.

In **Aim 1**, I will map the changes in the translational program of RGC signaling in the first week following optic nerve crush (ONC) injury in *X. laevis*. My approach is cell-type specific, thus avoiding confounding issues of previous investigations which were unable to distinguish between the (likely vastly different) responses of several cell types. It is also unbiased and comprehensive, utilizing an RNA-sequencing protocol in order to detect only actively translating mRNAs without introducing the selective bias inherent in other approaches. The identification of early key injury-responsive genes in this manner will enable us to prioritize genes for future study.

In **Aim 2**, I will expand upon a previous study by comparing the post-injury translational responses of Wt animals to animals which lack dual leucine zipper kinase (*dlk*), an axonal injury signal which we have previously found to be both intrinsic to RGCs and indispensable for RGC axonal regeneration in *X .laevis*. By understanding how lack of *dlk* affects the activation of signaling pathways upon injury, we will be able to generate a list of targets dependent upon Dlk which could be potential therapeutic targets for achieving optic nerve regeneration in humans. Taken together, these Aims will leverage a known regeneration-associated gene to map out the transcriptional response following injury in a regeneration-capable species, which could lead to a breakthrough in understanding the most critical genes and pathways responsible for axonal regeneration.

Background:

The previous study outlined in Chapter 2 details our discovery that the MAPKKK dual leucine zipper kinase (*dlk*) is necessary for optic nerve regeneration in *Xenopus laevis*. Two key findings which emerged in this work point to a mechanistic role for Dlk which invites further investigation. First, we found that Dlk likely functions cell-autonomously in RGCs, as the absence of *dlk* in RGCs was enough to prevent their axonal regeneration even when transplanted into a wild-type nerve environment. Secondly, we found that the phosphorylation of known downstream target c-Jun was completely dependent upon Dlk, suggesting that not only does Dlk activate known cell-death and possibly cell-regeneration pathways, it is the only axonal injury signal to do so in *X. laevis*. Taken together, this data leads us to believe that *dlk* is an early axonal injury signal intrinsic to RGCs which mechanistically controls the activation of RGC axonal regeneration by transcriptional regulation of relevant pathways in the cell soma.

Given that c-Jun itself is a signaling molecule with dozens of targets and far-reaching effects, it seems likely that *dlk*, as the sole activator of c-Jun following RGC injury, also regulates a large number of pathways. It stands to reason that only some these are important for RGC axonal regeneration, and that others triggered by axonal injury may serve different functions irrelevant for RGC axonal regrowth. Thus, understanding the transcriptional changes which occur as a result of Dlk-dependent activation will point to therapeutic targets which may be both more specific and more effective than *dlk* itself to promote axonal regeneration.

Many studies into the molecular programming within the injured ON have involved various types of RNA profiling. Some investigations have profiled whole-retina or whole-ONH samples post-ONC via either microarray (87, 308, 309) or RNA-sequencing (114, 115). Others

have profiled or attempted to profile a single cell-type at a time, most commonly using laser capture microdissection (LCM) to isolate RGCs (259, 310). However, even this technique only enriches for RGC's 4-5 fold, as the ganglion cell layer contains as many amacrine cells as RGCs.

Since our previous work found that *Dlk* functions cell-autonomously in RGCs to promote axonal regeneration, a cell-type specific method which allows us to isolate RGCs alone is required. One such method, Translating Ribosome Affinity Pulldown (TRAP), offers unparalleled enrichment of a single cell type, plus unbiased RNA sequencing analysis. TRAP method involves the expression of an eGFP-tagged ribosomal subunit (eGFP-L10a) under the control of a cell-type specific promoter (311). Following cyclohexamide treatment to freeze ribosomes onto mRNAs, anti-eGFP antibodies are used for affinity pull down of the EGFP tagged ribosomes still associated with their mRNA transcripts. Subsequent RNA sequencing thus contains only those mRNA transcripts actively being translated by a single cell type at the time of dissection. Following the TRAP isolation step, the obtained mRNA can be utilized in a variety of RNA sequencing modalities. One such application is an RNA-seq protocol dubbed TagSeq, which can be an affordable and comprehensive way to achieve sequencing of large numbers of libraries. TagSeq involves a modified cDNA library preparation, which uses a molecular barcode-tagged oligo-dT targeting the polyadenylated 3' tail of each RNA molecule (312, 313). Focusing sequencing efforts on the 3' ends of mRNAs in this way allows for significance with a far lower number of reads than that required for conventional RNA-seq (312). Like most mRNA protocols, TagSeq also allows for multiplexing of different libraries, further reducing cost and increasing the potential for additional replicates, thus increasing the power of the analyses.

Aim 1: Understanding the Transcriptional Response of RGCs after Injury

The TRAP technique has been successfully used by our lab to study RGC's post-ONC in frog (250). In that study, we utilized a retinal ganglion cell (RGC) specific frog line for TRAP analysis of translatome changes at 0, 1, 3, 5, 7, 11 days, and 3 months post-ON. The study demonstrated that different genes show peak expression at different days, suggesting that the timing of induction of factors relative to each other may be critical to the overall response. However, that study did not include replicates, which limited the type of statistics that could be used to find significant changes in differentially regulated genes. Thus, using this study as a guide, I will perform TRAP in adult *X. laevis* RGCs at 0, 1, 3, and 7 days post-ONC. One retina from each of four animals will be crushed and pooled at each timepoint for each replicate, and each replicate will be processed together on the same day. Sequencing will be performed by TagSeq, and bioinformatic experts from UC Davis's Genomics Core will be able to assist with data processing and analysis.

Key methods: The general TRAP method has been previously described by others for mouse tissues and modified by us for use in *X. laevis* tissues (250, 270, 311) former study used tissue freshly dissected and immediately processed upon the day of dissection. However, my experiments with using fresh tissue vs. tissue which has been snap-frozen in liquid nitrogen upon dissection showed no difference in RNA quality as assessed by RIN scores. Thus, future experiments will divide the tissue dissections and TRAP RNA isolations into two days. First, tissues will be dissected and frozen immediately upon dissection. Then, at a later date, all 4 samples per replicate will be removed from storage and immediately processed (concurrent to thawing) to begin the TRAP isolation. We have also added a significant improvement in tissue homogenization procedure. In a prior experiment, we determined that the Wheaten glass-on-glass Dounce tissue grinder returned far superior quality RNA to those obtained with the Teflon tissue homogenizers used in the initial study; however, later experiments still had difficulty standardizing the degree of tissue homogenization. To address this, conjunction with the UC Davis Core Facilities, we designed a custom Dremel drill attachment for the Wheaton glass dounce tissue grinders, which creates a

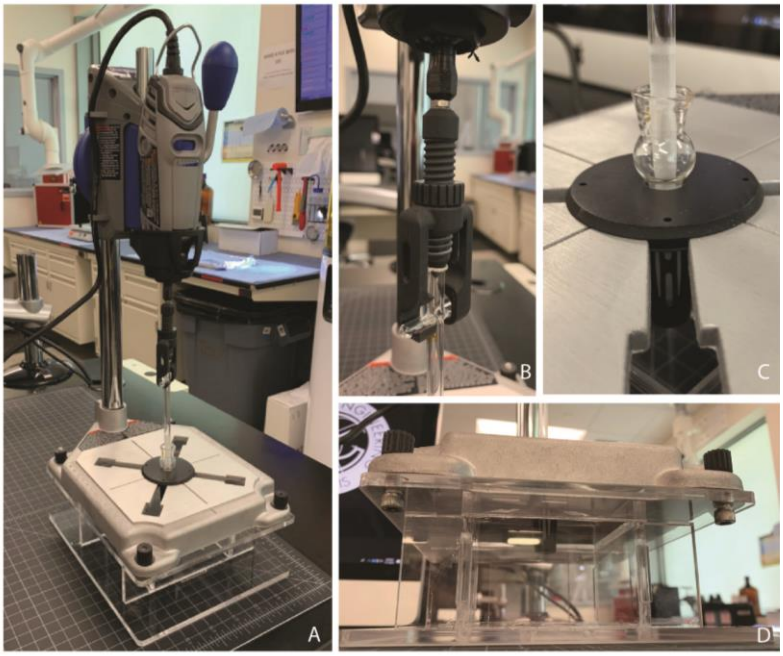

Figure A1.1. Custom Dremel drill attachment for consistent homogenization of tissues. B, Dual attachment arms grip pestle of Wheaton glass-on-glass dounce homogenizer. C, Base attachment calibrated to hold dounce tube. D, Metal drill base screws onto a tray built beneath base which can be filled with ice to keep tissues cold during homogenization. Not shown, foot pedal attachment allows for consistent homogenization speed while manually operating the up-and-down movement of drill attachment.

consistent speed of tissue homogenization and also allows the samples to be kept cold by way of a custom ice tray attachment which holds the glass tube stable during homogenization (Figure 1).

Current progress: 7 replicate TRAP purifications have been performed to date, of which 4 have sufficiently high RIN scores to warrant inclusion in the TagSeq sequencing (Figure 2). Tissues have been collected and frozen for an 8th and final replicate to be performed within 30-60 days.

WT Isl2b: EGFP-L10a Timecourse

	0d	1d	3d	7d	Include?
Replicate 1	7.1	6.6	6.4	8.3	Yes
Replicate 2	7.8	8	8	5.9	Yes
Replicate 3	8	7.6	7.6	7.6	Yes
Replicate 4	8	7	7.8	1	No
Replicate 5	8.4	8.2	8	8.5	Yes
Replicate 6	7.5	6.9	4.9	9	No
Replicate 7	3.3	4.7	4	8.3	No
Replicate 8	-	-	-	-	TBD

Figure A1.2. RIN scores tallied for TRAP replicate mRNA already collected. Replicates 1, 2, 3, and 5 are of sufficiently high and consistent quality to proceed onto TagSeq mRNA sequencing.

Expected results and future directions: I predict that the gene expression profiles will be the most divergent from mock (uncrushed) retinas at day 7, a timepoint at which significant denervation of the optic tectum has begun to occur and at which degradation of the optic nerve and influx of myeloid cells into the nerve has begun to occur. I further expect to repeat several key findings found by our prior study using Gene Ontology (GO): that genes related to oxidative stress and metabolic and biosynthesis capacity of RGCs, will be strongly upregulated, and that RGC-specific genes will be downregulated (250). Given that the prior study did not include replicates, I expect that sequencing of 4-5 complete replicate sets will allow us to better account for potential noise and will result in a smaller list of differentially regulated genes by comparing results across all replicates. Following this bioinformatic analysis, selected targets will be validated via qPCR analysis on separately collected TRAP mRNA samples prior to inclusion in further studies to examine their individual impact on ON regeneration.

Aim 2: Comparing the Injury Transcriptional Response of *Dlk* KO and Wt RGCs

Our prior discovery that *dlk* is necessary for RGC axonal regeneration in *X. laevis* tadpoles offers a unique opportunity to further expand our sequencing-based approach to understanding the molecular underpinnings of axonal regeneration. Given that *dlk* is a MAP3K which is known to regulate a variety of downstream factors, comparing the molecular pathways active following injury in RGCs deficient in *dlk* to wild-type RGCs is a simple and elegant way to understand which specific pathways *dlk* regulates within RGCs. To that end, I plan to perform TRAP mRNA isolation and TagSeq sequencing using adult *X. laevis* retinal tissue from *dlk* KO adults at 7d post-ONC or mock crush and compare these to WT adult *X. laevis* ONC and mock-crushed retinas at the same timepoint. As for Experiment 1, four retinas from four separate animals will be collected and pooled for each group. Similar to Experiment 1, multiple replicates will be processed and sent for sequencing together.

Current progress and next steps: 7 retina samples from WT adult frogs and 5 pooled retina samples from *dlk* KO frogs at 7d post-ONC have been collected, frozen in liquid nitrogen and stored at -80 degrees. For the mock-crushed cohort, WT and *dlk* KO animals have been bred and are being raised to the correct age (2-3 months of age) to perform the ONC or mock crush and tissue collections. Since all *dlk* KO animals used in the samples collected thus far were F1 animals from F0 mosaic animals, each animal was genotyped and confirmed to be complete KO animals (each carries only frameshift mutations in *dlk* on each chromosome) prior to ONC and tissue collection. All *dlk* KO animals currently being raised are full KO animals bred from the same male used for the initial cohort crossed to one of his female full-KO progeny. For each

replicate, one WT ONC, one WT mock-crush, one *dlk* KO ONC and one *dlk* KO mock-crushed retina sample (4 retinas pooled per sample) will be processed on the same day using the TRAP technique to isolate mRNA. Each mRNA sample will be assayed by Bioanalyzer to confirm RIN scores indicating good-quality RNA prior to inclusion in TagSeq sequencing. I plan to send a minimum of 4 and ideally 5 replicates (of 4 groups each) of this experiment for TagSeq sequencing. As for Experiment 1, bioinformatics experts at the UCD Genomics Core will assist in processing and analyzing sequence reads.

Expected results and future directions: A prior study which sequenced whole-retina mRNA from *Dlk* KO mice has previously revealed that loss of *dlk* changes the molecular signal of injured retinas to be more similar to uininjured retinas than injured Dlk+ retinas; furthermore, 92 of the top 100 differentially-regulated genes in this study displayed a dependence on *dlk* (78). Given this data, our prior study profiling adult RGCs (250), and my own preliminary data from Chapter 2 suggesting that *dlk* functions as a regeneration-specific gene, I likewise expect that the mock-crushed *dlk* KO and WT groups will be more similar to each other than to either of the crushed retinas. Furthermore, I expect that *dlk* KO ONC samples will be more similar to mock-crushed WT retinas than to WT ONC retinas. However, given that *X. laevis* is a regeneration-capable model, I expect that in this case, the differentially regulated genes in the WT ONC animals compared to the *dlk* KO ONC animals will include some novel genes never before reported in the known literature involving murine species. I would expect that that this subset of genes, which is up- or down-regulated in *X. laevis* WT animals but not in *dlk* KO animals, could represent the critical factors which regulate the regeneration response of *X. laevis* as opposed to the apoptotic response of murine RGCs following injury.

Conclusion

The natural ability of amphibians to regrow their optic nerves suggests that they regulate different molecular pathways compared to their mammalian counterparts. Thus far, our lab has identified at least one key gene, *dlk*, which is critical for the regenerative response of amphibian axons, though it is likely to just help transduce the injury signal back from the axon to the soma, something likely shared by amphibians and mammals. Thus, a comprehensive cell-type specific profiling of the post-injury response in Wt *X. laevis* animals compared to that of Dlk-deficient animals should reveal an array of RGC-intrinsic signaling pathways dependent upon *dlk*, but some of those pathways must be different in amphibians and mammals. Those differences may hold the key to therapeutic regeneration of RGC axons. Analyses of these differences in expression, complemented by functional assessments which are now possible on a previously impossible scale due to the development of tadpole ONC model, will begin to piece together the specific function of genes essential to initiating and shaping successful RGC axonal regeneration. Thus, taken together, this project should identify new molecular targets with potential as regeneration-promoting therapies in the future.

Appendix II: Screening of Putative Regeneration-Associated Genes via F0 CRISPR Knockout Model creation and Tadpole ONC Assay

Upon development of the tadpole ONC assay, we began creating F0 global knockout models for genes which we believed might be involved in RGC axonal regeneration in *X. laevis*. We selected both genes which have been studied in other axonal regeneration models as well as novel candidate genes which came up in our previously published study on translational profiling of RGCs (250). Of the initial genes targeted, we were only able to find sgRNAs of suitable KO efficiency for about half of these genes, and many of these required testing several sgRNAs per gene to find one effective guide. Table A2.1 details all the genes for which I have designed and tested at least one sgRNA; the sequences of all effective sgRNAs (consensus sequence includes PAM) are noted, as are the efficiency of KO for each sgRNA as calculated by either TIDE analysis or TA cloning and Sanger sequencing of individual clones. In the end, none of these initial F0 KO lines resulted in a measurable regeneration defect until we screened our sgRNAs for *dlk*, and our further experiments with this gene are detailed in Chapter II.

Gene	sgRNAs tested	sgRNA Chosen (Consensus sequence)	KO Efficiency	Line(s) Made?
gap43	2	GCTTCCGTGGACATATAATCAGG	75% (TA)	Yes
jun	5	CAAGCTCGCTTCCCCGGAGTTGG		Yes
optn	5 (2L, 3S)	L: TCAGAATTGCAGCTGAAACTCGG S: TGAAAACGAGGTGTTAAGGAAGG	L: 50% (TA) S: 100% (TA)	Yes
atf3	2	None	0% (TA)	
atf4	2	None	0% (TA)	
bnip3L	1	None (incomplete TA cloning results)	0% (TA)	
bnip3	2	None (incomplete TA cloning results)	0% (TA)	
igf2	2	None	0% (TA)	

myc	2	GGTTGACCATGTCCCCTCCCAGG	50% (TA)	
gadd45G	2	ATGACTCTGGAAGAAGTTCACGG	80% (TA)	
rasd1	2 (3 designed)	None	20% (TA)	
itgb5	4	L: GGATGCTGAAGTTGCACTCCGGG S: AGTAGCGCGTCCCCAACTCCGGG	42-84% (TIDE, individual)	Yes
mfge8	8 (4S, 4L)	L: GCCAAGTACTGTCTGATTCTGGG S: GGGGGCATCTGCAAACATCTTGG		Yes
aqp4	1^{+}	CCAAAGCGTAAAGACATAACAGG	62.5% (TA)	Yes
itgb3	3	GCTACGAGAACGGTGCTGACTGG	12-68% (TIDE, individual)	Yes
mertk	2	None		
axl	4 (2S, 2L)	None		
dlk	3	GACAGACCATGTCGGGCATTGGG	95% S, 98% L (TIDE)	Yes
*Uch1L*1	4 (2S, 2L)	L: AGTCTGTATCTAGACGGGAACGG S: GGCACCAGACACACCCAACTGGG	91% L (TIDE)	Yes
lzk	2	None	13% (TIDE) (Both guides injected together)	
bax	4 (2S, 2L)	N/a (not tested)	N/A	

Table A2.1. sgRNAs designed for screening via CRISPR F0 knockout and tadpole ONC assay. A complete list of all sgRNA designed and intended for screening using our novel tadpole ONC regeneration assay combined with F0 CRISPR creation. For some genes, (see notes in Column 2, "sgRNAs tested"), guides needed to be designed against each chromosome (S and L) of the *X. laevis* allotetraploid genome separately. Some guides have been designed but not yet used for F0 knockout creation (noted in Column 3). For some early guides, we used TA cloning to measure the efficiency of knockout; efficiency is thus reported as a percentage of all TA clones which were sequence-confirmed to carry an indel of any kind out of all TA clones successfully sequenced. Typically, 4 TA clones were

sequenced per sample, with the exception of Aqp4, for which only 3 clones were sequenced. For later guides, Tracking of Indels by Decomposition (TIDE, see notes in Methods of Chapter 2) was used to measure efficiency of knockout, and estimated total indel percentage as calculated by TIDE analysis is included in Column 4 for these guides. All guides for which F0 founder knockout animals were retained and raised into lines which are now maintained as part of the lab animal population are indicated in the Column 5. [+] This guide was co-designed by the author and a former rotation student, Elizabeth Schinski; Elizabeth carried out the TA cloning to determine efficiency on this guide.

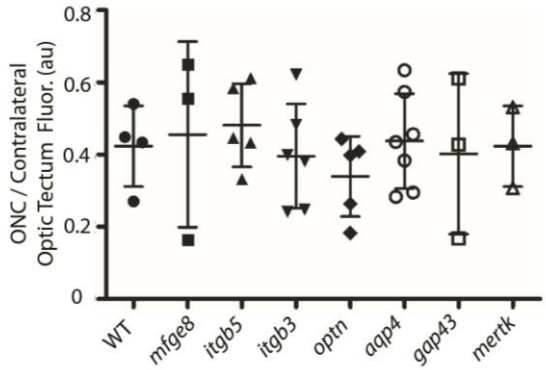

Figure A2.2. Knockout of various genes does not affect tectal reinnervation in *X. laevis*. When seven different genes known or suspected to be associated with either debris clearance or axonal regeneration are individually targeted for KO in F0 sgRNA-injected animals, no defect in tectal innervation is seen in any KO line at 12 days post-ONC.

A significant amount of previously published and unpublished work by the lab has focused on the clearance of debris from the optic nerve, in *Xenopus* as well as murine and primate species, with an eye towards determining if a debris-clearance defect might underlie certain optic neuropathies such as glaucoma in humans (1, 14, 294). As such, we wondered whether clearance of debris might also affect regeneration of the optic nerve. To that end, many of the sgRNAs in the above list were designed specifically to test this hypothesis, as they target genes known to be involved in debris clearance mechanisms. Once we had successfully validated reasonably effective sgRNAs to a number of these genes, we proceeded onto the tadpole ONC regeneration assay (described in Chapter 2, Figure 2.1) using founder F0 knockout animals produced from our CRISPR-Cas9 injections. However, none of our knockout animals showed a defect in regeneration compared to wild-type control animals (Figure A2.2). Though this initially suggested that the genes in question were irrelevant for regeneration, later TIDE genotyping analysis of selected individual animals from this cohort (see genotyping results for *itgb3* and *itgb5* knockout anmimals in Figure A2.1, above)

suggested the alternative explanation that none of our sgRNA KOs were sufficiently complete enough to show a regeneration phenotype. As such, further work with these knockout models will require breeding these F0 founder animals, which are now at sexual maturity, to full KO status prior to re-evaluating the effect of any of these genes on optic nerve regeneration and tectal reinnervation in *X. laevis*.

Appendix III: Conditional Tissue-Specific Cas9 Knockout Models in *X. laevis*

Introduction

Besides the monumental amount of sequencing work which I originally planned to complete for my Ph.D, a small amount of which will finally be completed as part of the work proposed in Appendix I, a second ambitious project proposed for my qualifying exam was the creation of the first conditional, tissue-specific Cas9 knockout lines in *Xenopus*. In brief, these knockout lines would be created in two steps. The first step involved the creation of driver lines, each of which would express a nuclear-localized, FLAG-tagged Cas9 protein under the control of a different inducible tissue-specific promoter, which would result in translation of the Cas9 protein only when doxycycline was added to the tadpole media. These lines would be raised to sexual maturity for step two. Then, using these lines as the background, new transgenes would be inserted into these driver lines which would result in constitutive, global expression of small sgRNA molecules. These transgenes would consist of a small Pol III promoter driving an sgRNA consensus sequence inserted into an sgRNA scaffolding sequence. When the driver line was induced to begin translation of the Cas9 protein in our cell type of choice, these sgRNAs would thus be present in the same cells and this combination would (we hoped) result in the knockout of our gene of interest in only a single cell type. We proposed that this strategy would enable us to avoid a problem we predicted would occur as we created global knockout models for various genes via F0 CRISPR injections at the one-cell stage; that is, we expected that many of the genes we were most interested in studying for their potential effect on regeneration were likely to be embryonic lethal when absent. Thankfully, this did not end up being the case for any of the genes which we have studied to date, which was doubly fortunate as my driver Cas9 lines never proved

effective. In retrospect, the lack of embryonic lethality in F0 KOs in frogs might not be so surprising given that most embryonic lethality occurs during gastrulation, and much of early development in Xenopus relies on maternal transcripts. However, given the vast amount of work which was done on this project and a final result which was tantalizingly close to success in at least one driver line, I will here present a brief description of the driver lines created, the Pol III constructs created, and the experiments I have completed to date to validate their effectiveness.

Cas9 Driver Lines

Isl2b: rtTA-TetBi-YFP-3xFLAG-NLS-SpCas9-NLS

The cloning of this plasmid was the first project I undertook upon joining the Marsh-Armstrong lab, under the direction and design of Chung-Ha Davis, who should be earning his Ph.D at about this same time. To create this line, a 5690-bp fragment was amplified from pTREtightBI-3xFLAG-NLS-spCas9(200bBGpA)-NLS-nYFP using primers CAGgctagcGATATCctaCTTGTACAGCTCGTCCATGC and GATCCGGCCGCGGCCGCGAATTAAAAAACCTCCCAC. A 6479-bp fragment was then amplified from pCS2(Isl2b1kb): rtTA using primers GCATGGACGAGCTGTACAAGtagGATATCgctagcCTG and GTGGGAGGTTTTTTAATTCGCGGCCGCGGCCGGATC. These two fragments were ligated together using Gibson assembly to create pCS2(Isl2b 1kb): rtTA-TetBi-YFP-3xFLAG-NLS-SpCas9-NLS. This construct was used to create the final construct pCS2(Isl2b 20kb): rtT-TetBi-YFP-3xFLAG-NLS-SpCas9-NLS by recombineering, essentially as previously described (1).

This final ~30kb construct was then digested with Not1 and a transgenic *X. laevis* line created by REMI transgenesis as previously described (291).

Blbp: rtTA-TetBi-YFP-3xFLAG-NLS-SpCas9-NLS

To create a plasmid in which the RGC-specific Isl2b: promoter of the first construct was replaced by the astrocyte-specific Blbp construct, pCS2(Isl2b 1kb): rtTA-TetBi-YFP-3xFLAG-NLS-SpCas9-NLS partially digested with HindIII and re-ligated together via blunt-end ligation to retain only the HindIII site located between the Isl2b(1kb) promoter region and the rtTA. This ΔHindIII version was then digested with HindIII and SalI to remove the Isl2b(1 kb) promoter region. A 1726-basepair region was then amplified from pCS2(Blbp):mCherry-Gap43 (1) using primers GCTATTACGCCAgtcgacCCTATGAAAGAGTGTGTT and CTTCTGACGGGaagcttACAAGGCAGTGGAACAGATC and ligated together with the digested plasmid above using Gibson assembly. This construct was then digested with Not1 and a transgenic *X. laevis* line created by REMI transgenesis as previously described (291).

Coronin: rtTA + pTREtightBI-3xFLAG-NLS-spCas9(200bBGpA)-NLS-nYFP

Despite a long cloning effort to create a single plasmid replacing the cell-type specific promoter with our preferred promoter for driving expression in myeloid cells (zfCoronin1a, described in Chapter III), due to the size of the DNA pieces my efforts were in the end unsuccessful. Therefore, a transgenic *X. laevis* line was created by co-injection of the previously cloned plasmids pCS2(Coronin1a): rtTA and pTREtightBI-3xFLAG-NLS-spCas9(200bBGpA)-NLS-nYFP using REMI transgenesis.

pCS2(CMV): 6xHis-3xFLAG-NLS-SpCas9-NLS

Initially, this plasmid was intended to create a transgenic line from which oocytes could be harvested to produce a large quantity of His-tagged Cas9 protein, which could be isolated by a nickel column protein purification method and ultimately eliminate the need to purchase purified Cas9 protein for usage in F0 CRISPR global KO injections. No line was created and this plasmid was never utilized for that purpose, but it did prove useful in a later validation experiment described in the Validation of SpCas9 Lines section. To create this line, a 4320-bp fragment was amplified from pTREtightBI-3xFLAG-NLS-spCas9(200bBGpA)-NLS-nYFP using primers CCCGGGGCCACCgccaccATGggaCATCACCATCACCATCACgccaccATGGACT and GGCGCCGCGGCCGCTCATTTCTTTTTCTTAGC. A 3794-bp fragment was then amplified from pCS2(CMV): GFP using primers GGTGGCCCCGGGAAGCT and GCGGCCGCGGCGCCA. These fragments were then ligated together using Gibson assembly.

Pol III Promoter Constructs

As I began cloning the Cas9 driver constructs, Chung-Ha took on the task of creating three separate Pol III constructs to drive RNA transcription of our chosen gene. Each construct contained a different PolIII promoter region located directly upstream of dual BsmBII restriction enzyme sites placed immediately before a 76-bp gRNA scaffolding sequence. Using these degenerate restriction enzyme sites, we could design and insert our sgRNA consensus sequences essentially using the Golden Gate cloning method (314). The resulting constructs are listed below:

pXtU6Long-Bsmbi-Sp-gRNA-Bsmbi: contains a 508-bp region from the U6 promoter region amplified from *Xenopus tropicalis* cDNA upstream of the gRNA scaffolding sequence.

pXtU6Short-Bsmbi-Sp-gRNA-Bsmbi: contains a 273-bp region from the U6 promoter region amplified from *Xenopus tropicalis* cDNA upstream of the gRNA scaffolding region.

pXtH1t-Bsmbi-Sp-gRNA-Bsmbi: contains a 509-bp region from the XtH1 promoter region amplified from *Xenopus tropicalis* cDNA upstream of the gRNA scaffolding region

Once Chung-Ha finished these constructs and moved on to his own graduate work at Stanford, we realized that we would need a selectable marker to be able to screen for these constructs when they were injected into *Xenopus* embryos via REMI transgenesis. As such, after cloning and testing five new fluorescent transgenes, I selected mCerulean3 as my selectable marker of choice, under the control of a cardiac actin promoter (CA600) previously utilized by the lab in a handful of other constructs and which drives expression strongly in muscle tissues. To create this construct, a 1634-basepair region was amplified from pCS2(CA600): mCerulean3 using primers CCGCGGCGCCAATGCAtaaTCCACTGCATTCTG and CTGGGTACCGGGCCCAAGaattAAAAAACCTCCCACAC. Each of the three stable expression vectors was digested with Nsi1, and then each vector was ligated together separately with the fragment from pCS2(CA600): mCerulean3 using Gibson assembly.

Following the creation of the above three Pol III promoter constructs, I received a suggestion and from Dr. Tom Glaser that I create a fourth modified construct using the human U6 promoter, which is well-published to drive strongly in cultured cells (315). To replace our

PolIII promoters with this new promoter, I amplified a 283-bp region around the human U6 promoter using primers CTATTACGCCAGTCGACtttcccatgattccttc and gagacgTCAGcgtctcCcGGTGTTTCGTCCTTTC. I then amplified a 4421-bp region from pXtU6Long-Bsmbi-Sp-gRNA-Bsmbi using primers GTCGACTGGCGTAATAGCGAAG and GgagacgCTGAcgtctcCGTTTTAG. These fragments were ligated together using Gibson assembly.

While completing these constructs, I was concurrently testing sgRNAs designed to knockout various genes of interest using F0 CRISPR model creation (see Table A2.1 and Methods, Chapter 2). Upon integration of the selectable marker mCerulean3 Into the stable expression constructs, I began to ligate confirmed sgRNAs for these genes into them for later use in REMI transgenesis injections into our Cas9 driver lines, and a table of these constructs follows (Table A3.1).

Stable Expression Vector	sgRNAs inserted (by gene name)
pXtU6Long-Bsmbi-Sp-gRNA-Bsmbi/CA600-mCerulean3	Gap43, OPTN-L, Aqp4, Itgb5-1L, Itgb5-1S, Mfge8-2L, Dlk
pXtU6Short-Bsmbi-Sp-gRNA-Bsmbi/CA600-mCerulean3	Gap43, OPTN-L, Aqp4, Itgb5-1L, Itgb5-1S, Mfge8-2L,
pXtH1-Bsmbi-Sp-gRNA-Bsmbi/CA600-mCerulean3	Gap43, OPTN-L, Aqp4, Itgb5-1L, Itgb5-1S, Mfge8-2L
HsU6-Bsmbi-Sp-gRNA-Bsmbi/CA600-mCerulean3	None yet

Table A3.1. Stable expression vectors with addition of specific sgRNA consensus sequences. Into each of the four stable expression vectors, Golden Gate cloning enabled modular insertion of various sgRNA consensus sequences corresponding to genes of interest targeted for tissue-specific, conditional Cas9 KO using our Cas9 driver lines. sgRNAs for all genes listed in the second column were validated for efficiency of KO above 50% prior to ligation into each stable expression construct.

Validation of SpCas9 Lines

Astrocyte Cas9 driver line strongly drives expression of Cas9

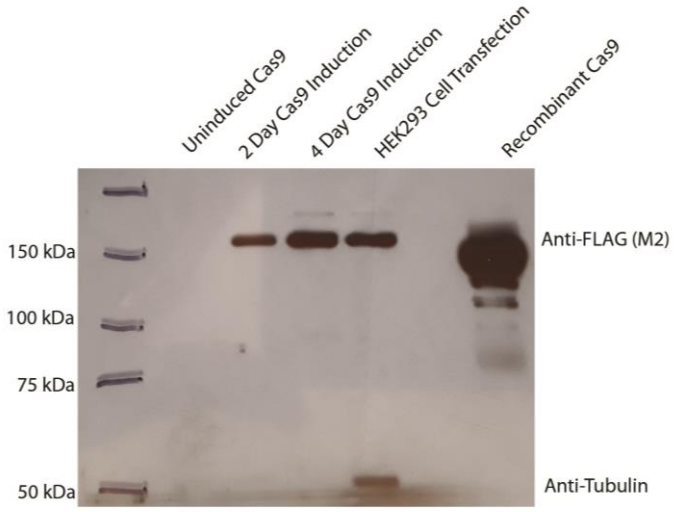

Figure A3.2. Astrocyte Cas9 driver line expresses Cas9 upon induction of transgene. Uninduced control animals (first lane) do not produce Cas9 protein, but both animals which were induced for 2 days (second lane) or those induced for 4 days (third lane) with 50 ug/mL doxycycline produce quantities of Cas9 protein comparable to the ubiquitous promoter CMV transfected into HEK293 cells (fourth lane). The size of the Cas9 protein produced is comparable to that of purified recombinant Cas9 protein.

To confirm that our driver lines were capable of driving Cas9 expression in our tissues of interest, we chose to test our Blbp Cas9 driver line first (*Blbp: rtTA-TetBi-YFP-3xFLAG-NLS-SpCas9-NLS*). As the Blbp promoter drives in astrocytes both in the retina and in the brain, the number of cells expressing Cas9 (and therefore levels of Cas9 protein) in this line should be orders of magnitude higher than in the other two lines in which only RGCs or only immune cells are expressing the Cas9 protein. We induced Cas9 expression for 0 days (no induction), 2 days, or 4 days on young *X. laevis* tadpoles and collected brains at 10 days of age from these animals. For an additional control, a collaborator (thank you to Dr. Jisoo Han for her generous help) also transfected HEK293 cells with our 6xHis-tagged Cas9 construct (described above) and cells were dissociated and collected 2 days post-transfection. Following protein isolation, all four samples were analyzed via Western blot alongside the additional control of purified Cas9-NLS protein purchased from QB3 MacroLab (UC Berkeley). When stained using the M2 anti-Flag antibody, animals induced for either 2 or 4 days produced large amounts of

Cas9 protein; uninduced animals did not produce Cas9 protein (Figure A3.1). Amount of Cas9 protein produced was visually comparable to that produced by the HEK 293 cells after 2 days of induction, and was comparable in molecular weight to the purified, purchased Cas9-NLS protein. Overall, these results confirmed that our Cas9 driver lines express Cas9 protein only when induced by doxycycline application to the tadpole media.

RGC Cas9 driver line expresses Cas9, but Cas9 localization is non-nuclear and may be toxic

Having confirmed the conditional nature of our novel Cas9 system, we next needed to assess the tissue specificity of our Cas9 protein production by confirming the localization of the Cas9 protein within our driver lines. To do this, we chose the RGC-specific Cas9 driver line (Isl2b: rtTA-TetBi-YFP-3xFLAG-NLS-SpCas9-NLS) as our test line and induced expression of

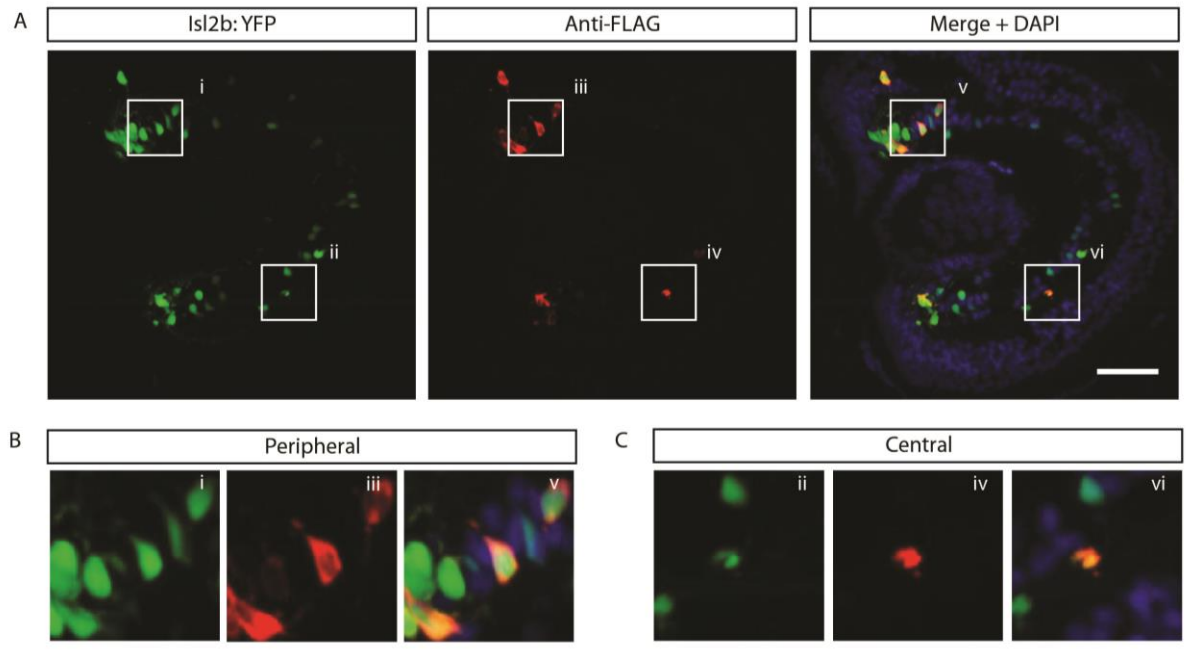

Figure A3.3. Expression of Cas9 in RGC driver line is non-nuclear and may be toxic to RGCs. A-B. In tadpoles in which RGCs inducibly express both YFP and a FLAG-tagged Cas9 protein, induced expression of the Cas9 protein for 2 days shows Cas9 localization to be cytoplasmic, while YFP expression seems to be nuclear. C. Limited expression of Cas9 protein in the central retina combined with abnormal RGC morphology suggests expression of Cas9 may be toxic to RGCs.

the Cas9 protein for two days in tadpoles from 6-8 dpf by addition of 50 ug/mL doxycycline to the tadpole media. We examined the expression of both the YFP protein and the Cas9 protein via visualization with a FLAG antibody (M2) to take advantage of the 3xFLAG tag of the Cas9 fusion protein. We found that while the YFP expressed in many, though not all, cells of the RGC layer at this timepoint, anti-FLAG labeling was found in only a subset of these YFP-labeled cells. Furthermore, we noticed that the localization of the YFP protein appeared nuclear, but the localization of the FLAG antibody appeared decidedly cytoplasmic, with no nuclear localization signal (Figure A3.3A-B). Furthermore, the morphology of those few RGCs in the central region of the retina which seemed to express FLAG-tagged Cas9, the appearance of these FLAG+ retinas appeared abnormal, rounded and atrophied, indicative of cell death (Figure A3.3C). Together, these results seem to suggest that despite the dual NLS sequences of the Cas9 fusion protein, the Cas9 does not appear able to enter the nucleus of RGCs upon transgene induction, and furthermore, that expression of the Cas9 may actually be toxic to RGCs of the retina.

Attempted astrocyte-specific knockout of Dlk largely unsuccessful, but may work at very low efficiency

Upon validation of very high-efficiency

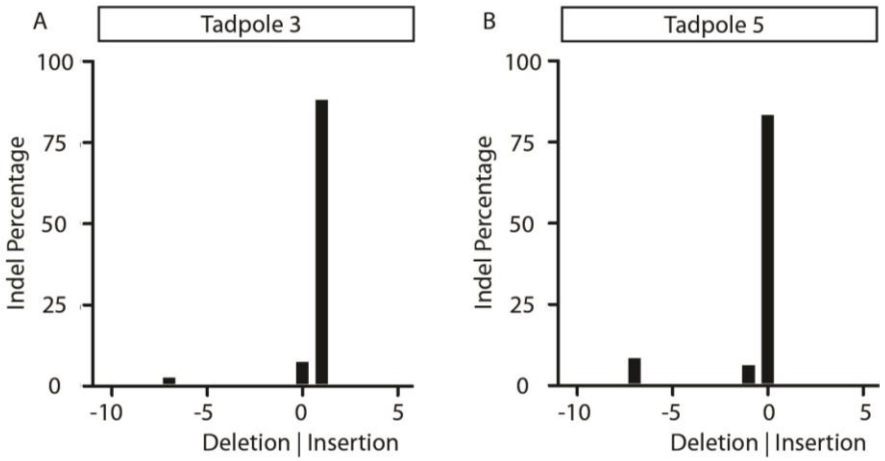

Figure A3.4. Pilot test of tissue-specific, inducible Cas9 system shows possible genome editing at low levels in 2 of 5 tadpoles tested. When a stable expression construct in which the XtU6Long Pol III drives expression of *Dlk*, and Cas9 production is induced in retinal progenitor cells at 2dpf via the Blbp promoter, a small percentage of indels seem to be produced via genome editing. Note that the -7 and -1 indels produced here are characteristic of this specific sgRNA.

sgRNAs against *Dlk,* which led to our identification of Dlk as a regeneration-critical factor in *X. laevis,* a renewed interest emerged in testing the cell-autonomous mechanism of *Dlk* action within RGCs. Though our RGC-specific Cas9 driver line proved unsuccessful due to the non-nucelar nature of the Cas9 localization within RGCs, our astrocyte Cas9 driver line (Blbp: rtTA-TetBi-YFP-3xFLAG-NLS-SpCas9-NLS) utilizes a promoter which drives in mature astrocytes in adult retinas, but early in development, drives in the vast majority of all retinal progenitor cells (1). As such, induction of the promoter at a very early stage, only 1-3 dpf, would result in Cas9 expression in the vast majority of retinal cells at a mitotic stage in which the nuclear envelope would be forming de novo around differentiating cells, and thus, our Cas9 protein could be more easily incorporated into these mitotic cells despite not typically being able to pass through the nuclear pores of a fully differentiated retinal cell.

Thus, to test the ability of our Cas9 system to knock out a specific gene in an inducible, tissue-specific way, we performed REMI transgenesis using sperm nuclei from our Blbp: rtTA-TetBi-YFP-3xFLAG-NLS-SpCas9-NLS driver line and a Pol III stable expression construct containing our *Dlk* sgRNA, pU6Long-Dlk/CA600:mCerulean. At 2dpf, we induced expression of Cas9 via application of 20 µg/mL doxycycline. This lower concentration of doxycycline was intended to avoid the potential problem of toxicity by overproduction of Cas9 protein. At 7 dpf, we collected the eyes from 5 tadpoles which expressed both YFP in brain and retina and mCerulean3 in muscle actin, pooled both eyes per animal, and performed genomic DNA isolation for each animal individually for genotyping analysis by PCR amplification and TIDE deconvolution of the PCR sequence traces. Of these five animals, three animals received TIDE indel scores of >95% and no clearly distinguishable indels predicted, which we interpreted to mean that no genomic editing had occurred in these animals (data not shown). However, in two

of the animals, TIDE analysis showed an indel percentage of 10.7% in one tadpole and 15.3% in another (Figure A3.4). Even more compellingly, the two indels predicted for each tadpole, a -7 deletion and a -1 deletion, are indels which are very commonly seen in our global *Dlk* KO tadpoles when using this specific sgRNA sequence. Though the indel percentages were low, it seems possible that our conditional, tissue-specific Cas9 system may be driving a small amount of true genome editing when induced very early in young embryos.

Future directions

Using precise genome editing techniques confined to tissues of interest may be essential for success when working with genes which could prove embryonic lethal when targeted with global knockout techniques. Moreover, when studying a complex biological process such as axonal regeneration which may involve several different cell types, it is important to understand which genes are acting in certain cell types but not in others. Finally, regeneration as a process might involve activating the correct genes at the right time, meaning that temporal control of gene activation must also be considered in experiments. For these reasons, we set out to create the first inducible, tissue-specific Cas9 knockout system in the regeneration-capable species *Xenopus laevis*. Despite our initial success at creating an inducible Cas9, later experiments showed poor to nonexistent nuclear localization, possible toxicity effects and an inconclusively low extent of genome editing.

Future work in the lab will focus on solving these problems I encountered during this initial design and testing phase. Redesigning of the Cas9 driver lines to involve a split Cas9 protein may enable better transport of two smaller proteins rather than one large protein into the nucleus. This may or may not also solve the problem of toxicity; it may if the toxicity of the

Cas9 protein was due to large aggregates of Cas9 in the cytoplasm which were unable to be nuclearly localized. It also might be possible to utilize dead-Cas9 variants fused to transcriptional repressors alongside guides targeting regulatory regions (316). This strategy could bypass Cas9 toxicity if the toxicity is due to low-level off-target nuclease activity exacerbated by the high levels of Cas9 expression in our current lines. If toxicity persists even with these models, it will be necessary to carry out titration experiments to find the lowest concentration of doxycycline (and thus Cas9 production) which can result in genome editing. Finally, it seems likely that our low degree of genome editing was due at least in part to a low transcription rate of our sgRNA, and that a more efficient Pol III promoter, perhaps the newest HsU6 construct in our current inventory, might prove more effective. While significant validation and redesign will need to be done, I am optimistic that my experiments will pave the way for the lab to finally achieve the conditional, tissue-specific Cas9 system which we have been working towards.

Many thanks to Dr. Chung-Ha Davis for his cloning genius, to Dr. Tom Glaser for his advice and HsU6 construct, and to Dr. Jisoo Han for her invaluable help with Western blots and for carrying out the transfection of HEK293 cells.

References

1. Mills EA, Davis CH, Bushong EA, Boassa D, Kim KY, Ellisman MH, et al. Astrocytes phagocytose focal dystrophies from shortening myelin segments in the optic nerve of Xenopus laevis at metamorphosis. Proc Natl Acad Sci U S A. 2015;112(33):10509-14.
2. Hill RW, Wyse GA, Anderson M. Animal Physiology. 3rd ed. ed. Sunderland, MA: Sinauer Associates, Inc. Publishers; 2012.
3. Butt AM, Pugh M, Hubbard P, James G. Functions of optic nerve glia: axoglial signalling in physiology and pathology. Eye (Lond). 2004;18(11):1110-21.
4. Miron VE, Kuhlmann T, Antel JP. Cells of the oligodendroglial lineage, myelination, and remyelination. Biochim Biophys Acta. 2011;1812(2):184-93.
5. Amaral DG. The anatomical organization of the central nervous system. Principles of neural science. 2000;4:317-36.
6. Sternini C. Organization of the peripheral nervous system: autonomic and sensory ganglia. J Investig Dermatol Symp Proc. 1997;2(1):1-7.
7. Chen ZL, Yu WM, Strickland S. Peripheral regeneration. Annu Rev Neurosci. 2007;30:209-33.
8. Masland RH. The neuronal organization of the retina. Neuron. 2012;76(2):266-80.
9. Wässle H, Boycott BB. Functional architecture of the mammalian retina. Physiol Rev. 1991;71(2):447-80.
10. Masland RH. The fundamental plan of the retina. Nat Neurosci. 2001;4(9):877-86.
11. Kim T, Soto F, Kerschensteiner D. An excitatory amacrine cell detects object motion and provides feature-selective input to ganglion cells in the mouse retina. Elife. 2015;4.
12. Reichenbach A, Bringmann A. New functions of Müller cells. Glia. 2013;61(5):651-78.
13. Kreutzberg GW. Microglia: a sensor for pathological events in the CNS. Trends Neurosci. 1996;19(8):312-8.
14. Davis CH, Kim KY, Bushong EA, Mills EA, Boassa D, Shih T, et al. Transcellular degradation of axonal mitochondria. Proc Natl Acad Sci U S A. 2014;111(26):9633-8.
15. Liddelow SA, Guttenplan KA, Clarke LE, Bennett FC, Bohlen CJ, Schirmer L, et al. Neurotoxic reactive astrocytes are induced by activated microglia. Nature. 2017;541(7638):481-7.
16. Ronning KE, Karlen SJ, Miller EB, Burns ME. Molecular profiling of resident and infiltrating mononuclear phagocytes during rapid adult retinal degeneration using single-cell RNA sequencing. Sci Rep. 2019;9(1):4858.
17. Sernagor E, Eglen SJ, Wong RO. Development of retinal ganglion cell structure and function. Prog Retin Eye Res. 2001;20(2):139-74.
18. Polley EH, Zimmerman RP, Fortney RL. Neurogenesis and Maturation of Cell Morphology in the Development of the Mammalian Retina. In: Finlay BL, Sengelaub DR, editors. Development of the Vertebrate Retina Perspectives in Vision Research. Boston: Springer; 1989.
19. Martersteck EM, Hirokawa KE, Evarts M, Bernard A, Duan X, Li Y, et al. Diverse Central Projection Patterns of Retinal Ganglion Cells. Cell Rep. 2017;18(8):2058-72.
20. Laboissonniere LA, Goetz JJ, Martin GM, Bi R, Lund TJS, Ellson L, et al. Molecular signatures of retinal ganglion cells revealed through single cell profiling. Sci Rep. 2019;9(1):15778.

21. Baden T, Berens P, Franke K, Román Rosón M, Bethge M, Euler T. The functional diversity of retinal ganglion cells in the mouse. Nature. 2016;529(7586):345-50.
22. Cajal SRy. La retine des vertebres. La cellule. 1893;9:17-257.
23. Cleland BG, Levick WR, Wässle H. Physiological identification of a morphological class of cat retinal ganglion cells. J Physiol. 1975;248(1):151-71.
24. Sanes JR, Masland RH. The types of retinal ganglion cells: current status and implications for neuronal classification. Annu Rev Neurosci. 2015;38:221-46.
25. Famiglietti EV, Kolb H. Structural basis for ON-and OFF-center responses in retinal ganglion cells. Science. 1976;194(4261):193-5.
26. Huberman AD, Wei W, Elstrott J, Stafford BK, Feller MB, Barres BA. Genetic identification of an On-Off direction-selective retinal ganglion cell subtype reveals a layer-specific subcortical map of posterior motion. Neuron. 2009;62(3):327-34.
27. Hattar S, Liao HW, Takao M, Berson DM, Yau KW. Melanopsin-containing retinal ganglion cells: architecture, projections, and intrinsic photosensitivity. Science. 2002;295(5557):1065-70.
28. Ecker JL, Dumitrescu ON, Wong KY, Alam NM, Chen SK, LeGates T, et al. Melanopsin-expressing retinal ganglion-cell photoreceptors: cellular diversity and role in pattern vision. Neuron. 2010;67(1):49-60.
29. Berson DM, Dunn FA, Takao M. Phototransduction by retinal ganglion cells that set the circadian clock. Science. 2002;295(5557):1070-3.
30. Rheaume BA, Jereen A, Bolisetty M, Sajid MS, Yang Y, Renna K, et al. Single cell transcriptome profiling of retinal ganglion cells identifies cellular subtypes. Nat Commun. 2018;9(1):2759.
31. Dhande OS, Stafford BK, Lim JA, Huberman AD. Contributions of Retinal Ganglion Cells to Subcortical Visual Processing and Behaviors. Annu Rev Vis Sci. 2015;1:291-328.
32. Dhande OS, Huberman AD. Retinal ganglion cell maps in the brain: implications for visual processing. Curr Opin Neurobiol. 2014;24(1):133-42.
33. Tham YC, Li X, Wong TY, Quigley HA, Aung T, Cheng CY. Global prevalence of glaucoma and projections of glaucoma burden through 2040: a systematic review and meta-analysis. Ophthalmology. 2014;121(11):2081-90.
34. Nickells RW, Howell GR, Soto I, John SW. Under pressure: cellular and molecular responses during glaucoma, a common neurodegeneration with axonopathy. Annu Rev Neurosci. 2012;35:153-79.
35. Dahlmann-Noor AH, Vijay S, Limb GA, Khaw PT. Strategies for optic nerve rescue and regeneration in glaucoma and other optic neuropathies. Drug Discov Today. 2010;15(7-8):287-99.
36. Howell GR, Libby RT, Jakobs TC, Smith RS, Phalan FC, Barter JW, et al. Axons of retinal ganglion cells are insulted in the optic nerve early in DBA/2J glaucoma. J Cell Biol. 2007;179(7):1523-37.
37. Rotchford AP, Johnson GJ. Glaucoma in Zulus: a population-based cross-sectional survey in a rural district in South Africa. Arch Ophthalmol. 2002;120(4):471-8.
38. Cho HK, Kee C. Population-based glaucoma prevalence studies in Asians. Surv Ophthalmol. 2014;59(4):434-47.
39. Sommer A, Tielsch JM, Katz J, Quigley HA, Gottsch JD, Javitt J, et al. Relationship between intraocular pressure and primary open angle glaucoma among white and black Americans. The Baltimore Eye Survey. Arch Ophthalmol. 1991;109(8):1090-5.

40. Klein BE, Klein R, Sponsel WE, Franke T, Cantor LB, Martone J, et al. Prevalence of glaucoma. The Beaver Dam Eye Study. Ophthalmology. 1992;99(10):1499-504.
41. Bonomi L, Marchini G, Marraffa M, Bernardi P, De Franco I, Perfetti S, et al. Prevalence of glaucoma and intraocular pressure distribution in a defined population. The Egna-Neumarkt Study. Ophthalmology. 1998;105(2):209-15.
42. Hood DC, Raza AS, de Moraes CG, Liebmann JM, Ritch R. Glaucomatous damage of the macula. Prog Retin Eye Res. 2013;32:1-21.
43. Weinreb RN, Aung T, Medeiros FA. The pathophysiology and treatment of glaucoma: a review. JAMA. 2014;311(18):1901-11.
44. Ghaffarieh A, Levin LA. Optic nerve disease and axon pathophysiology. Int Rev Neurobiol. 2012;105:1-17.
45. Biousse V, Newman NJ. Ischemic Optic Neuropathies. N Engl J Med. 2015;373(17):1677.
46. Behbehani R. Clinical approach to optic neuropathies. Clin Ophthalmol. 2007;1(3):233-46.
47. Martinez-Perez R, Albonette-Felicio T, Hardesty DA, Carrau RL, Prevedello DM. Outcome of the surgical decompression for traumatic optic neuropathy: a systematic review and meta-analysis. Neurosurg Rev. 2020.
48. Degnan AJ, Levy LM. Pseudotumor cerebri: brief review of clinical syndrome and imaging findings. AJNR Am J Neuroradiol. 2011;32(11):1986-93.
49. Lee AG, Mader TH, Gibson CR, Brunstetter TJ, Tarver WJ. Space flight-associated neuro-ocular syndrome (SANS). Eye (Lond). 2018;32(7):1164-7.
50. Yoles E, Schwartz M. Degeneration of spared axons following partial white matter lesion: implications for optic nerve neuropathies. Exp Neurol. 1998;153(1):1-7.
51. Levkovitch-Verbin H, Quigley HA, Martin KR, Zack DJ, Pease ME, Valenta DF. A model to study differences between primary and secondary degeneration of retinal ganglion cells in rats by partial optic nerve transection. Invest Ophthalmol Vis Sci. 2003;44(8):3388-93.
52. Carelli V, La Morgia C, Valentino ML, Barboni P, Ross-Cisneros FN, Sadun AA. Retinal ganglion cell neurodegeneration in mitochondrial inherited disorders. Biochim Biophys Acta. 2009;1787(5):518-28.
53. Lenaers G, Hamel C, Delettre C, Amati-Bonneau P, Procaccio V, Bonneau D, et al. Dominant optic atrophy. Orphanet J Rare Dis. 2012;7:46.
54. Kersten HM, Danesh-Meyer HV, Kilfoyle DH, Roxburgh RH. Optical coherence tomography findings in Huntington's disease: a potential biomarker of disease progression. J Neurol. 2015;262(11):2457-65.
55. La Morgia C, Di Vito L, Carelli V, Carbonelli M. Patterns of Retinal Ganglion Cell Damage in Neurodegenerative Disorders: Parvocellular vs Magnocellular Degeneration in Optical Coherence Tomography Studies. Front Neurol. 2017;8:710.
56. Li Y, Schlamp CL, Nickells RW. Experimental induction of retinal ganglion cell death in adult mice. Invest Ophthalmol Vis Sci. 1999;40(5):1004-8.
57. Berkelaar M, Clarke DB, Wang YC, Bray GM, Aguayo AJ. Axotomy results in delayed death and apoptosis of retinal ganglion cells in adult rats. J Neurosci. 1994;14(7):4368-74.
58. Villegas-Pérez MP, Vidal-Sanz M, Rasminsky M, Bray GM, Aguayo AJ. Rapid and protracted phases of retinal ganglion cell loss follow axotomy in the optic nerve of adult rats. J Neurobiol. 1993;24(1):23-36.

59. Wolf JA, Stys PK, Lusardi T, Meaney D, Smith DH. Traumatic axonal injury induces calcium influx modulated by tetrodotoxin-sensitive sodium channels. J Neurosci. 2001;21(6):1923-30.
60. George EB, Glass JD, Griffin JW. Axotomy-induced axonal degeneration is mediated by calcium influx through ion-specific channels. J Neurosci. 1995;15(10):6445-52.
61. Witte ME, Schumacher AM, Mahler CF, Bewersdorf JP, Lehmitz J, Scheiter A, et al. Calcium Influx through Plasma-Membrane Nanoruptures Drives Axon Degeneration in a Model of Multiple Sclerosis. Neuron. 2019;101(4):615-24.e5.
62. Stirling DP, Cummins K, Wayne Chen SR, Stys P. Axoplasmic reticulum Ca(2+) release causes secondary degeneration of spinal axons. Ann Neurol. 2014;75(2):220-9.
63. Choi HJ, Sun D, Jakobs TC. Astrocytes in the optic nerve head express putative mechanosensitive channels. Mol Vis. 2015;21:749-66.
64. Sappington RM, Sidorova T, Long DJ, Calkins DJ. TRPV1: contribution to retinal ganglion cell apoptosis and increased intracellular Ca2+ with exposure to hydrostatic pressure. Invest Ophthalmol Vis Sci. 2009;50(2):717-28.
65. Williams PR, Marincu BN, Sorbara CD, Mahler CF, Schumacher AM, Griesbeck O, et al. A recoverable state of axon injury persists for hours after spinal cord contusion in vivo. Nat Commun. 2014;5:5683.
66. Goll DE, Thompson VF, Li H, Wei W, Cong J. The calpain system. Physiol Rev. 2003;83(3):731-801.
67. Knöferle J, Koch JC, Ostendorf T, Michel U, Planchamp V, Vutova P, et al. Mechanisms of acute axonal degeneration in the optic nerve in vivo. Proc Natl Acad Sci U S A. 2010;107(13):6064-9.
68. Kerschensteiner M, Schwab ME, Lichtman JW, Misgeld T. In vivo imaging of axonal degeneration and regeneration in the injured spinal cord. Nat Med. 2005;11(5):572-7.
69. Beirowski B, Nógrádi A, Babetto E, Garcia-Alias G, Coleman MP. Mechanisms of axonal spheroid formation in central nervous system Wallerian degeneration. J Neuropathol Exp Neurol. 2010;69(5):455-72.
70. Conforti L, Gilley J, Coleman MP. Wallerian degeneration: an emerging axon death pathway linking injury and disease. Nat Rev Neurosci. 2014;15(6):394-409.
71. Blanquie O, Bradke F. Cytoskeleton dynamics in axon regeneration. Curr Opin Neurobiol. 2018;51:60-9.
72. Ertürk A, Hellal F, Enes J, Bradke F. Disorganized microtubules underlie the formation of retraction bulbs and the failure of axonal regeneration. J Neurosci. 2007;27(34):9169-80.
73. Ruschel J, Hellal F, Flynn KC, Dupraz S, Elliott DA, Tedeschi A, et al. Axonal regeneration. Systemic administration of epothilone B promotes axon regeneration after spinal cord injury. Science. 2015;348(6232):347-52.
74. Wang XW, Yang SG, Zhang C, Hu MW, Qian J, Ma JJ, et al. Knocking Out Non-muscle Myosin II in Retinal Ganglion Cells Promotes Long-Distance Optic Nerve Regeneration. Cell Rep. 2020;31(3):107537.
75. Misgeld T, Kerschensteiner M, Bareyre FM, Burgess RW, Lichtman JW. Imaging axonal transport of mitochondria in vivo. Nat Methods. 2007;4(7):559-61.
76. Han SM, Baig HS, Hammarlund M. Mitochondria Localize to Injured Axons to Support Regeneration. Neuron. 2016;92(6):1308-23.

77. Shin JE, Cho Y, Beirowski B, Milbrandt J, Cavalli V, DiAntonio A. Dual leucine zipper kinase is required for retrograde injury signaling and axonal regeneration. Neuron. 2012;74(6):1015-22.
78. Watkins TA, Wang B, Huntwork-Rodriguez S, Yang J, Jiang Z, Eastham-Anderson J, et al. DLK initiates a transcriptional program that couples apoptotic and regenerative responses to axonal injury. Proc Natl Acad Sci U S A. 2013;110(10):4039-44.
79. Welsbie DS, Yang Z, Ge Y, Mitchell KL, Zhou X, Martin SE, et al. Functional genomic screening identifies dual leucine zipper kinase as a key mediator of retinal ganglion cell death. Proc Natl Acad Sci U S A. 2013;110(10):4045-50.
80. Welsbie DS, Mitchell KL, Jaskula-Ranga V, Sluch VM, Yang Z, Kim J, et al. Enhanced Functional Genomic Screening Identifies Novel Mediators of Dual Leucine Zipper Kinase-Dependent Injury Signaling in Neurons. Neuron. 2017;94(6):1142-54.e6.
81. Yin Y, Cui Q, Gilbert HY, Yang Y, Yang Z, Berlinicke C, et al. Oncomodulin links inflammation to optic nerve regeneration. Proc Natl Acad Sci U S A. 2009;106(46):19587-92.
82. Kurimoto T, Yin Y, Habboub G, Gilbert HY, Li Y, Nakao S, et al. Neutrophils express oncomodulin and promote optic nerve regeneration. J Neurosci. 2013;33(37):14816-24.
83. Yin Y, Henzl MT, Lorber B, Nakazawa T, Thomas TT, Jiang F, et al. Oncomodulin is a macrophage-derived signal for axon regeneration in retinal ganglion cells. Nat Neurosci. 2006;9(6):843-52.
84. Andries L, De Groef L, Moons L. Neuroinflammation and Optic Nerve Regeneration: Where Do We Stand in Elucidating Underlying Cellular and Molecular Players? Curr Eye Res. 2020;45(3):397-409.
85. Shechter R, London A, Varol C, Raposo C, Cusimano M, Yovel G, et al. Infiltrating blood-derived macrophages are vital cells playing an anti-inflammatory role in recovery from spinal cord injury in mice. PLoS Med. 2009;6(7):e1000113.
86. O'Koren EG, Mathew R, Saban DR. Fate mapping reveals that microglia and recruited monocyte-derived macrophages are definitively distinguishable by phenotype in the retina. Sci Rep. 2016;6:20636.
87. Qu J, Jakobs TC. The Time Course of Gene Expression during Reactive Gliosis in the Optic Nerve. PLoS One. 2013;8(6):e67094.
88. Sun D, Lye-Barthel M, Masland RH, Jakobs TC. Structural remodeling of fibrous astrocytes after axonal injury. J Neurosci. 2010;30(42):14008-19.
89. Wohl SG, Schmeer CW, Witte OW, Isenmann S. Proliferative response of microglia and macrophages in the adult mouse eye after optic nerve lesion. Invest Ophthalmol Vis Sci. 2010;51(5):2686-96.
90. Kim SH, Munemasa Y, Kwong JM, Ahn JH, Mareninov S, Gordon LK, et al. Activation of autophagy in retinal ganglion cells. J Neurosci Res. 2008;86(13):2943-51.
91. Hu Y, Park KK, Yang L, Wei X, Yang Q, Cho KS, et al. Differential effects of unfolded protein response pathways on axon injury-induced death of retinal ganglion cells. Neuron. 2012;73(3):445-52.
92. Chen DF, Jhaveri S, Schneider GE. Intrinsic changes in developing retinal neurons result in regenerative failure of their axons. Proc Natl Acad Sci U S A. 1995;92(16):7287-91.
93. Goldberg JL, Klassen MP, Hua Y, Barres BA. Amacrine-signaled loss of intrinsic axon growth ability by retinal ganglion cells. Science. 2002;296(5574):1860-4.
94. Syc-Mazurek SB, Libby RT. Axon injury signaling and compartmentalized injury response in glaucoma. Prog Retin Eye Res. 2019;73:100769.

95. Maes ME, Schlamp CL, Nickells RW. BAX to basics: How the BCL2 gene family controls the death of retinal ganglion cells. Prog Retin Eye Res. 2017;57:1-25.
96. Chinnaiyan AM, O'Rourke K, Lane BR, Dixit VM. Interaction of CED-4 with CED-3 and CED-9: a molecular framework for cell death. Science. 1997;275(5303):1122-6.
97. Ellis HM, Horvitz HR. Genetic control of programmed cell death in the nematode C. elegans. Cell. 1986;44(6):817-29.
98. Conradt B, Wu YC, Xue D. Programmed Cell Death During Caenorhabditis elegans Development. Genetics. 2016;203(4):1533-62.
99. Zou H, Henzel WJ, Liu X, Lutschg A, Wang X. Apaf-1, a human protein homologous to C. elegans CED-4, participates in cytochrome c-dependent activation of caspase-3. Cell. 1997;90(3):405-13.
100. Desagher S, Osen-Sand A, Nichols A, Eskes R, Montessuit S, Lauper S, et al. Bid-induced conformational change of Bax is responsible for mitochondrial cytochrome c release during apoptosis. J Cell Biol. 1999;144(5):891-901.
101. Nechushtan A, Smith CL, Hsu YT, Youle RJ. Conformation of the Bax C-terminus regulates subcellular location and cell death. EMBO J. 1999;18(9):2330-41.
102. Lowe SW, Cepero E, Evan G. Intrinsic tumour suppression. Nature. 2004;432(7015):307-15.
103. Bonfanti L, Strettoi E, Chierzi S, Cenni MC, Liu XH, Martinou J-C, et al. Protection of retinal ganglion cells from natural and axotomy-induced cell death in neonatal transgenic mice overexpressing bcl-2. J Neurosci. 1996;16(13):4186-94.
104. Semaan SJ, Li Y, Nickells RW. A single nucleotide polymorphism in the Bax gene promoter affects transcription and influences retinal ganglion cell death. ASN Neuro. 2010;2(2):e00032.
105. Janssen KT, Mac Nair CE, Dietz JA, Schlamp CL, Nickells RW. Nuclear atrophy of retinal ganglion cells precedes the bax-dependent stage of apoptosis. Invest Ophthalmol Vis Sci. 2013;54(3):1805-15.
106. Donahue RJ, Maes ME, Grosser JA, Nickells RW. BAX-Depleted Retinal Ganglion Cells Survive and Become Quiescent Following Optic Nerve Damage. Mol Neurobiol. 2020;57(2):1070-84.
107. Rishal I, Fainzilber M. Axon-soma communication in neuronal injury. Nat Rev Neurosci. 2014;15(1):32-42.
108. Keshet Y, Seger R. The MAP kinase signaling cascades: a system of hundreds of components regulates a diverse array of physiological functions. Methods Mol Biol. 2010;661:3-38.
109. Holland SM, Collura KM, Ketschek A, Noma K, Ferguson TA, Jin Y, et al. Palmitoylation controls DLK localization, interactions and activity to ensure effective axonal injury signaling. Proc Natl Acad Sci U S A. 2016;113(3):763-8.
110. Shin JE, Ha H, Kim YK, Cho Y, DiAntonio A. DLK regulates a distinctive transcriptional regeneration program after peripheral nerve injury. Neurobiol Dis. 2019;127:178-92.
111. Hunt D, Hossain-Ibrahim K, Mason MR, Coffin RS, Lieberman AR, Winterbottom J, et al. ATF3 upregulation in glia during Wallerian degeneration: differential expression in peripheral nerves and CNS white matter. BMC Neurosci. 2004;5:9.

112. Lindwall C, Kanje M. Retrograde axonal transport of JNK signaling molecules influence injury induced nuclear changes in p-c-Jun and ATF3 in adult rat sensory neurons. Mol Cell Neurosci. 2005;29(2):269-82.
113. Hunt D, Raivich G, Anderson PN. Activating transcription factor 3 and the nervous system. Front Mol Neurosci. 2012;5:7.
114. Yasuda M, Tanaka Y, Ryu M, Tsuda S, Nakazawa T. RNA sequence reveals mouse retinal transcriptome changes early after axonal injury. PLoS One. 2014;9(3):e93258.
115. Yasuda M, Tanaka Y, Omodaka K, Nishiguchi KM, Nakamura O, Tsuda S, et al. Transcriptome profiling of the rat retina after optic nerve transection. Sci Rep. 2016;6:28736.
116. Fernandes KA, Harder JM, Fornarola LB, Freeman RS, Clark AF, Pang IH, et al. JNK2 and JNK3 are major regulators of axonal injury-induced retinal ganglion cell death. Neurobiol Dis. 2012;46(2):393-401.
117. Harder JM, Williams PA, Soto I, Foxworth NE, Fernandes KA, Freeburg NF, et al. Jnk2 deficiency increases the rate of glaucomatous neurodegeneration in ocular hypertensive DBA/2J mice. Cell Death Dis. 2018;9(6):705.
118. Rodríguez-Muela N, Germain F, Mariño G, Fitze PS, Boya P. Autophagy promotes survival of retinal ganglion cells after optic nerve axotomy in mice. Cell Death Differ. 2012;19(1):162-9.
119. Boya P, Esteban-Martínez L, Serrano-Puebla A, Gómez-Sintes R, Villarejo-Zori B. Autophagy in the eye: Development, degeneration, and aging. Prog Retin Eye Res. 2016;55:206-45.
120. Hammarlund M, Nix P, Hauth L, Jorgensen EM, Bastiani M. Axon regeneration requires a conserved MAP kinase pathway. Science. 2009;323(5915):802-6.
121. Libby RT, Li Y, Savinova OV, Barter J, Smith RS, Nickells RW, et al. Susceptibility to neurodegeneration in a glaucoma is modified by Bax gene dosage. PLoS Genet. 2005;1(1):17-26.
122. Fujiki M, Zhang Z, Guth L, Steward O. Genetic influences on cellular reactions to spinal cord injury: activation of macrophages/microglia and astrocytes is delayed in mice carrying a mutation (WldS) that causes delayed Wallerian degeneration. J Comp Neurol. 1996;371(3):469-84.
123. Beirowski B, Babetto E, Coleman MP, Martin KR. The WldS gene delays axonal but not somatic degeneration in a rat glaucoma model. Eur J Neurosci. 2008;28(6):1166-79.
124. Williams PA, Harder JM, Foxworth NE, Cardozo BH, Cochran KE, John SWM. Nicotinamide and WLD. Front Neurosci. 2017;11:232.
125. Conforti L, Tarlton A, Mack TG, Mi W, Buckmaster EA, Wagner D, et al. A Ufd2/D4Cole1e chimeric protein and overexpression of Rbp7 in the slow Wallerian degeneration (WldS) mouse. Proc Natl Acad Sci U S A. 2000;97(21):11377-82.
126. Mack TG, Reiner M, Beirowski B, Mi W, Emanuelli M, Wagner D, et al. Wallerian degeneration of injured axons and synapses is delayed by a Ube4b/Nmnat chimeric gene. Nat Neurosci. 2001;4(12):1199-206.
127. Wang J, Zhai Q, Chen Y, Lin E, Gu W, McBurney MW, et al. A local mechanism mediates NAD-dependent protection of axon degeneration. J Cell Biol. 2005;170(3):349-55.
128. Gilley J, Coleman MP. Endogenous Nmnat2 is an essential survival factor for maintenance of healthy axons. PLoS Biol. 2010;8(1):e1000300.
129. Gerdts J, Brace EJ, Sasaki Y, DiAntonio A, Milbrandt J. SARM1 activation triggers axon degeneration locally via NAD^+ destruction. Science. 2015;348(6233):453-7.

130. Osterloh JM, Yang J, Rooney TM, Fox AN, Adalbert R, Powell EH, et al. dSarm/Sarm1 is required for activation of an injury-induced axon death pathway. Science. 2012;337(6093):481-4.
131. Fernandes KA, Mitchell KL, Patel A, Marola OJ, Shrager P, Zack DJ, et al. Role of SARM1 and DR6 in retinal ganglion cell axonal and somal degeneration following axonal injury. Exp Eye Res. 2018;171:54-61.
132. Summers DW, Milbrandt J, DiAntonio A. Palmitoylation enables MAPK-dependent proteostasis of axon survival factors. Proc Natl Acad Sci U S A. 2018;115(37):E8746-E54.
133. Summers DW, Frey E, Walker LJ, Milbrandt J, DiAntonio A. DLK Activation Synergizes with Mitochondrial Dysfunction to Downregulate Axon Survival Factors and Promote SARM1-Dependent Axon Degeneration. Mol Neurobiol. 2020;57(2):1146-58.
134. Shin JE, Miller BR, Babetto E, Cho Y, Sasaki Y, Qayum S, et al. SCG10 is a JNK target in the axonal degeneration pathway. Proc Natl Acad Sci U S A. 2012;109(52):E3696-705.
135. Gerdts J, Summers DW, Milbrandt J, DiAntonio A. Axon Self-Destruction: New Links among SARM1, MAPKs, and NAD+ Metabolism. Neuron. 2016;89(3):449-60.
136. Lunn ER, Perry VH, Brown MC, Rosen H, Gordon S. Absence of Wallerian Degeneration does not Hinder Regeneration in Peripheral Nerve. Eur J Neurosci. 1989;1(1):27-33.
137. Herrera SC, Bach EA. JAK/STAT signaling in stem cells and regeneration: from. Development. 2019;146(2).
138. Pernet V, Joly S, Jordi N, Dalkara D, Guzik-Kornacka A, Flannery JG, et al. Misguidance and modulation of axonal regeneration by Stat3 and Rho/ROCK signaling in the transparent optic nerve. Cell Death Dis. 2013;4:e734.
139. Müller A, Hauk TG, Fischer D. Astrocyte-derived CNTF switches mature RGCs to a regenerative state following inflammatory stimulation. Brain. 2007;130(Pt 12):3308-20.
140. Müller A, Hauk TG, Leibinger M, Marienfeld R, Fischer D. Exogenous CNTF stimulates axon regeneration of retinal ganglion cells partially via endogenous CNTF. Mol Cell Neurosci. 2009;41(2):233-46.
141. Fischer D, Pavlidis M, Thanos S. Cataractogenic lens injury prevents traumatic ganglion cell death and promotes axonal regeneration both in vivo and in culture. Invest Ophthalmol Vis Sci. 2000;41(12):3943-54.
142. Fischer D, Leibinger M. Promoting optic nerve regeneration. Prog Retin Eye Res. 2012;31(6):688-701.
143. Smith PD, Sun F, Park KK, Cai B, Wang C, Kuwako K, et al. SOCS3 deletion promotes optic nerve regeneration in vivo. Neuron. 2009;64(5):617-23.
144. Moore DL, Blackmore MG, Hu Y, Kaestner KH, Bixby JL, Lemmon VP, et al. KLF family members regulate intrinsic axon regeneration ability. Science. 2009;326(5950):298-301.
145. Apara A, Galvao J, Wang Y, Blackmore M, Trillo A, Iwao K, et al. KLF9 and JNK3 Interact to Suppress Axon Regeneration in the Adult CNS. J Neurosci. 2017;37(40):9632-44.
146. Darnell JE. STATs and gene regulation. Science. 1997;277(5332):1630-5.
147. Schaefer TS, Sanders LK, Nathans D. Cooperative transcriptional activity of Jun and Stat3 beta, a short form of Stat3. Proc Natl Acad Sci U S A. 1995;92(20):9097-101.
148. Shen S, Niso-Santano M, Adjemian S, Takehara T, Malik SA, Minoux H, et al. Cytoplasmic STAT3 represses autophagy by inhibiting PKR activity. Mol Cell. 2012;48(5):667-80.

149. Luo X, Ribeiro M, Bray ER, Lee DH, Yungher BJ, Mehta ST, et al. Enhanced Transcriptional Activity and Mitochondrial Localization of STAT3 Co-induce Axon Regrowth in the Adult Central Nervous System. Cell Rep. 2016;15(2):398-410.
150. Sarbassov DD, Ali SM, Sabatini DM. Growing roles for the mTOR pathway. Curr Opin Cell Biol. 2005;17(6):596-603.
151. Homma K, Koriyama Y, Mawatari K, Higuchi Y, Kosaka J, Kato S. Early downregulation of IGF-I decides the fate of rat retinal ganglion cells after optic nerve injury. Neurochem Int. 2007;50(5):741-8.
152. Sun F, Park KK, Belin S, Wang D, Lu T, Chen G, et al. Sustained axon regeneration induced by co-deletion of PTEN and SOCS3. Nature. 2011;480(7377):372-5.
153. Park KK, Liu K, Hu Y, Smith PD, Wang C, Cai B, et al. Promoting axon regeneration in the adult CNS by modulation of the PTEN/mTOR pathway. Science. 2008;322(5903):963-6.
154. Leibinger M, Andreadaki A, Fischer D. Role of mTOR in neuroprotection and axon regeneration after inflammatory stimulation. Neurobiol Dis. 2012;46(2):314-24.
155. Agostinone J, Alarcon-Martinez L, Gamlin C, Yu WQ, Wong ROL, Di Polo A. Insulin signalling promotes dendrite and synapse regeneration and restores circuit function after axonal injury. Brain. 2018;141(7):1963-80.
156. Ma JJ, Ju X, Xu RJ, Wang WH, Luo ZP, Liu CM, et al. Telomerase Reverse Transcriptase and p53 Regulate Mammalian Peripheral Nervous System and CNS Axon Regeneration Downstream of c-Myc. J Neurosci. 2019;39(46):9107-18.
157. Floriddia EM, Rathore KI, Tedeschi A, Quadrato G, Wuttke A, Lueckmann JM, et al. p53 Regulates the neuronal intrinsic and extrinsic responses affecting the recovery of motor function following spinal cord injury. J Neurosci. 2012;32(40):13956-70.
158. Yamanaka S, Takahashi K. [Induction of pluripotent stem cells from mouse fibroblast cultures]. Tanpakushitsu Kakusan Koso. 2006;51(15):2346-51.
159. Lu Y, Brommer B, Tian X, Krishnan A, Meer M, Wang C, et al. Reprogramming to recover youthful epigenetic information and restore vision. Nature. 2020;588(7836):124-9.
160. Ambros V, Horvitz HR. Heterochronic mutants of the nematode Caenorhabditis elegans. Science. 1984;226(4673):409-16.
161. Tsialikas J, Romer-Seibert J. LIN28: roles and regulation in development and beyond. Development. 2015;142(14):2397-404.
162. Wang XW, Li Q, Liu CM, Hall PA, Jiang JJ, Katchis CD, et al. Lin28 Signaling Supports Mammalian PNS and CNS Axon Regeneration. Cell Rep. 2018;24(10):2540-52.e6.
163. Zhang Y, Williams PR, Jacobi A, Wang C, Goel A, Hirano AA, et al. Elevating Growth Factor Responsiveness and Axon Regeneration by Modulating Presynaptic Inputs. Neuron. 2019;103(1):39-51.e5.
164. Belin S, Nawabi H, Wang C, Tang S, Latremoliere A, Warren P, et al. Injury-induced decline of intrinsic regenerative ability revealed by quantitative proteomics. Neuron. 2015;86(4):1000-14.
165. Kurimoto T, Yin Y, Omura K, Gilbert HY, Kim D, Cen LP, et al. Long-distance axon regeneration in the mature optic nerve: contributions of oncomodulin, cAMP, and pten gene deletion. J Neurosci. 2010;30(46):15654-63.
166. de Lima S, Habboub G, Benowitz LI. Combinatorial therapy stimulates long-distance regeneration, target reinnervation, and partial recovery of vision after optic nerve injury in mice. Int Rev Neurobiol. 2012;106:153-72.

167. Pernet V, Di Polo A. Synergistic action of brain-derived neurotrophic factor and lens injury promotes retinal ganglion cell survival, but leads to optic nerve dystrophy in vivo. Brain. 2006;129(Pt 4):1014-26.
168. KUFFLER SW. Discharge patterns and functional organization of mammalian retina. J Neurophysiol. 1953;16(1):37-68.
169. Gupta N, Yücel YH. What changes can we expect in the brain of glaucoma patients? Surv Ophthalmol. 2007;52 Suppl 2:S122-6.
170. Dacey DM, Petersen MR. Dendritic field size and morphology of midget and parasol ganglion cells of the human retina. Proc Natl Acad Sci U S A. 1992;89(20):9666-70.
171. Hannibal J, Christiansen AT, Heegaard S, Fahrenkrug J, Kiilgaard JF. Melanopsin expressing human retinal ganglion cells: Subtypes, distribution, and intraretinal connectivity. J Comp Neurol. 2017;525(8):1934-61.
172. Tran NM, Shekhar K, Whitney IE, Jacobi A, Benhar I, Hong G, et al. Single-Cell Profiles of Retinal Ganglion Cells Differing in Resilience to Injury Reveal Neuroprotective Genes. Neuron. 2019;104(6):1039-55.e12.
173. Duan X, Qiao M, Bei F, Kim IJ, He Z, Sanes JR. Subtype-specific regeneration of retinal ganglion cells following axotomy: effects of osteopontin and mTOR signaling. Neuron. 2015;85(6):1244-56.
174. Norsworthy MW, Bei F, Kawaguchi R, Wang Q, Tran NM, Li Y, et al. Sox11 Expression Promotes Regeneration of Some Retinal Ganglion Cell Types but Kills Others. Neuron. 2017;94(6):1112-20.e4.
175. Lim JH, Stafford BK, Nguyen PL, Lien BV, Wang C, Zukor K, et al. Neural activity promotes long-distance, target-specific regeneration of adult retinal axons. Nat Neurosci. 2016;19(8):1073-84.
176. Peng YR, Shekhar K, Yan W, Herrmann D, Sappington A, Bryman GS, et al. Molecular Classification and Comparative Taxonomics of Foveal and Peripheral Cells in Primate Retina. Cell. 2019;176(5):1222-37.e22.
177. Kaplan E. The M, P, and K pathways of the primate visual system. In: Chalupa LM, Werner JS, editors. The Visual Neurosciences. 1. Cambridge, MA: MIT Press; 2004. p. 481-93.
178. Li Y, Andereggen L, Yuki K, Omura K, Yin Y, Gilbert HY, et al. Mobile zinc increases rapidly in the retina after optic nerve injury and regulates ganglion cell survival and optic nerve regeneration. Proc Natl Acad Sci U S A. 2017;114(2):E209-E18.
179. Casson RJ. Possible role of excitotoxicity in the pathogenesis of glaucoma. Clin Exp Ophthalmol. 2006;34(1):54-63.
180. Itoh N, Nagata S. A novel protein domain required for apoptosis. Mutational analysis of human Fas antigen. J Biol Chem. 1993;268(15):10932-7.
181. Nakazawa T, Nakazawa C, Matsubara A, Noda K, Hisatomi T, She H, et al. Tumor necrosis factor-alpha mediates oligodendrocyte death and delayed retinal ganglion cell loss in a mouse model of glaucoma. J Neurosci. 2006;26(49):12633-41.
182. Sawada H, Fukuchi T, Tanaka T, Abe H. Tumor necrosis factor-alpha concentrations in the aqueous humor of patients with glaucoma. Invest Ophthalmol Vis Sci. 2010;51(2):903-6.
183. Cueva Vargas JL, Osswald IK, Unsain N, Aurousseau MR, Barker PA, Bowie D, et al. Soluble Tumor Necrosis Factor Alpha Promotes Retinal Ganglion Cell Death in Glaucoma via Calcium-Permeable AMPA Receptor Activation. J Neurosci. 2015;35(35):12088-102.

184. Ebadi M, Bashir RM, Heidrick ML, Hamada FM, Refaey HE, Hamed A, et al. Neurotrophins and their receptors in nerve injury and repair. Neurochem Int. 1997;30(4-5):347-74.
185. Mey J, Thanos S. Intravitreal injections of neurotrophic factors support the survival of axotomized retinal ganglion cells in adult rats in vivo. Brain Res. 1993;602(2):304-17.
186. Di Polo A, Aigner LJ, Dunn RJ, Bray GM, Aguayo AJ. Prolonged delivery of brain-derived neurotrophic factor by adenovirus-infected Müller cells temporarily rescues injured retinal ganglion cells. Proc Natl Acad Sci U S A. 1998;95(7):3978-83.
187. Pease ME, McKinnon SJ, Quigley HA, Kerrigan-Baumrind LA, Zack DJ. Obstructed axonal transport of BDNF and its receptor TrkB in experimental glaucoma. Invest Ophthalmol Vis Sci. 2000;41(3):764-74.
188. Quigley HA, McKinnon SJ, Zack DJ, Pease ME, Kerrigan-Baumrind LA, Kerrigan DF, et al. Retrograde axonal transport of BDNF in retinal ganglion cells is blocked by acute IOP elevation in rats. Invest Ophthalmol Vis Sci. 2000;41(11):3460-6.
189. Leibinger M, Müller A, Andreadaki A, Hauk TG, Kirsch M, Fischer D. Neuroprotective and axon growth-promoting effects following inflammatory stimulation on mature retinal ganglion cells in mice depend on ciliary neurotrophic factor and leukemia inhibitory factor. J Neurosci. 2009;29(45):14334-41.
190. Jessen KR, Mirsky R, Lloyd AC. Schwann Cells: Development and Role in Nerve Repair. Cold Spring Harb Perspect Biol. 2015;7(7):a020487.
191. Ramon y Cajal S. Degeneration and Regeneration of the Nervous System. New York: Oxford University Press; 1991.
192. Bray GM, Villegas-Pérez MP, Vidal-Sanz M, Aguayo AJ. The use of peripheral nerve grafts to enhance neuronal survival, promote growth and permit terminal reconnections in the central nervous system of adult rats. J Exp Biol. 1987;132:5-19.
193. Vidal-Sanz M, Bray GM, Villegas-Pérez MP, Thanos S, Aguayo AJ. Axonal regeneration and synapse formation in the superior colliculus by retinal ganglion cells in the adult rat. J Neurosci. 1987;7(9):2894-909.
194. Vidal-Sanz M, Bray GM, Aguayo AJ. Regenerated synapses persist in the superior colliculus after the regrowth of retinal ganglion cell axons. J Neurocytol. 1991;20(11):940-52.
195. Schwab ME, Thoenen H. Dissociated neurons regenerate into sciatic but not optic nerve explants in culture irrespective of neurotrophic factors. J Neurosci. 1985;5(9):2415-23.
196. Schnell L, Schwab ME. Axonal regeneration in the rat spinal cord produced by an antibody against myelin-associated neurite growth inhibitors. Nature. 1990;343(6255):269-72.
197. McKerracher L, David S, Jackson DL, Kottis V, Dunn RJ, Braun PE. Identification of myelin-associated glycoprotein as a major myelin-derived inhibitor of neurite growth. Neuron. 1994;13(4):805-11.
198. Chen MS, Huber AB, van der Haar ME, Frank M, Schnell L, Spillmann AA, et al. Nogo-A is a myelin-associated neurite outgrowth inhibitor and an antigen for monoclonal antibody IN-1. Nature. 2000;403(6768):434-9.
199. Wang KC, Koprivica V, Kim JA, Sivasankaran R, Guo Y, Neve RL, et al. Oligodendrocyte-myelin glycoprotein is a Nogo receptor ligand that inhibits neurite outgrowth. Nature. 2002;417(6892):941-4.
200. Domeniconi M, Cao Z, Spencer T, Sivasankaran R, Wang K, Nikulina E, et al. Myelin-associated glycoprotein interacts with the Nogo66 receptor to inhibit neurite outgrowth. Neuron. 2002;35(2):283-90.

201. Kottis V, Thibault P, Mikol D, Xiao ZC, Zhang R, Dergham P, et al. Oligodendrocyte-myelin glycoprotein (OMgp) is an inhibitor of neurite outgrowth. J Neurochem. 2002;82(6):1566-9.
202. Fischer D, He Z, Benowitz LI. Counteracting the Nogo receptor enhances optic nerve regeneration if retinal ganglion cells are in an active growth state. J Neurosci. 2004;24(7):1646-51.
203. Dickendesher TL, Baldwin KT, Mironova YA, Koriyama Y, Raiker SJ, Askew KL, et al. NgR1 and NgR3 are receptors for chondroitin sulfate proteoglycans. Nat Neurosci. 2012;15(5):703-12.
204. Kucher K, Johns D, Maier D, Abel R, Badke A, Baron H, et al. First-in-Man Intrathecal Application of Neurite Growth-Promoting Anti-Nogo-A Antibodies in Acute Spinal Cord Injury. Neurorehabil Neural Repair. 2018;32(6-7):578-89.
205. McKeon RJ, Schreiber RC, Rudge JS, Silver J. Reduction of neurite outgrowth in a model of glial scarring following CNS injury is correlated with the expression of inhibitory molecules on reactive astrocytes. J Neurosci. 1991;11(11):3398-411.
206. Fitch MT, Doller C, Combs CK, Landreth GE, Silver J. Cellular and molecular mechanisms of glial scarring and progressive cavitation: in vivo and in vitro analysis of inflammation-induced secondary injury after CNS trauma. J Neurosci. 1999;19(19):8182-98.
207. Fabes J, Anderson P, Yáñez-Muñoz RJ, Thrasher A, Brennan C, Bolsover S. Accumulation of the inhibitory receptor EphA4 may prevent regeneration of corticospinal tract axons following lesion. Eur J Neurosci. 2006;23(7):1721-30.
208. Bradbury EJ, Moon LD, Popat RJ, King VR, Bennett GS, Patel PN, et al. Chondroitinase ABC promotes functional recovery after spinal cord injury. Nature. 2002;416(6881):636-40.
209. Anderson MA, Burda JE, Ren Y, Ao Y, O'Shea TM, Kawaguchi R, et al. Astrocyte scar formation aids central nervous system axon regeneration. Nature. 2016;532(7598):195-200.
210. Mimura F, Yamagishi S, Arimura N, Fujitani M, Kubo T, Kaibuchi K, et al. Myelin-associated glycoprotein inhibits microtubule assembly by a Rho-kinase-dependent mechanism. J Biol Chem. 2006;281(23):15970-9.
211. Harboe M, Torvund-Jensen J, Kjaer-Sorensen K, Laursen LS. Ephrin-A1-EphA4 signaling negatively regulates myelination in the central nervous system. Glia. 2018;66(5):934-50.
212. Lehmann M, Fournier A, Selles-Navarro I, Dergham P, Sebok A, Leclerc N, et al. Inactivation of Rho signaling pathway promotes CNS axon regeneration. J Neurosci. 1999;19(17):7537-47.
213. Fischer D, Petkova V, Thanos S, Benowitz LI. Switching mature retinal ganglion cells to a robust growth state in vivo: gene expression and synergy with RhoA inactivation. J Neurosci. 2004;24(40):8726-40.
214. Ellis RE, Jacobson DM, Horvitz HR. Genes required for the engulfment of cell corpses during programmed cell death in Caenorhabditis elegans. Genetics. 1991;129(1):79-94.
215. Zhou Z, Hartwieg E, Horvitz HR. CED-1 is a transmembrane receptor that mediates cell corpse engulfment in C. elegans. Cell. 2001;104(1):43-56.
216. Suzuki E, Nakayama M. MEGF10 is a mammalian ortholog of CED-1 that interacts with clathrin assembly protein complex 2 medium chain and induces large vacuole formation. Exp Cell Res. 2007;313(17):3729-42.
217. Hanayama R, Tanaka M, Miwa K, Shinohara A, Iwamatsu A, Nagata S. Identification of a factor that links apoptotic cells to phagocytes. Nature. 2002;417(6885):182-7.

218. Fadok VA, Voelker DR, Campbell PA, Cohen JJ, Bratton DL, Henson PM. Exposure of phosphatidylserine on the surface of apoptotic lymphocytes triggers specific recognition and removal by macrophages. J Immunol. 1992;148(7):2207-16.
219. Cordeiro MF, Normando EM, Cardoso MJ, Miodragovic S, Jeylani S, Davis BM, et al. Real-time imaging of single neuronal cell apoptosis in patients with glaucoma. Brain. 2017;140(6):1757-67.
220. Schmitz-Valckenberg S, Guo L, Maass A, Cheung W, Vugler A, Moss SE, et al. Real-time in vivo imaging of retinal cell apoptosis after laser exposure. Invest Ophthalmol Vis Sci. 2008;49(6):2773-80.
221. Yuan TF, Liang YX, Peng B, Lin B, So KF. Local proliferation is the main source of rod microglia after optic nerve transection. Sci Rep. 2015;5:10788.
222. Paolicelli RC, Bolasco G, Pagani F, Maggi L, Scianni M, Panzanelli P, et al. Synaptic pruning by microglia is necessary for normal brain development. Science. 2011;333(6048):1456-8.
223. Rice RA, Spangenberg EE, Yamate-Morgan H, Lee RJ, Arora RP, Hernandez MX, et al. Elimination of Microglia Improves Functional Outcomes Following Extensive Neuronal Loss in the Hippocampus. J Neurosci. 2015;35(27):9977-89.
224. Fan R, Xu F, Previti ML, Davis J, Grande AM, Robinson JK, et al. Minocycline reduces microglial activation and improves behavioral deficits in a transgenic model of cerebral microvascular amyloid. J Neurosci. 2007;27(12):3057-63.
225. Bosco A, Inman DM, Steele MR, Wu G, Soto I, Marsh-Armstrong N, et al. Reduced retina microglial activation and improved optic nerve integrity with minocycline treatment in the DBA/2J mouse model of glaucoma. Invest Ophthalmol Vis Sci. 2008;49(4):1437-46.
226. Hilla AM, Diekmann H, Fischer D. Microglia Are Irrelevant for Neuronal Degeneration and Axon Regeneration after Acute Injury. J Neurosci. 2017;37(25):6113-24.
227. Jessen KR, Mirsky R. Origin and early development of Schwann cells. Microsc Res Tech. 1998;41(5):393-402.
228. GUTH L. Regeneration in the mammalian peripheral nervous system. Physiol Rev. 1956;36(4):441-78.
229. Stoll G, Griffin JW, Li CY, Trapp BD. Wallerian degeneration in the peripheral nervous system: participation of both Schwann cells and macrophages in myelin degradation. J Neurocytol. 1989;18(5):671-83.
230. Huebner EA, Strittmatter SM. Axon regeneration in the peripheral and central nervous systems. Results Probl Cell Differ. 2009;48:339-51.
231. Makwana M, Raivich G. Molecular mechanisms in successful peripheral regeneration. FEBS J. 2005;272(11):2628-38.
232. Benowitz LI, He Z, Goldberg JL. Reaching the brain: Advances in optic nerve regeneration. Exp Neurol. 2017;287(Pt 3):365-73.
233. Hellsten U, Harland RM, Gilchrist MJ, Hendrix D, Jurka J, Kapitonov V, et al. The genome of the Western clawed frog Xenopus tropicalis. Science. 2010;328(5978):633-6.
234. Howe K, Clark MD, Torroja CF, Torrance J, Berthelot C, Muffato M, et al. The zebrafish reference genome sequence and its relationship to the human genome. Nature. 2013;496(7446):498-503.
235. Sperry R. Optic nerve regeneration with return of vision in anurans. American Physiological Society; 1944.

236. GAZE RM. Regeneration of the optic nerve in Xenopus laevis. Q J Exp Physiol Cogn Med Sci. 1959;44:290-308.
237. Meyer RL, Sakurai K, Schauwecker E. Topography of regenerating optic fibers in goldfish traced with local wheat germ injections into retina: evidence for discontinuous microtopography in the retinotectal projection. J Comp Neurol. 1985;239(1):27-43.
238. Straznicky K, Gaze RM. The growth of the retina in Xenopus laevis: an autoradiographic study. J Embryol Exp Morphol. 1971;26(1):67-79.
239. Johns PR. Growth of the adult goldfish eye. III. Source of the new retinal cells. J Comp Neurol. 1977;176(3):343-57.
240. Fausett BV, Goldman D. A role for alpha1 tubulin-expressing Müller glia in regeneration of the injured zebrafish retina. J Neurosci. 2006;26(23):6303-13.
241. Ramachandran R, Fausett BV, Goldman D. Ascl1a regulates Müller glia dedifferentiation and retinal regeneration through a Lin-28-dependent, let-7 microRNA signalling pathway. Nat Cell Biol. 2010;12(11):1101-7.
242. Zhao XF, Wan J, Powell C, Ramachandran R, Myers MG, Goldman D. Leptin and IL-6 family cytokines synergize to stimulate Müller glia reprogramming and retina regeneration. Cell Rep. 2014;9(1):272-84.
243. Bosco L. Transdifferentiation of ocular tissues in larval Xenopus laevis. Differentiation. 1988;39(1):4-15.
244. Yoshii C, Ueda Y, Okamoto M, Araki M. Neural retinal regeneration in the anuran amphibian Xenopus laevis post-metamorphosis: transdifferentiation of retinal pigmented epithelium regenerates the neural retina. Dev Biol. 2007;303(1):45-56.
245. Zou S, Tian C, Ge S, Hu B. Neurogenesis of retinal ganglion cells is not essential to visual functional recovery after optic nerve injury in adult zebrafish. PLoS One. 2013;8(2):e57280.
246. Liu Y, Yu H, Deaton SK, Szaro BG. Heterogeneous nuclear ribonucleoprotein K, an RNA-binding protein, is required for optic axon regeneration in Xenopus laevis. J Neurosci. 2012;32(10):3563-74.
247. Diekmann H, Kalbhen P, Fischer D. Characterization of optic nerve regeneration using transgenic zebrafish. Front Cell Neurosci. 2015;9:118.
248. Matsukawa T, Arai K, Koriyama Y, Liu Z, Kato S. Axonal regeneration of fish optic nerve after injury. Biol Pharm Bull. 2004;27(4):445-51.
249. Zhao Y, Szaro BG. The return of phosphorylated and nonphosphorylated epitopes of neurofilament proteins to the regenerating optic nerve of Xenopus laevis. J Comp Neurol. 1994;343(1):158-72.
250. Whitworth GB, Misaghi BC, Rosenthal DM, Mills EA, Heinen DJ, Watson AH, et al. Translational profiling of retinal ganglion cell optic nerve regeneration in Xenopus laevis. Dev Biol. 2017;426(2):360-73.
251. Beaver RS, Dunlop SA, Harman AM, Stirling RV, Easter SS, Roberts JD, et al. Continued neurogenesis is not a pre-requisite for regeneration of a topographic retino-tectal projection. Vision Res. 2001;41(14):1765-70.
252. Bohn RC, Reier PJ. Retrograde degeneration of myelinated axons and re-organization in the optic nerves of adult frogs (Xenopus laevis) following nerve injury or tectal ablation. J Neurocytol. 1985;14(2):221-44.
253. SPERRY RW. The problem of central nervous reorganization after nerve regeneration and muscle transposition. Q Rev Biol. 1945;20:311-69.

254. Meyer RL. Mapping the normal and regenerating retinotectal projection of goldfish with autoradiographic methods. J Comp Neurol. 1980;189(2):273-89.
255. Adamson J, Burke J, Grobstein P. Recovery of the ipsilateral oculotectal projection following nerve crush in the frog: evidence that retinal afferents make synapses at abnormal tectal locations. J Neurosci. 1984;4(10):2635-49.
256. Meyer RL. Tetrodotoxin inhibits the formation of refined retinotopography in goldfish. Brain Res. 1983;282(3):293-8.
257. Schmidt JT, Edwards DL. Activity sharpens the map during the regeneration of the retinotectal projection in goldfish. Brain Res. 1983;269(1):29-39.
258. Bastmeyer M, Beckmann M, Schwab ME, Stuermer CA. Growth of regenerating goldfish axons is inhibited by rat oligodendrocytes and CNS myelin but not but not by goldfish optic nerve tract oligodendrocytelike cells and fish CNS myelin. J Neurosci. 1991;11(3):626-40.
259. Veldman MB, Bemben MA, Thompson RC, Goldman D. Gene expression analysis of zebrafish retinal ganglion cells during optic nerve regeneration identifies KLF6a and KLF7a as important regulators of axon regeneration. Dev Biol. 2007;312(2):596-612.
260. Matsukawa T, Morita K, Omizu S, Kato S, Koriyama Y. Mechanisms of RhoA inactivation and CDC42 and Rac1 activation during zebrafish optic nerve regeneration. Neurochem Int. 2018;112:71-80.
261. Dhara SP, Rau A, Flister MJ, Recka NM, Laiosa MD, Auer PL, et al. Cellular reprogramming for successful CNS axon regeneration is driven by a temporally changing cast of transcription factors. Sci Rep. 2019;9(1):14198.
262. Szaro BG, Loh YP. Changes in axonal transport and glial proteins during optic nerve regeneration in Xenopus laevis. Curr Top Dev Biol. 1987;21:217-54.
263. Lewis C. The Abolition of Man. London: Oxford University Press; 1943.
264. Cook MW, Levin LA, Joseph MP, Pinczower EF. Traumatic optic neuropathy. A meta-analysis. Arch Otolaryngol Head Neck Surg. 1996;122(4):389-92.
265. Biousse V, Newman NJ. Ischemic Optic Neuropathies. N Engl J Med. 2015;372(25):2428-36.
266. Sperry RW. Effect of 180 degree rotation of the retinal field on visuomotor coordination. J Exper Zool. 1943;92:263-79.
267. Sperry RW. Restoration of vision after crossing of optic nerves and after contralateral transplantation of eye. J Neurophysiol. 1945;8:15-28.
268. Session AM, Uno Y, Kwon T, Chapman JA, Toyoda A, Takahashi S, et al. Genome evolution in the allotetraploid frog Xenopus laevis. Nature. 2016;538(7625):336-43.
269. Belrose JL, Prasad A, Sammons MA, Gibbs KM, Szaro BG. Comparative gene expression profiling between optic nerve and spinal cord injury in Xenopus laevis reveals a core set of genes inherent in successful regeneration of vertebrate central nervous system axons. BMC Genomics. 2020;21(1):540.
270. Watson FL, Mills EA, Wang X, Guo C, Chen DF, Marsh-Armstrong N. Cell type-specific translational profiling in the Xenopus laevis retina. Dev Dyn. 2012;241(12):1960-72.
271. Pittman AJ, Law MY, Chien CB. Pathfinding in a large vertebrate axon tract: isotypic interactions guide retinotectal axons at multiple choice points. Development. 2008;135(17):2865-71.
272. Hoskins SG, Grobstein P. Development of the ipsilateral retinothalamic projection in the frog Xenopus laevis. I. Retinal distribution of ipsilaterally projecting cells in normal and experimentally manipulated frogs. J Neurosci. 1985;5(4):911-9.

273. Levine RL. An autoradiographic study of the retinal projection in Xenopus laevis with comparisons to Rana. J Comp Neurol. 1980;189(1):1-29.
274. Coleman M. Axon degeneration mechanisms: commonality amid diversity. Nat Rev Neurosci. 2005;6(11):889-98.
275. Marsh-Armstrong N, Huang H, Remo BF, Liu TT, Brown DD. Asymmetric growth and development of the Xenopus laevis retina during metamorphosis is controlled by type III deiodinase. Neuron. 1999;24(4):871-8.
276. Miesfeld JB, Ghiasvand NM, Marsh-Armstrong B, Marsh-Armstrong N, Miller EB, Zhang P, et al. The. Proc Natl Acad Sci U S A. 2020;117(35):21690-700.
277. Willardsen MI, Suli A, Pan Y, Marsh-Armstrong N, Chien CB, El-Hodiri H, et al. Temporal regulation of Ath5 gene expression during eye development. Dev Biol. 2009;326(2):471-81.
278. Willsey HR, Exner CRT, Xu Y, Everitt A, Sun N, Wang B, et al. Parallel in vivo analysis of large-effect autism genes implicates cortical neurogenesis and estrogen in risk and resilience. Neuron. 2021;109(8):1409.
279. Bhattacharya D, Marfo CA, Li D, Lane M, Khokha MK. CRISPR/Cas9: An inexpensive, efficient loss of function tool to screen human disease genes in Xenopus. Dev Biol. 2015;408(2):196-204.
280. Labun K, Montague TG, Krause M, Torres Cleuren YN, Tjeldnes H, Valen E. CHOPCHOP v3: expanding the CRISPR web toolbox beyond genome editing. Nucleic Acids Res. 2019;47(W1):W171-W4.
281. Brinkman EK, Chen T, Amendola M, van Steensel B. Easy quantitative assessment of genome editing by sequence trace decomposition. Nucleic Acids Res. 2014;42(22):e168.
282. Yan D, Wu Z, Chisholm AD, Jin Y. The DLK-1 kinase promotes mRNA stability and local translation in C. elegans synapses and axon regeneration. Cell. 2009;138(5):1005-18.
283. Xiong X, Wang X, Ewanek R, Bhat P, Diantonio A, Collins CA. Protein turnover of the Wallenda/DLK kinase regulates a retrograde response to axonal injury. J Cell Biol. 2010;191(1):211-23.
284. Holt CE, Harris WA. Order in the initial retinotectal map in Xenopus: a new technique for labelling growing nerve fibres. Nature. 1983;301(5896):150-2.
285. Khakhalin AS. Analysis of Visual Collision Avoidance in. Cold Spring Harb Protoc. 2021;2021(4).
286. Dong W, Lee RH, Xu H, Yang S, Pratt KG, Cao V, et al. Visual avoidance in Xenopus tadpoles is correlated with the maturation of visual responses in the optic tectum. J Neurophysiol. 2009;101(2):803-15.
287. Khakhalin AS, Koren D, Gu J, Xu H, Aizenman CD. Excitation and inhibition in recurrent networks mediate collision avoidance in Xenopus tadpoles. Eur J Neurosci. 2014;40(6):2948-62.
288. Ko KW, Devault L, Sasaki Y, Milbrandt J, DiAntonio A. Live imaging reveals the cellular events downstream of SARM1 activation. Elife. 2021;10.
289. Yokota S, Takihara Y, Arimura S, Miyake S, Takamura Y, Yoshimura N, et al. Altered Transport Velocity of Axonal Mitochondria in Retinal Ganglion Cells After Laser-Induced Axonal Injury In Vitro. Invest Ophthalmol Vis Sci. 2015;56(13):8019-25.
290. Fague L, Liu YA, Marsh-Armstrong N. The basic science of optic nerve regeneration. Ann Transl Med. 2021;9(15):1276.

291. Amaya E, Kroll KL. A method for generating transgenic frog embryos. Methods Mol Biol. 1999;97:393-414.
292. Das B, Brown DD. Controlling transgene expression to study Xenopus laevis metamorphosis. Proc Natl Acad Sci U S A. 2004;101(14):4839-42.
293. Zhang XH, Tee LY, Wang XG, Huang QS, Yang SH. Off-target Effects in CRISPR/Cas9-mediated Genome Engineering. Mol Ther Nucleic Acids. 2015;4:e264.
294. Nguyen JV, Soto I, Kim KY, Bushong EA, Oglesby E, Valiente-Soriano FJ, et al. Myelination transition zone astrocytes are constitutively phagocytic and have synuclein dependent reactivity in glaucoma. Proc Natl Acad Sci U S A. 2011;108(3):1176-81.
295. Inoue T, Hosokawa M, Morigiwa K, Ohashi Y, Fukuda Y. Bcl-2 overexpression does not enhance in vivo axonal regeneration of retinal ganglion cells after peripheral nerve transplantation in adult mice. J Neurosci. 2002;22(11):4468-77.
296. Cenni MC, Bonfanti L, Martinou JC, Ratto GM, Strettoi E, Maffei L. Long-term survival of retinal ganglion cells following optic nerve section in adult bcl-2 transgenic mice. Eur J Neurosci. 1996;8(8):1735-45.
297. Leon S, Yin Y, Nguyen J, Irwin N, Benowitz LI. Lens injury stimulates axon regeneration in the mature rat optic nerve. J Neurosci. 2000;20(12):4615-26.
298. Cui Q, Yin Y, Benowitz LI. The role of macrophages in optic nerve regeneration. Neuroscience. 2009;158(3):1039-48.
299. Simkin J, Gawriluk TR, Gensel JC, Seifert AW. Macrophages are necessary for epimorphic regeneration in African spiny mice. Elife. 2017;6.
300. Godwin JW, Pinto AR, Rosenthal NA. Macrophages are required for adult salamander limb regeneration. Proc Natl Acad Sci U S A. 2013;110(23):9415-20.
301. Leach LL, Hanovice NJ, George SM, Gabriel AE, Gross JM. The immune response is a critical regulator of zebrafish retinal pigment epithelium regeneration. Proc Natl Acad Sci U S A. 2021;118(21).
302. Chen S, Lathrop KL, Kuwajima T, Gross JM. Retinal ganglion cell survival after severe optic nerve injury is modulated by crosstalk between Jak/Stat signaling and innate immune responses in the zebrafish retina. Development. 2022;149(8).
303. Iliff JJ, Wang M, Liao Y, Plogg BA, Peng W, Gundersen GA, et al. A paravascular pathway facilitates CSF flow through the brain parenchyma and the clearance of interstitial solutes, including amyloid β. Sci Transl Med. 2012;4(147):147ra11.
304. Tabor KM, Bergeron SA, Horstick EJ, Jordan DC, Aho V, Porkka-Heiskanen T, et al. Direct activation of the Mauthner cell by electric field pulses drives ultrarapid escape responses. J Neurophysiol. 2014;112(4):834-44.
305. Mathias JR, Zhang Z, Saxena MT, Mumm JS. Enhanced cell-specific ablation in zebrafish using a triple mutant of Escherichia coli nitroreductase. Zebrafish. 2014;11(2):85-97.
306. Bergemann D, Massoz L, Bourdouxhe J, Carril Pardo CA, Voz ML, Peers B, et al. Nifurpirinol: A more potent and reliable substrate compared to metronidazole for nitroreductase-mediated cell ablations. Wound Repair Regen. 2018;26(2):238-44.
307. Gibson DG, Young L, Chuang RY, Venter JC, Hutchison CA, Smith HO. Enzymatic assembly of DNA molecules up to several hundred kilobases. Nat Methods. 2009;6(5):343-5.
308. Yang Z, Quigley HA, Pease ME, Yang Y, Qian J, Valenta D, et al. Changes in gene expression in experimental glaucoma and optic nerve transection: the equilibrium between protective and detrimental mechanisms. Invest Ophthalmol Vis Sci. 2007;48(12):5539-48.

309. Agudo M, Pérez-Marín MC, Lönngren U, Sobrado P, Conesa A, Cánovas I, et al. Time course profiling of the retinal transcriptome after optic nerve transection and optic nerve crush. Mol Vis. 2008;14:1050-63.
310. Hackler L, Masuda T, Oliver VF, Merbs SL, Zack DJ. Use of laser capture microdissection for analysis of retinal mRNA/miRNA expression and DNA methylation. Methods Mol Biol. 2012;884:289-304.
311. Heiman M, Kulicke R, Fenster RJ, Greengard P, Heintz N. Cell type-specific mRNA purification by translating ribosome affinity purification (TRAP). Nat Protoc. 2014;9(6):1282-91.
312. Lohman BK, Weber JN, Bolnick DI. Evaluation of TagSeq, a reliable low-cost alternative for RNAseq. Mol Ecol Resour. 2016;16(6):1315-21.
313. Meyer E, Aglyamova GV, Matz MV. Profiling gene expression responses of coral larvae (Acropora millepora) to elevated temperature and settlement inducers using a novel RNA-Seq procedure. Mol Ecol. 2011;20(17):3599-616.
314. Engler C, Kandzia R, Marillonnet S. A one pot, one step, precision cloning method with high throughput capability. PLoS One. 2008;3(11):e3647.
315. Ran FA, Hsu PD, Wright J, Agarwala V, Scott DA, Zhang F. Genome engineering using the CRISPR-Cas9 system. Nat Protoc. 2013;8(11):2281-308.
316. Qi LS, Larson MH, Gilbert LA, Doudna JA, Weissman JS, Arkin AP, et al. Repurposing CRISPR as an RNA-guided platform for sequence-specific control of gene expression. Cell. 2013;152(5):1173-83.